

COMPOSITE THERMO-HYDROFORMING OF MILITARY BALLISTIC
HELMETS

By

Nicholas Eric Kuuttila

A THESIS

Submitted to
Michigan State University
in partial fulfillment of the requirements
for the degree of

Mechanical Engineering—Master of Science

2014

ABSTRACT

COMPOSITE THERMO-HYDROFORMING OF MILITARY BALLISTIC HELMETS

By

Nicholas Eric Kuuttilla

Composite thermo-hydroforming is an MSU patented process similar to sheet metal hydroforming. This process uses heated and pressurized fluid to form composite blanks to a punch of desired geometry. Prior to this study, a small 40 ton press served as a proof of concept by forming 4” diameter hemispheres, allowing the lab to acquire a larger 300 ton press. This study focuses on the modification and design of the 300 ton press and using it to form advanced combat helmets using the ballistic composite Spectra Shield SR-3136. Good results are achieved in the forming process showing that composite hydroforming is a viable means for manufacturing thermoplastic composite materials. The process showed good results in the ability to form these deep drawn parts by reducing wrinkling of the final product.

Concurrent to these forming experiments, the forming process is numerically modeled using Abaqus/CAE. The material is modeled using a Preferred Fiber Orientation model developed by a past student of the hydroforming lab. The model is adapted to work with a thick composite laminate consisting of many layers. Model parameters are also updated to work with a significantly thicker laminate than has been used in the past. Results of the numerical modeling show good correlation with the forming experiments. The model still shows need for improvement due to the premature onset and severity of the out of plane warping observed.

Copyright by
NICHOLAS ERIC KUUTTILA
2014

I dedicate this work to my mother and father.
Thanks for the love and encouragement, but mostly thanks for supporting my continued education.

ACKNOWLEDGMENTS

Thank you to everyone who helped guide me along the path of research and discovery. Thanks to Dr. Loos and Dr. Hossain for their expertise and support in material characterization. Thanks to all that helped at Mott Community College for supplying the lab with pre-cut blanks. Thanks also to BAE Systems and TARDEC for supporting this work through funding, materials and tooling.

Thank you to my hardworking undergraduate assistants; Scott Belonge, Luke Ferguson, Matt Ayers, Ryan Volkman and Tim Maul.

Most of all, thanks to my adviser, Dr. Farhang Pourboghra, who has not only advised me but mentored me as well throughout the majority of my higher education. Thanks for the opportunities and for the continued support.

TABLE OF CONTENTS

| | |
|---|------|
| LIST OF TABLES | viii |
| LIST OF FIGURES | ix |
| Introduction..... | 1 |
| Composite Thermo Hydroforming..... | 2 |
| Topics Investigated During This Study | 4 |
| Literature Review..... | 7 |
| Consolidation of CFRTP Composites..... | 7 |
| Material Characterization Methods..... | 12 |
| Thermoplastic Composite Forming Methods | 14 |
| Numerical Methods for Simulating the Forming of Composites..... | 17 |
| Consolidation of Flat Panels and Material Characterization..... | 20 |
| SR-3136 | 20 |
| Blank Consolidation and Shape | 20 |
| Material Characterization..... | 23 |
| Shear Modulus | 23 |
| Young’s Modulus..... | 27 |
| Polypropylene Reinforced Carbon Fiber | 31 |
| Blank Consolidation..... | 31 |
| Consolidation Properties Tool | 34 |
| Future Recommendations | 36 |
| Experimental Methods | 37 |
| Experimental Setup..... | 38 |
| High Pressure System (HPS) | 38 |
| Pressure Producing Skid (PPS) | 40 |
| Forming Dies | 44 |
| Punches | 50 |
| Oil Heater..... | 52 |
| Infrared Heater..... | 53 |
| Computer Control System..... | 55 |
| Forming Process..... | 57 |
| Results and Discussion | 63 |
| Phase 1 | 64 |
| Phase 2 | 65 |
| Phase 3 | 67 |
| Phase 4..... | 73 |
| Future Recommendations | 83 |
| Numerical Methods..... | 85 |
| Preferred Fiber Orientation (PFO) Material Model | 85 |
| Constitutive Model..... | 86 |
| Obtaining Material Properties..... | 88 |

| | |
|--|-----|
| Preferred Orientations | 91 |
| Implementation in Abaqus | 95 |
| Simulation Changes and Adaptions | 96 |
| Multiple Layer Simulation | 97 |
| Transverse Shear Stiffness | 100 |
| Transverse Young's Modulus | 102 |
| Use of Material Characterization Data..... | 102 |
| Results and Discussion | 103 |
| Impact of Transverse Shear Stiffness..... | 104 |
| Square Blank Simulation Results..... | 106 |
| Over-prediction of Shear Stiffness..... | 110 |
| Comparison to Experimental Results..... | 112 |
| Future Recommendations | 116 |
| Conclusions..... | 118 |
| REFERENCES | 120 |

LIST OF TABLES

| | |
|--|-----|
| Table 1 – Shear Modulus | 26 |
| Table 2 – Tensile Test Data | 30 |
| Table 4 – Consolidation Conditions..... | 34 |
| Table 3 – CF-PP Layup Tool | 35 |
| Table 5 - Traction Separation Properties | 100 |
| Table 6 – Original Transverse Shear Properties | 101 |
| Table 7 – Simulation Properties..... | 106 |

LIST OF FIGURES

| | |
|--|----|
| Figure 1 - Matched Die Molding | 3 |
| Figure 2 – CMA Blank Shape Prediction Capabilities | 22 |
| Figure 3 – Shear Modulus Test Specimens..... | 24 |
| Figure 4 – Shear Fixtures | 25 |
| Figure 5 – Shear Stress Strain Curves..... | 26 |
| Figure 6 – Difficulties with Tensile Specimens..... | 28 |
| Figure 7 – Dog Bone Specimens | 28 |
| Figure 8 – Tensile Test Results..... | 29 |
| Figure 9 – Tensile Specimen from Russell Study..... | 31 |
| Figure 10 – CF-PP Consolidation Mold | 32 |
| Figure 11 – HPS Components..... | 39 |
| Figure 12 – Simplified Hydraulic Schematic of PPS and Forming Die..... | 41 |
| Figure 13 – The Blank Sandwich..... | 42 |
| Figure 14 – PPS Cooling Loop | 43 |
| Figure 15 – Regulator Operating Configurations..... | 44 |
| Figure 16 – Original Hydroforming Dies | 45 |
| Figure 17 – Redesigned Hydroforming Die Set..... | 47 |
| Figure 18 – Reduction in Punch Cavity Gap | 48 |
| Figure 19 – Hydrostatic Clamping..... | 49 |
| Figure 20 – Tongue and Groove Feature | 50 |
| Figure 21 – Section View of Punch-Ram Adapter Interface | 51 |
| Figure 22 – ACH Punch..... | 51 |
| Figure 23 – Hemispherical Punch..... | 52 |

| | |
|---|----|
| Figure 24 – IR Heating Array | 54 |
| Figure 25 – Forming - Step 1 | 58 |
| Figure 26 – Forming - Step 2..... | 59 |
| Figure 27 – Forming - Step 3..... | 60 |
| Figure 28 – Forming - Step 4..... | 61 |
| Figure 29 – Forming - Step 5..... | 62 |
| Figure 30 – Forming - Step 6..... | 63 |
| Figure 31 – First Hydroforming Results | 65 |
| Figure 32 – Double Sided Forming Pressure on Dyneema Blank | 66 |
| Figure 33 - Rapid Decompression of the Fluid Cavity | 68 |
| Figure 34 – Blank Formed with Single-Side Forming Pressure | 69 |
| Figure 35 - Fiber Orientations of Dyneema Blank..... | 70 |
| Figure 36 - Reducing Blank Anisotropy | 71 |
| Figure 37 – Specialized Stacking Sequence | 72 |
| Figure 38 – CMA Predicted Blank Shape..... | 74 |
| Figure 39 – Limited Forming Pressure | 75 |
| Figure 40 - Forming Pressure and Punch/Clamp Displacement | 76 |
| Figure 41 – Improvement in Results..... | 78 |
| Figure 42 - Blank Lifting Problem..... | 79 |
| Figure 43 - Change in Clamping Scheme | 81 |
| Figure 44 – Clamping Scheme Difficulties..... | 82 |
| Figure 45 – Material and Structural Coordinate Systems | 87 |
| Figure 46 – Stiffness Summing Used in PFO Model..... | 91 |
| Figure 47 – Rotation of PFO’s to the Structural Frame..... | 93 |
| Figure 48 – Modification of the Structural Coordinate System and Fiber Orientations | 94 |
| Figure 49 – User Subroutines Within Abaqus/CAE | 95 |

| | |
|--|-----|
| Figure 50 - Model Setup | 96 |
| Figure 51 – Fracture Modes | 98 |
| Figure 52 - Traction-Separation Curves..... | 99 |
| Figure 53 - Tansverse Shear | 101 |
| Figure 54 – Transverse Shear Stiffness Effects | 105 |
| Figure 55 – Deformed Blank Shape..... | 107 |
| Figure 56 - Previous Simulation Results..... | 108 |
| Figure 57 – Fiber Shear Contour Plot | 109 |
| Figure 58 - Q_{66} Contour Plot..... | 110 |
| Figure 59 - Shear Stiffness vs Volume Fraction | 111 |
| Figure 60 - Frame Rotation Effect on Shear Stiffness | 111 |
| Figure 61 - Pressure Profiles..... | 113 |
| Figure 62 - Force-Displacment Comparison..... | 114 |
| Figure 63 – Blank Shape and Wrinkling Region Comparison..... | 115 |

Introduction

The use of composite materials in high strength, light weight structures has been occurring for decades. Fiberglass reinforced plastics have been employed since the 1950's in the building of high performance cars and boat hulls. More recently, carbon fiber composites have gained acceptance in the aerospace industry as a high strength structural material, capable of exceeding the strength of steel. It has only been a couple of decades that carbon fiber and other high performing composites has become affordable enough to appear in consumer goods such as automobile components and sporting goods. These products are the first among many consumer products that will employ carbon fiber composites as the material becomes more affordable. Currently these products are still cost prohibitive to the average consumer. Nevertheless, costs continue to decrease and the strength and weight reduction benefits are becoming more attractive, especially to the automotive industry as CAFE standards continue to push for higher fuel efficiency (50 MPG by 2025).

The costs of raw materials alone do not shed light on the reason for the high cost of composites. A vast majority of composites employ matrix systems such as polyester, vinylester, and epoxy. This class of plastics, known as thermosets, is applied to the reinforcing fibers in liquid form and either heat or a chemical hardener is used to catalyze cross linking of the polymer chains which permanently hardens the resin. This type of resin has several advantages such as relatively low curing temperature, a low pre-cured viscosity, high stiffness and stability over a wide range of temperatures. However the drawbacks associated with this resin system are numerous. The curing cycle of the resin system can take hours, severely reducing the ability to mass produce components. Additionally, components that have been damaged are not able to be repaired easily and more often than not need to be completely replaced. Recycling these resins is also difficult.

Many of these shortcomings can be addressed by employing thermoplastic resin systems. Thermoplastics soften and melt at elevated temperatures and solidify when cooled. This allows manufacturing cycles that are a fraction of the time when comparing them to thermosets. This also allows the repair and joining of components through fusion bonding and thermoplastic welding techniques [1]. As opposed to thermoset resins, thermoplastics do not cross link but instead form a solid structure by an entangled network of amorphous or semi-crystalline polymer chains. This gives the thermoplastic polymer the ability to reach large deformations before failure, leading to increased energy absorption over thermoset polymers. Thermoplastics are also easily recycled which leads to waste reduction benefits [2].

A few drawbacks exist when working with thermoplastic resins. Thermoplastics often require a higher processing temperature than thermosets. PEEK, for example, melts at approximately 340° C and requires processing around 385° C. Many thermoplastics do not bond well to fiber constituents resulting in poor interface adhesion and reduced mechanical properties. This problem can be avoided with good consolidation techniques and the use of a binding agent at the fiber-matrix interface. Benefits in using thermoplastics still outweigh the costs. This study highlights the design and manufacturing processes used in the manufacture of a thermoplastic military helmet.

Composite Thermo Hydroforming

As discussed above, a key advantage of thermoplastic matrix composites is the ability to be heated and reformed several times before the final net shape is created. A wide number of forming processes can be used to form composites utilizing this type of matrix. Perhaps the most common of these methods is matched die molding. This method is similar to sheet metal forming in that the composite is acted on by a die of the desired geometry. This die pushes the composite into a cavity which is a mirror image of the other die but slightly larger. As the two matched dies come together the composite is compressed into a cavity that dictates its final shape and thickness. The basic tooling and process can be seen in Figure 1.

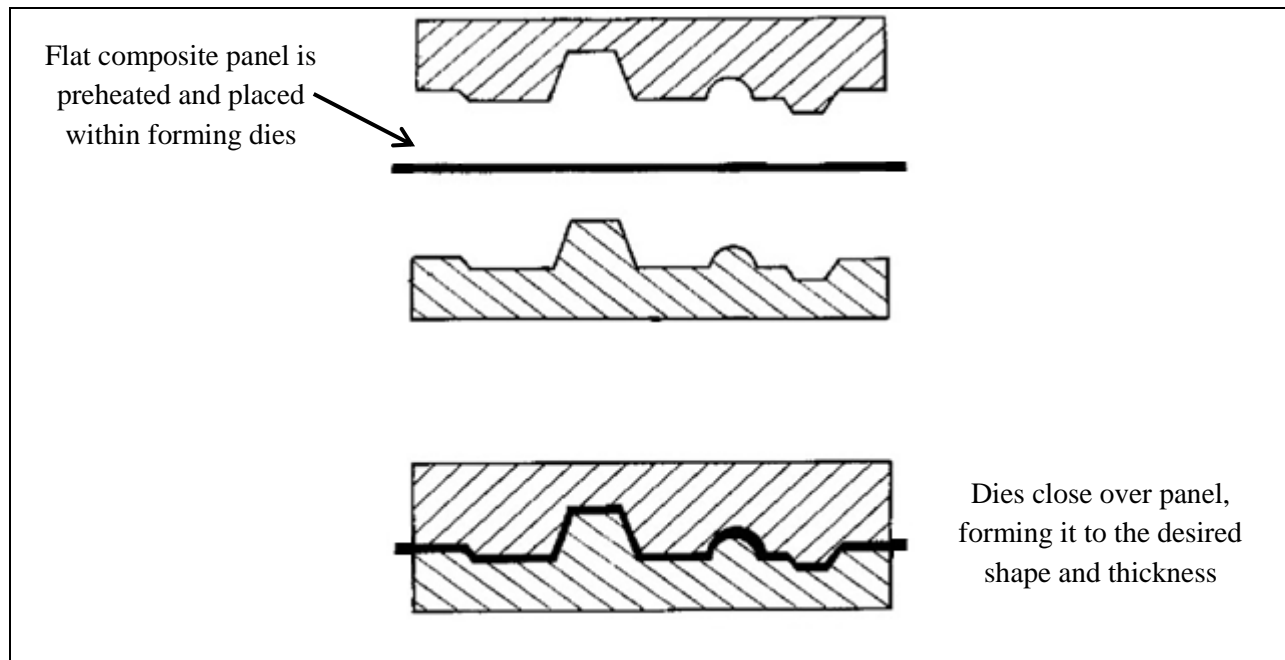


Figure 1 - Matched Die Molding

Typically the tooling used in match die forming is heated to keep the composite at the proper forming temperature as it is deformed to its final shape. Heating and cooling of the tooling is necessary to keep the composite at its forming temperature and to accelerate the solidification process. This heating and cooling can significantly increase process time. The dies are only able to exert force downward onto each other. In the case of deep drawn parts, the normal direction of the die surface may differ significantly from the force application vector. This makes controlling thickness and applying even forming pressure difficult. This can lead to parts that are not well consolidated or have significant variations in thickness.

Thermo hydro-forming is a composite forming process that utilizes a heated pressurized fluid to conform the composite material to a punch of the desired part geometry. This process is similar to sheet metal hydro-forming in that it utilizes pressurized fluid to form the blank to a male plug (punch). This process was developed and patented in the Michigan State University Advanced Materials Manufacturing Laboratory. The hydroforming press and process will be described in more detail in the Experimental Methods section.

This method of forming presents several advantages over match die forming. Since fluid is used to form the material, only a single punch is needed where as in matched die forming a male and female

die is required to form the part, leading to reductions in tooling cost and complexity. The heated pressurized fluid can be used to keep the composite at the appropriate forming temperature, eliminating the need for tool heating. Since the forming force utilized is applied by pressurized fluid, the force vector that conforms the material to the punch is always normal to the material surface. This evenly distributed forming force has been shown to reduce out of plane warping significantly; especially in high shear areas of the formed part. This allows the hydroforming process to form deep drawn parts and other challenging part geometries. This is the greatest benefit that composite hydroforming offers over other thermoplastic composite forming methods.

Topics Investigated During This Study

The focus of this study was to develop a thermoplastic composite processing methodology and system. This goes far beyond just the forming of the composite blank. Rather, it involves developing a deep understanding of the microstructure, mechanical response and failure mechanisms of the composite system being formed. Understanding these properties is critical in developing a process and setting forming conditions that will produce a high quality part.

The first portion of the study involves understanding the consolidation of the composite material to be formed. Two separate composite systems were investigated during this study; carbon fiber reinforced polypropylene and the ballistic composite Spectra Shield SR-3136. Spectra Shield is a thermoplastic composite consisting of highly crystalline ultra-high molecular weight polyethylene fibers reinforced by a sparse matrix consisting of a proprietary mixture of lower density polyethylene. A single layer of this film is made up of four unidirectional layers of UHMWPE fibers oriented [0/90/0/90]. This film is cut and laid up to the desired areal density where it is then consolidated using a heated platen press. Honeywell provides a recommended pressing temperature time and pressure in order to achieve the best ballistic performance possible.

The carbon fiber polypropylene composite was selected to display the versatility of the thermo hydro-forming system. This composite is formed from 5x5 satin woven 6k carbon fiber and block

copolymer polypropylene film. The constituents are laid up into a special mold in alternating order forming a sandwich structure. The mold is then loaded into a heated platen press where heat and pressure are applied to the mold forming the plate. For this material, only a consolidation study is performed.

The next portion of this study is obtaining the mechanical properties of the consolidated composites. Mechanical properties are obtained to provide material models with the needed engineering constants in order to make the simulation produce realistic results. A preferred fiber orientation (PFO) material model is utilized in this study to predict the results of the composite forming process. Several common engineering constants are required for the characterization of the laminated composite in this material model. The methods used to obtain these constants will be discussed later in the Material Characterization section.

The main focus of this study is the forming of composite blanks into useful parts. A 300 ton thermo hydroforming press is used to form the flat blanks into military ballistic helmets. This press is based off a small 40 ton press that served as a proof of concept for the process of composite hydroforming. The 40 ton press was successful in forming 4" diameter hemispheres out of polypropylene reinforced fiberglass. The 300 ton press is capable of forming pieces in excess of 10" in diameter and up to a depth of 8". Forming pressures of up to 2400 psi can be applied, allowing the forming of thick laminated plates. Many changes were made to the press in order to produce high quality parts. Changes included developing a new bladder system to protect the composite, implementing new die sets and changing the blank clamping scheme. These methods and process changes will be described in more detail in the Experimental Methods section.

Finite element analysis was performed in order to develop a deeper understanding of the blank material and of the hydroforming press. Simulations were performed in Abaqus CAE using a user defined material model. As stated before, a PFO model that was developed by Mike Zampaloni during his PhD studies was utilized [3]. The main advantage of this model is its ability to track the alignment of the reinforcing fibers as the material is deformed during the forming process. Several updates were made to the material model during this study, including the implementation of cohesive surfaces, updating the

transverse shear stiffness and using material properties obtained during material characterization. The results of these simulations were compared to experimental forming results in order to assess the validity of the material model. The material model can also be used to predict the effect that changing the forming conditions will have on the final part. A simulation with sufficient accuracy will ideally be used to determine the optimal forming conditions without having to physically form a single part. The numerical simulations and material model will be further discussed in the Numerical Methods section.

Literature Review

Consolidation of CFRTP Composites

Consolidation quality of composites has a profound effect on their mechanical properties. Excessive void content and poor fiber matrix adhesion can greatly limit the mechanical properties of the consolidated laminate. In the 1980's, thermoplastic composites began to gain traction because of the potential to significantly reduce manufacturing costs. Up to this point, composite materials had been employing thermoset matrix systems such as polyester, vinylester and epoxy.

In order to engineer optimal matrix fiber adhesion for thermoset or thermoplastic composites, the microstructure of the interface must be well understood. Bascom and Drzal studied the interface of carbon fibers as the bonding mechanisms used in carbon fiber composites which was not well understood at this time [4]. Techniques used to construct carbon lattices from polyacrylonitrile (PAN) are presented. The ways in which these lattice structures pack as they are drawn into fibers has great effect on the crystal alignment of the fiber and consequently the mechanical response. The surface of a carbon fiber is composed of the same material structure as can be found at the core of the fiber which is graphitic crystals (hexagonally packed carbon atoms). Oxidation is used to bond functional groups to the surface of the fiber which can be used in bonding mechanisms for epoxy. In order for this to happen the resin must make intimate contact with the inclusions. This is true for both thermoplastic and thermoset composites.

Recent studies have been conducted by Semoto et al. showing the formation of bonds between epoxy resins and functionalized oxygen based molecules on the surface of graphite lattices [5]. This study involved molecular dynamic simulation of hydrogen bonds between a fragment of epoxy resin and OH and COOH functionalized molecules on the surface of carbon fibers that are the product of oxidation surface treatments. The simulation shows strong atomic bonds reinforcing the interface adhesion between fiber and matrix constituents but is highly idealized and beyond the scope of this study. Nevertheless, this

study shows the crucial importance of functionalized bonds in the adhesion in carbon fiber-epoxy composites.

Thermoplastic polymers do not typically form these strong bonds with fibers but instead rely on an entangled polymer chain network to transfer load to the fibers. Upon melting these molecular chains become less entangled and can slide and flow past one another. However the long chains do not break down resulting in relatively high molten viscosities. Ye performed a study which investigates how the high viscosities of these polymers can affect consolidation of composites [6]. The composite system used in this study is woven CF pre-impregnated with polyether ether ketone (PEEK). The consolidation of a laminate from individual prepreg sheets is performed using a heated platen press. Ye found that heat, pressure, and time are the three main variables that affect the consolidation quality of the composite. In order to achieve the best properties, the fiber yarns (tows) must be wet out with molten polymer. The key factors shown to vary the wet out of the fiber tows is their permeability, their radius, the matrix viscosity and the pressure of the molten matrix. For laminates consolidated under varying conditions, the void volume fraction, ultimate tensile stress and transverse shear modulus are measured. It is shown that increases in void volume fraction lead to decreases in the measured mechanical properties.

By analyzing the matrix flow equation of the previous paper, it is clear that reductions in matrix viscosity will lead to faster consolidation with fewer voids. Decreasing a thermoplastic polymers viscosity can be accomplished by raising its temperature above the melt point. For many high performing polymers such as PEEK, the temperature cannot be raised significantly above the melting point because of the onset of thermal degradation. Thermal degradation and its effect on the microstructure of polymers is described by Beyler [7]. During thermal degradation, thermoplastic polymers are attempting to volatilize but cannot due to their high molecular weight (polymer chain length). As the degradation temperature is passed, polymer chains begin to break apart. This reduction in molecular weight can significantly reduce the mechanical properties of the material and further heating will bring on the formation of char as broken polymer chains begin to cross link forming chemical species that are more carbon rich. Therefore, it is ideal to thermoform with polymers that possess a large gap between the

melting temperature and thermal gradient temperature to take advantage of reductions in viscosity.

Polypropylene is ideal in this application as the melting temperature and degradation temperature differ by $\sim 88^{\circ}$ C.

Polypropylene has become a material of interest for fiber reinforced composites recently due to its low price. Mass production industries such as automotive, packaging and consumer goods have taken an increased interest in PP composites due to their potential for high performance, low cost and excellent formability. Zampaloni et al. investigated the consolidation and forming of kenaf natural fiber reinforced polypropylene [8]. Several consolidation techniques and PP blends were evaluated during this study. A method was developed to consolidate PP-Kenaf composites into sheets. A small amount of maleated polypropylene (MaPP) was added to the PP blend to improve bond quality between the kenaf fibers and PP matrix. Zampaloni also showed that these pre-consolidated sheets can be effectively formed by the hydroforming process similar to the one used in this study.

MaPP is commonly used to strengthen the bond between PP and reinforcing fibers. In his study of PP composites, Shubhra states the MaPP can be used to increase the matrix-inclusion bond strength and stiffness of several types of thermoplastic composites including fiber types of hemp, cotton, carbon, glass, and several others [9]. On the molecular level, most reinforcing fibers used in composite applications are polar in nature or have polar molecular groups on the surface. Since the molecular structure of PP is non-polar, only mechanical forces such as friction and polymer chain entanglement resist separation at the fiber-matrix interface. The introduction of polar maleic anhydride (MA) to the polymer chain, allows a physical bond to attach between the fiber and matrix. A small amount of MaPP is required to improve the properties of the PP composite (only about 2-4% by weight of the matrix). Excess MaPP has been shown to decrease tensile and bending strength.

Several studies have been focused on adding MaPP to CF-PP composites as well. Karsli et.al. show increases in the strength and stiffness of composites prepared by twin screw extrusion of chopped fiber CF-PP composites [10]. The composites in this study were prepared with a 2-20% fiber weight fraction. Maleic anhydride grafted polypropylene (MAH-g-PP) was added to the matrix constituent in

amounts 0-5% by weight. Since preparation of the samples was carried out via plastic injection molding, the MAH-g-PP was evenly distributed throughout the matrix. Increases in both tensile strength at break and tensile modulus were obtained by increasing both the fiber and binder content. Micrographs of the failure sites showed an increase in fiber-matrix adhesion in the MAH-g-PP blended composite over those without the matrix compatibilizer.

Giruaud et. al. investigated the effects of other sizing agents for CF reinforced PEEK [11]. The composite is consolidated using a resin film infusion technique similar to the one in this study. Prior to consolidation, a sizing of polyetherimide (PEI) is applied to continuous CF tows by spraying a prepared emulsion of the polymer sizing directly onto the fiber surface. The emulsion consists of polymer suspended in water and other solvents which is sprayed directly onto the fiber surface. Micrographs show an enhancement in bond quality for the sized fibers when compared to the un-sized fibers.

Ultra high molecular weight polyethylene (UHMWPE) composites are a more recent development in the world of composites. These composites have a high fiber volume fraction (typically 80% or above) and are employed primarily in blast or ballistic protection devices (body and vehicle armor). Since these materials are in an early stage of development, literature on particular types of UHMWPE composites is sparse. Most of the literature presented for these types of materials focuses on products that are similar but not exactly the same as SR-3136.

One of the only pieces of literature existing specifically for SR-3136 comes from the manufacturer and provides consolidation and forming recommendations [12]. This document recommends that the processing temperature should be between 240°F and 260°F when using the compression molding process. A pressure between 500 and 5000 psi should be applied to fully consolidate the sheets. The laminate is then cooled under pressure until the center of the material is below 125°F. This document also states that improved ballistic performance may be achieved through the use of higher consolidation pressure. It should be noted that these recommendations are made for the entire Spectra Shield line and not just for SR-3136. Optimal forming conditions for SR-3136 may lie somewhere within these relatively broad guidelines.

UHMWPE fibers have been used to reinforce high demand structures over the past couple of decades. Since the fibers have a density less than water, they have been utilized in marine applications to take advantage of their buoyancy. Heavy duty ropes, sails and fishing lines as well as body and vehicle armor have been offered by both Honeywell and DSM, the two main manufacturers of UHMWPE fiber composites. These fibers have been offered in various forms as well, ranging from matrix free braids and woven fabrics to unidirectional prepreg which is held together with a sparse matrix constituent that is typically held proprietary.

Xu et. al studied UHMWPE composites in their matrix free form called Spectra Cloth [13]. A method for forming this cloth was developed called high-temperature high-pressure sintering. This method involves bringing the polymer cloth close to its melting temperature allowing just the surface of the fibers melt. Pressure is applied allowing the molten fiber surfaces to unite and become bonded to one another. Care must be taken to avoid over-melting the fibers during processing however. Excessive melting destroys the highly crystalline structure of the fibers leading to drastically reduced strength and stiffness.

In a later study, Xu and Farris compare the ballistic performance and formability of Spectra cloth with Dyneema Fraglight and Spectra Plus PCR [14]. Dyneema is a non-woven felt-like material with random fiber orientations, and the Spectra plus PCR consists of fibers impregnated with a proprietary matrix and stacked in a $[0^\circ/90^\circ]$ tape. Spectra cloth performed the best in impact energy absorption but only over a very narrow temperature window (2°C). Both the Dyneema and Spectra Plus PCR absorbed an impact energy of at least 60 KJ/m over a 10°C spread in processing temperature. Even though these values are slightly lower than the max energy absorbed by Spectra cloth (78.1 KJ/m @ 150°C) the wider band of acceptable processing temperature allows for better quality assurance in the end product. Comparisons in material formability showed that the Spectra cloth and Dyneema were easily formed with Dyneema requiring slightly less punch force. Problems with forming Spectra Plus PCR are attributed to matrix squeeze-out and other matrix flow issues. Since all of

these materials are processed using the same conditions and same method (match die molding), it is impossible to say whether or not optimizing the process for each material could result in better performance or ease of forming.

Greenhalgh et. al performed a more comprehensive study on the effects that processing parameters have on the response of Dyneema UHMWPE composites [15]. Micrographs revealed that the matrix constituent of this composite is very sparse and void ridden. Unlike in structural composites, this matrix structure assists in energy absorption and is a key feature in ballistic composites. Further analysis revealed that increases in processing pressure lead to changes in the inter-laminar matrix thickness. Differences in matrix thickness affect the toughness of different modes of fracture and delamination. Even though processing pressures show a difference in the failure mechanism, the overall target response between panels processed under low and high pressures is the same.

Material Characterization Methods

When analyzing the forming of materials of any type, it is important to understand their mechanical response to applied deformations. This is easily done with homogeneous materials that do not change their response when loading is applied along different orientations. Obtaining the response of composites is not as trivial due to the anisotropy created by the orientation of the reinforcing fibers. This type of material response and structure calls for the use of an orthotropic material model coupled with a plane stress assumption. This model will take into account the stiffness along the fiber axis and perpendicular to it as well as the Poisson's ratio and shear modulus. With these engineering terms, a reduced compliance matrix can be assembled that will predict the response for a given stress.

Zampaloni developed a material model which tracks preferred fiber orientations of random orientation, woven or unidirectional composite sheets [3]. The method was first developed to predict the response of randomly oriented fibers. With woven or unidirectional composites, it is easy to visually determine which orientations will give the stiffest response but this cannot be done with composite

possessing random fiber orientations. By using a squeeze flow test, he was able to determine which directions possessed the greatest amount of reinforcing fibers and which orientations had the least. By assuming that orientations with the greatest fiber content would be the stiffest, he was able to determine the orientations worth tracking in his material model. After identifying these orientations, material properties were extracted.

The first property to be determined is typically the Young's modulus. This is a routine characterization for composite materials and is typically performed in accordance with ASTM D 3039 [16]. This standard utilizes a rectangular specimen with specialized grip tabs to determine the axial response of the composite being evaluated. For this standard, both the Young's modulus and Poisson's ratio of a composite material can be determined.

This standard does not work well with all composites however. The use of this standard with UHMWPE composites often causes inter-laminar shear failure at the gripped area. Russell et al. developed a specialized gripping mechanism in order to resolve this issue [17]. The gauge section of the specimen is small in comparison to the gripped area. This ensures that failure does not occur in the gripped region.

Direct measurement of the shear modulus is also necessary. Two methods for evaluating the shear modulus are reviewed; the Iosipescu shear test [18] and V-notch rail shear test [19]. Both of these tests rely on a rectangular specimen with notches cut in order to concentrate shear stress at the neck. The main difference in these methods is how the specimen is loaded. The Iosipescu method uses a special fixture which loads the specimen along its edges by exerting compressive force. The V-Notched rail shear method grips the faces of the specimens using a special fixture and shears the specimen in tension. Since these methods apply different loads in different locations of the laminated coupons (face or edge) it is reasonable to expect that they will give slightly different values for the shear modulus. Yan-lei et al. performed a study where these two methods were evaluated [20]. Although the Iosipescu shear specimens can produce good results, they claim that edge crushing can be an issue due to the way that the specimen

is loaded. The V-notched rail shear method is preferred because of the elimination of this unacceptable failure mode and the use of a larger gauge section.

The determination of the two Young's moduli, the Poisson's ratio and the shear modulus are all that is needed to characterize the constitutive relation. For large deformations, however, inter-laminar separation plays a role. This effect becomes pronounced in materials where delamination commonly occurs, such as in UHMWPE fiber composites. This makes determining the inter-laminar traction separation response necessary in order to fully characterize the material. Liu et al. utilized a shear test method to determine the traction-separation response of Dyneema HB26 undergoing mode II inter-laminar fracture [21]. A special double notched beam is loaded in tension in order to initiate delamination. The shear stress can be calculated using the area of the planes in which fracture occurred and displacement is measured using a clip gauge. The exact traction separation quantities are then determined via the calibration of a similar FEA model.

Thermoplastic Composite Forming Methods

The manufacturing of composite materials requires many considerations in order to produce a high quality end part that is visually appealing and performs well. Many methods have been developed exclusively for thermoset materials. These methods include wet layup, vacuum molding, resin transfer molding, vacuum assisted resin transfer molding, autoclave, and a host of others. These methods take advantage of the low temperature and viscosity of the pre-cured resin and often rely on skilled laborers to mix and distribute the resin properly. The use of prepregs eliminates the need for the manual mixing of resin and ensures a uniform distribution. Once laid up, these composites are typically cured in an autoclave oven. It is by this method that the highest quality aerospace composite parts are made today. The need for skilled labor and massive autoclaves drives price up significantly as does the cost of the prepreg itself. Thermoplastic composites have the ability to surpass thermosets in the ease and cost of

manufacturing. Fully automated methods can be utilized for more consistent parts and shorter cycle times. These composites also feature a nearly infinite shelf life further increasing their economic value.

By the late 1980's, thermoplastic composites had risen in popularity and forming methods were developed with the ability to produce high quality composites. Richard Okine was among the first to evaluate these methods [22]. Several thermoplastic composite forming techniques were evaluated including match die forming, vacuum forming, diaphragm forming and hydroforming. Of these the most commonly used today is match die forming. Match die forming allows for excellent temperature control and the creation of parts with high quality surfaces. This technique has several drawbacks though. Deep drawn parts are difficult to form effectively since forming pressure is only applied axially. This leads to wrinkling and non-uniform part thickness. Resin can also be squeezed away from the fiber structure leading to resin poor areas.

Yin et.al. performed a more recent study which highlights some of the shortcomings of match die molding [23]. A layer of pellets is placed between two layers of plain weave carbon fiber and is placed in a furnace to melt the polymer. Once molten, the composite is transferred to the match die mold where it is quickly formed into the shape of a wingtip. Most of the formed parts exhibited a resin rich tip indicating molten polymer squeeze out. This is a common occurrence for deep drawn parts being formed using the match die technique due to the way the molds apply force.

McCool et al. performed a comprehensive study of match die molding [24]. During this study, effect of the composite formability and final part quality were investigated. Part temperature was closely monitored and the concept of a blank forming temperature "window" was investigated. The cooling rate of the mold was also changed in order to optimize the crystallinity of the polymer (PPS). A greater degree of crystallinity was shown to improve flexural strength, making the cooling rate, mold tool temperature and blank forming temperature all parameters of interest.

Another method of composite fabrication is injection molding, provided the fibers are relatively short. Karmaker and Youngquist explored methods to incorporate polypropylene injection molded parts reinforced with short natural fibers [25]. The reinforcing fiber constituent in this study was Jute at a

volume fraction of 50%. Uniform size fibers dispersed with random orientations give significant gains in stiffness and strength over the unfilled polymer. The addition of MAPP acting as a binder further increases the mechanical properties. Further analysis on the injection molding of short fiber composites was performed by Gupta and Wang [26]. This study concentrated on the effects that plastic injection molding had on the orientations of the dispersed fibers. It was found that both the injection location and distance from the boundary layer of the mold had significant effect on the fiber orientation as the fibers align themselves with the flow of the molten resin. This preferential material orientation must be taken into account in the design of molds utilizing this process.

Pourboghra et.al. patented a composite hydroforming process which demonstrated the ability to form composite materials using pressurized fluid [27]. This process uses pressurized and heated hydraulic fluid to form thermoplastic composites against a hard punch of desired geometry. The composite blank can be physically clamped using a blank holder mechanism or hydrostatic fluid pressure can be used to apply a more uniform clamping force. The main advantage this process presents over other forming techniques is that fluid pressure acts over the entire composite surface, reducing out of plane material warping. Since pressure is used as a “soft die”, part thickness remains uniform, unlike in match die forming. Resin squeeze out is also reduced due to uniform force being applied over the surface of the blank. Composite Hydroforming has been shown to work with a variety of material types.

Zampaloni showed the ability of this technique to form kenaf reinforced polypropylene natural composites [8], randomly oriented glass fiber composites [28], and woven glass fiber composites [3]. Since pressurized fluid is used to heat and cool the composite blank directly, process time can be drastically reduced making composite hydroforming an ideal manufacturing method for the automotive and aerospace industries.

Numerical Methods for Simulating the Forming of Composites

Simulating the forming of composite structures is an important and often necessary practice in order to determine optimal processing conditions and produce the highest quality parts. Through numerical modeling, a plethora of boundary conditions can be applied and their effects on the composite blank evaluated. Additionally, the modification of the laminate stacking sequence can also be varied, allowing the engineer to investigate how these changes will affect the formed part. In order to achieve the accurate simulation results, the composite laminate must be accurately modeled. This however is no easy task as composite materials are inherently anisotropic. Other considerations such as inter-laminar ply shearing, delamination and updates to the fiber orientations compound the complexity of the material models that are used.

The most classic way in which laminated composite materials can be characterized is with the ABD matrix [29]. The ABD matrix relies on a plane stress assumption allowing the 9x9 anisotropic material stiffness matrix to be reduced to a 3x3 matrix which characterizes that material's orientation dependent tensile stiffness qualities as well as shear stiffness. This matrix is extended to 6x6 in order to take into account the effects of bending stiffness and coupling that may exist between bending and in plane extension.

This model is able to make good predictions for composite structures after having been formed but it is not able to characterize the forming of composite materials with sufficient accuracy. Perhaps most importantly, the model is not able to take into account changes in fiber orientation. Strains produced by the forming operations change the orientation of the fibrous reinforcements which in turn change the properties of the material. Also, the ABD matrix assumes perfect bonding and load transfer between the layers of the laminate.

Several material models have been developed which take into account changes in fiber orientations. Yu et. al developed a material model which exclusively deals with plain weave composite fabrics [30]. This material model directly takes into account the structure of the fabric. Warp and weft

yarns are characterized by the number of fibers per tow and the apparent material properties of an individual fiber. A unit cell is built based on the constituents of the structure and fabric. Numerical simulations show that this model is able to accurately predict changes in the angle between the warp and weft fiber as the fabric is elongated when loaded 45° offset from the warp and weft orientation. Good results were also obtained when forming a hemisphere by a match die molding.

This material model was improved upon by including additional parameters that took into account the more complex phenomena when a woven fabric deforms. A significant improvement was made when taking into account the undulation geometry between the warp and weft yarns [31]. This study characterized the change in shear stress due to warp and weft yarn geometric considerations. The model predicts that shear stress increases in a non-linear fashion as shear angle increases. This is due to shear locking that occurs as the fibers interact with one another. This non-linear response in shear allowed for accurate predictions in wrinkling severity and location when simulating the deformation of a fabric as it experienced hydroforming type boundary conditions. An additional study took into account the asymmetric bending stiffness of the reinforcing fibers [32]. The asymmetric bending stiffness assumes that the reinforcing fibers do not possess the same stiffness in tension as they do in compression. This difference leads to a shift in the neutral axis of the fibers when equilibrating stresses during bending. This property is incorporated into the material model and shows good results when predicting the shape and fiber shear when a fabric is draped over complex geometry.

Boisse et al. developed a similar material model that takes into account geometric factors such as undulation geometry and shear locking [33]. This material model takes into account non-linear uniaxial loading results. As the fibers yarns are loaded they first need to straighten themselves due to the undulation inherent in biaxial weaving. As the fibers straighten out, the slope of the load increases and the fibers are directly strained leading to increased stiffness. This leads to an overall non-linear response. The behavior is evaluated biaxially to establish a weave geometry dependent Poisson's ratio. This model has been shown to accurately predict fiber shearing.

Another material model was developed during the PhD study of Mike Zampaloni [3]. A continuum model was developed that focused on tracking orientations of fiber features. These orientations of interest or preferred fiber orientations (PFO) refer to a particular orientation at which a composite sheet material is stiffest. Once determined, the orientations are characterized by obtaining the axial and transverse Young's modulus, Poisson's ratio and shear modulus. The model takes into account these PFOs and their related material properties along their initial orientations. During FEM simulations, a unique deformation gradient tensor acts upon each element which not only deforms the element but also changes the orientation of the PFO's. At the end of each step the stiffness of the PFOs are updated and used to calculate the material stiffness which changes as the PFOs change. This material model is used in this study and will be further described in the numerical methods section. The model has been used to determine the best forming conditions during the hydroforming process and has provided excellent predictions of the final formed shape using methods developed by Abedrabbo et al. [34].

The aforementioned models all possess a common flaw; they either assume perfect lamination between the composite layers or only model a single layer. The assumption of perfect bonding is insufficient due to the finite strength of the inter-laminar adhesive. During forming, and especially when deep drawing, the assumption of perfect bonding between layers can lead to complex out of plane warping that does not manifest itself in experiments. Typically this behavior follows a traction-separation response and can be incorporated into FEM models through cohesive elements. Harper et al. demonstrates how this behavior is implemented in the study of the mechanical response of panels delaminating [35]. Specialized cohesive zone elements are implemented at the predicted crack boundary, in this case the thin adhesive film between two laminated composite strips. These elements are given special fracture mechanics material properties. In its simplest form, fracture mechanics can be characterized by a bi-linear traction separation curve. An initial elastic stiffness gives the slope for the undamaged elongation on the adhesive until the damage initiation point is met. Displacements beyond this point undergo linear softening until failure.

Consolidation of Flat Panels and Material Characterization

The materials in this study are selected to exhibit the capabilities of the thermo-hydroforming process. Materials are laid up to their desired thickness or areal density and consolidated into flat plates. This allows the forming process to occur without having to consolidate simultaneously. Consolidation of the sheets prior to the final forming step allows for a reduction in processing time due to the extended heating, pressing and cooling time required to reduce void fraction and increase inter-laminar bond strength. Theoretically, a loose ply stack could be loaded into the press, formed and consolidated all in one step but increases to the cycle time would be expected. A far higher throughput can be achieved by using pre-consolidated laminates to avoid a bottleneck occurring at the final forming stage.

The laminates are consolidated and formed using a large heated platen press capable of housing circular blanks up to 36" in diameter. This press is used to consolidate both the spectra shield and carbon fiber blanks investigated during this study. Heating and cooling rate is not able to be precisely controlled with this press; both occur at a very slow pace. Also, the press makes use of four independently controlled heating elements which cool at drastically different rates, possibly leading to residual stresses and warping post cooling. If these flaws exist they are miniscule and have been ignored.

SR-3136

Blank Consolidation and Shape

Since Spectra Shield comes as a prepreg, a recommended consolidation procedure is provided by Honeywell [12]. The procedure for consolidating the flat sheets is based off the recommendations of this document. Other researchers claim that temperatures of up to 300°F can be used to sinter the fibers in UHMWPE composites that do not contain a matrix constituent [13]. The consolidation technique in this study required that a small portion of the highly crystalline fibers be melted and fused to its neighboring fibers requiring a higher processing temperature. Temperatures this high become dangerous due to the

onset of excessive fiber melting which ruins the highly crystalline structure of the polymer chains, greatly reducing their stiffness and strength. SR-3136 contains a sparse matrix constituent of low density polyethylene (LDPE) which melts at a lower temperature than the UHMWPE fiber, allowing the composite to be consolidated without the risk of damaging the load carrying fibers.

Taking into account the recommendations from Honeywell, the following procedure for consolidation of UHMWPE sheets was utilized:

1. The SR-3136 is cut to the desired shape and stacked to the desired thickness or areal density.
2. The ply stack is loaded into the heated platen press. Teflon release film is used as a barrier between the heated platens and the SR-3136 to prevent the composite from sticking to the press after cooling.
3. The press is closed such that the upper and lower platens make contact with the composite in order to ensure effective heat transfer. The temperature of the platens is set to the desired forming temperature of 250°F.
4. Once the platens reach 250°F an additional ten minute waiting period is utilized to allow the thermal gradient within the core of the composite to dissipate, ensuring the composite is evenly heated
5. After waiting 10 minutes, a pressure of 500 psi is applied to the composite (this pressure refers to the force exerted over the surface area of the blank, not hydraulic pressure). This pressure and temperature is held for 10 minutes.
6. After 10 minutes under heat and pressure, the heater elements are disabled and cooling measures are employed. The holding pressure is maintained throughout cooling.
7. Once the temperatures of all zones are below 150°F, pressure is released, the platens are opened and the composite can be removed.

Blank shape is determined through the use of an Abaqus/CAE add-on called Composite Modeler for Abaqus (CMA). This add-on is used primarily to construct models for complex composite

components that have irregular geometry or strange stacking sequences. The most useful tool in this add-on generates a flat pattern. The flat pattern represents the shape of the composite before it is draped over and formed to the punch. The flat pattern is generated for the desired final shape and includes the extra material that will be trimmed off after the parts have been formed. It is important to include this extra material because the material acts as a barrier which contains the pressurized forming fluid in the thermo-hydroforming process.

In order to generate the flat pattern, the shape of the formed part plus the excess material must be modeled as a sheet. This sheet model is then loaded in CMA and meshed. Once meshed, the composite type (unidirectional, bidirectional, woven, etc.), maximum shear angle and region are assigned. The flat pattern is then generated and shear angles are plotted over the surface of the formed part. This process is highlighted in Figure 2.

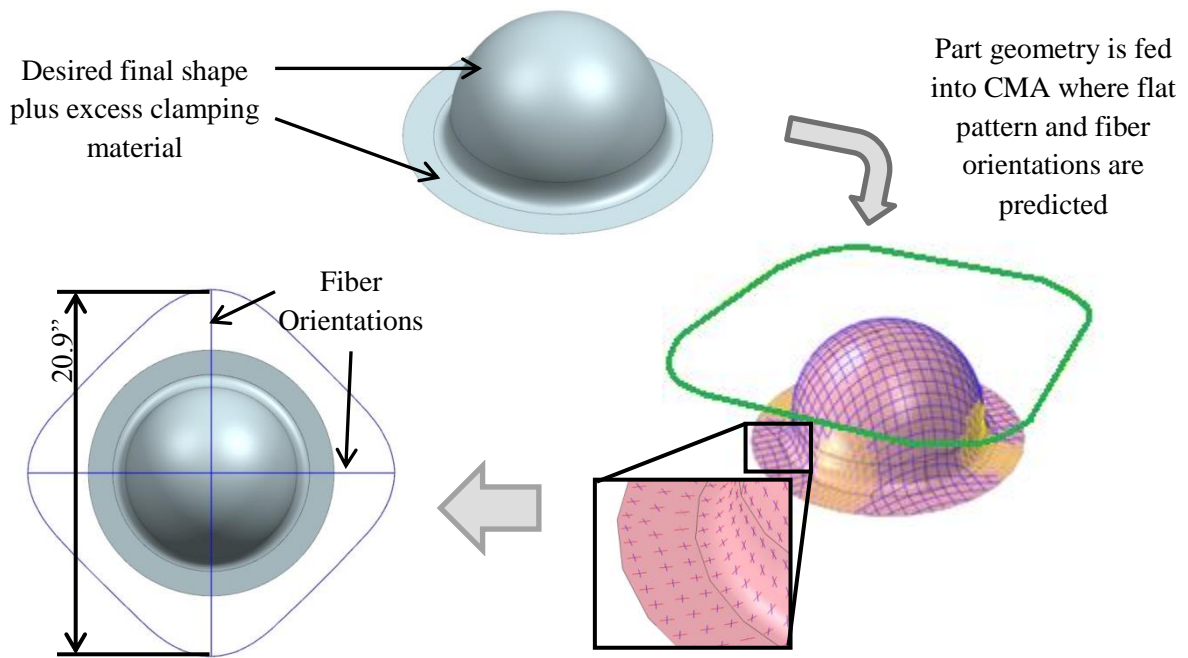


Figure 2 – CMA Blank Shape Prediction Capabilities

Flat pattern prediction is computed by calculating the Gaussian curvature over the entire surface and unfolding it onto a flat plane. This prediction only takes into account one layer and does not take into account stretching of the material but it provides a quick prediction for ply shape.

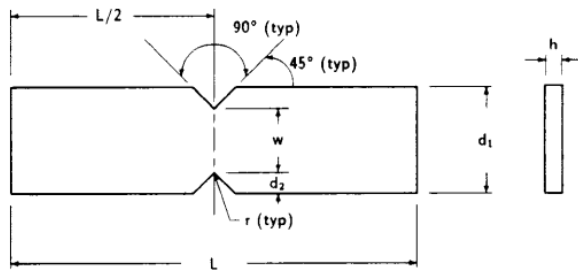
Material Characterization

Material characterizations for spectra shield SR-3136 and the CF-PP are aimed at populating the PFO material model with the appropriate parameters. The fiber properties for this model are linear elastic so the material parameters required are the Young's Modulus (E), Poisson's ratio (ν), and the shear modulus (G). It is preferred to characterize the traction separation response as well but machining the double notch shear specimen required to obtain these properties has presented many challenges.

Machining SR-3136 has led to many issues. Unlike epoxy reinforced composites, these materials are very difficult to machine. Standard mills and drill bits do not pull chips away from the material very well and typically lead to the edges of specimen being frayed. Delamination and back face deformation are other common flaws that occur during the machining of Spectra Shield. Water jetting has recently been attempted and has shown very good results with minimal delamination. This method alone should be used in the future to prepare test specimens.

Shear Modulus

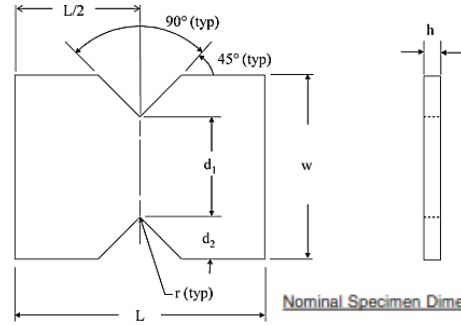
Perhaps the simplest specimens to prepare are the ones used to determine the shear modulus. Two standards were selected and utilized for the evaluation of the shear modulus; the v-notch rail shear test [19] and the Iosipescu shear test [18]. The specimens for these two tests are similar in that they are rectangular in shape and feature aligned notches to localize shear stress at a predictable and easily measurable cross section. See Figure 3 for the recommended geometry of the different shear specimens.



Nominal Specimen Dimensions

- $d_1 = 19 \text{ mm [0.75 in.]}$
- $d_2 = 3.8 \text{ mm [0.15 in.]}$
- $h = \text{as required}$
- $L = 76 \text{ mm [3.0 in.]}$
- $r = 1.3 \text{ mm [0.05 in.]}$
- $w = 11.4 \text{ mm [0.45 in.]}$

Iosipescu Specimen



Nominal Specimen Dimensions

- $d_1 = 31.0 \text{ mm [1.20 in.]}$
- $d_2 = 12.7 \text{ mm [0.50 in.]}$
- $h = \text{as required}$
- $L = 76.0 \text{ mm [3.0 in.]}$
- $r = 1.3 \text{ mm [0.05 in.]}$
- $w = 56.0 \text{ mm [2.20 in.]}$

Rail Shear Specimen

Figure 3 – Shear Modulus Test Specimens

The Iosipescu specimen is loaded by a special fixture that applies compressive forces that initiate shearing in the gauge section of the specimen. Force is applied on the edges of the specimen. The V-notch rail shear specimen is loaded on the faces of the gripping tabs which initiate shearing in the notched gauge section. The fixtures used to load these two specimens can be seen in Figure 4. Difficulties with the V-notch rail shear specimen were observed during initial tests. The fixture itself is very heavy and cumbersome resulting in the damage of specimens during mounting. For this reason the Iosipescu shear results will be reported and used.

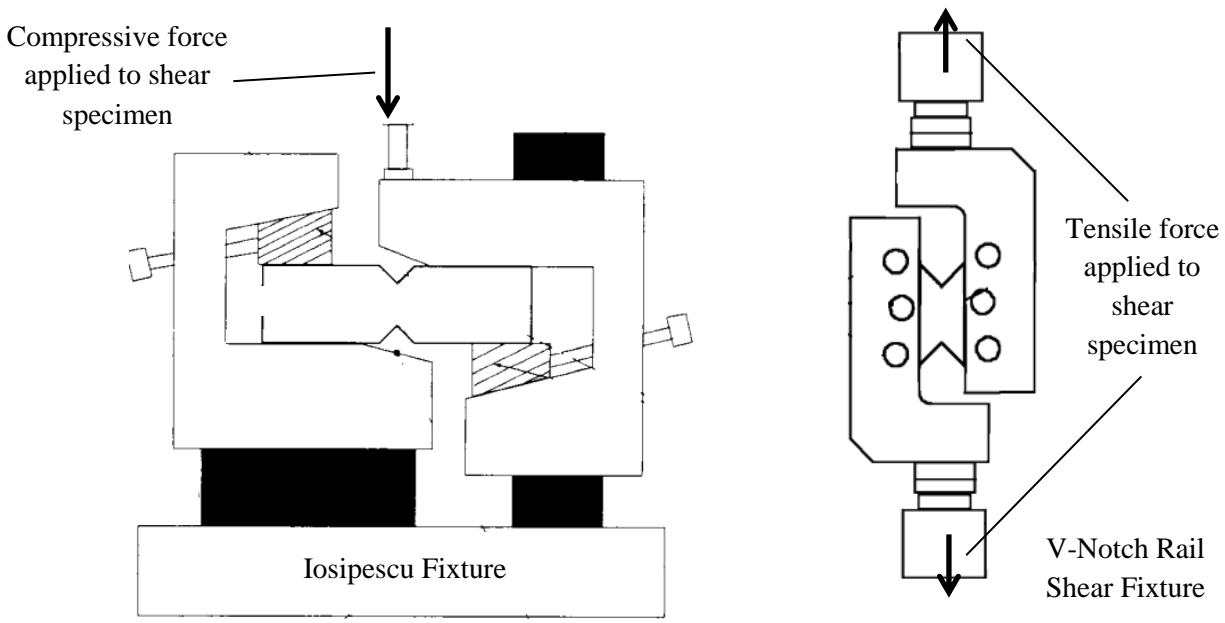


Figure 4 – Shear Fixtures

The Iosipescu specimens are evaluated using a uniaxial tensile testing machine. A load cell is used to measure the amount of force required to deform the specimen. The force is then normalized by the area to calculate the shear stress. Strain is obtained by a strain gauge mounted to the specimen in the direct vicinity of the gauge section. Strain is measured in the $+45^\circ$ and -45° directions. The absolute values of these strains are summed in order to obtain the shear strain. The shear modulus (G) is then calculated by taking the change in shear stress over the change in shear strain over a preselected chord. These methods are given in more detail in the ASTM recommendations ([19], [18]). Four specimens are prepared and tested to obtain the shear modulus. Figure 5 shows the obtained stress-strain curves.

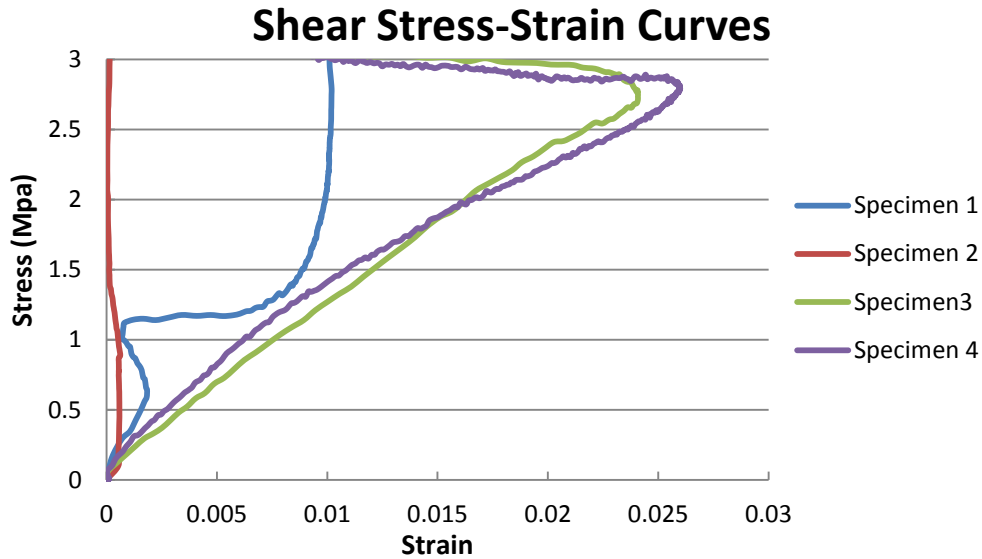


Figure 5 – Shear Stress Strain Curves

Specimen 1 and specimen 2 clearly give irregular results. The reason for these issues is difficulty in bonding the strain gauge to the specimen. The trends for these specimens indicate a high stress for a relatively low strain which is readily explained by ineffective strain gauge adhesion. Specimens 3 and 4 indicate the expected linear trend up to a point where once again, a decrease in strain is observed due again to failure of strain gauge adhesive. The chord is selected a safe distance away from this adhesive failure in order to obtain the most accurate data. The shear modulus values and their average can be seen in Table 1.

| Specimen | Cross-Section Area (mm ²) | $\Delta\tau$ (MPa) | $\Delta\varepsilon$ | Shear Modulus (MPa) |
|----------|---------------------------------------|--------------------|---------------------|---------------------|
| 3 | 38.76 | 0.50567 | 0.004337 | 116.59 |
| 4 | 39.56 | 0.55361 | 0.004066 | 136.16 |
| Average | | | | 126.37 |

Table 1 – Shear Modulus

Ideally, at least three successful test specimens are preferred but difficulty in obtaining good results prevented additional tests. Also, room temperature tests do not provide the necessary data to

characterize the composite as it is formed at elevated temperatures. Since the material model relies on a linear elastic-transversely isotropic assumption, no temperature dependent terms are used in the calculation of the materials stiffness. The most appropriate way to characterize the material would be at the temperature at which it is formed.

Young's Modulus

SR-3136 is difficult to fit empirical relations to due to poor fiber-matrix adhesion and void ridden matrix constituent. This makes using empirical relations to estimate the Young's modulus wildly inaccurate. Unfortunately, these issues also make material characterization difficult.

Characterization via ASTM standard D3039 was attempted first [16]. This standard recommends the use of a rectangular specimen that is gripped directly by the jaws of the machine. The first few attempts resulted in the gripped plies shearing away from the bulk of the laminate. This damages the material resulting in low force measurements. Emery cloth was utilized at the gripping interface per the recommendation of the standard. This resulted in the gripped plies shearing away from the bulk as well as the gripped layer being torn at the gripping boundary. Examples of this issue can be seen in Figure 6.

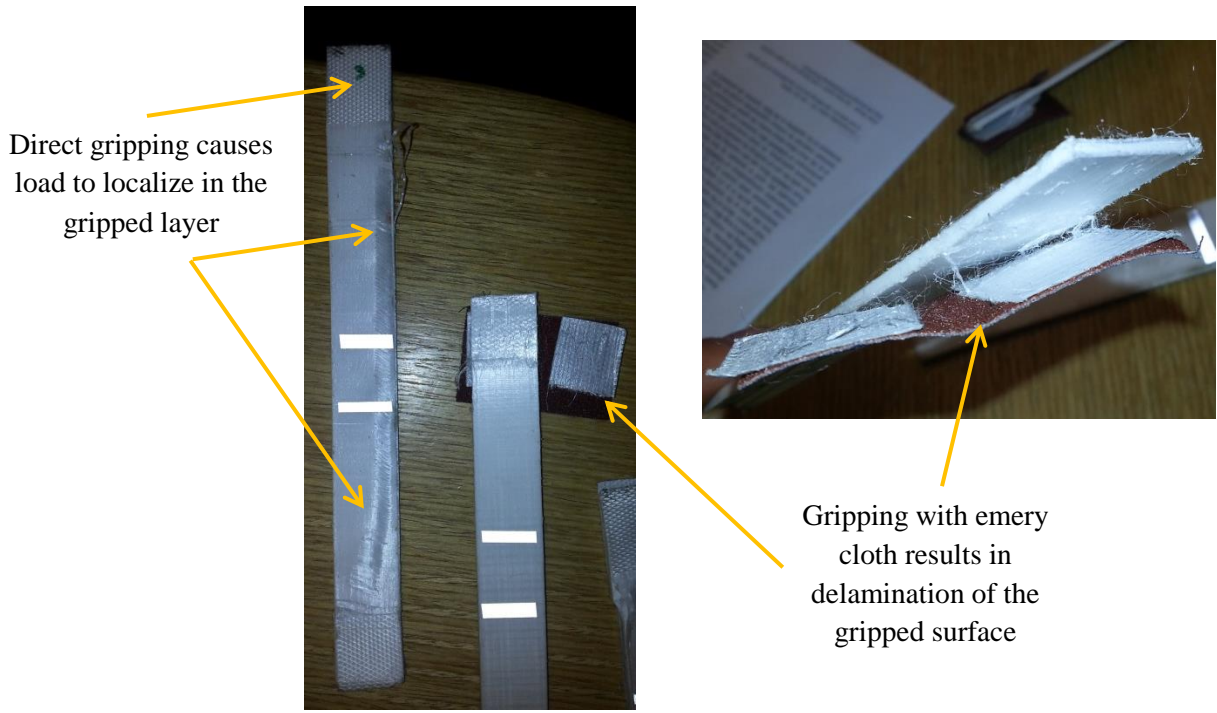


Figure 6 – Difficulties with Tensile Specimens

It was determined that this delamination was due to the low quality bond created by the void ridden LDPE matrix constituent. Based on this assumption, specimens were machined with a larger gripping face based on the geometry of the specimens in ASTM D638 [36]. These specimens showed better results but still seemed to be localizing most of the load on the gripped layers.

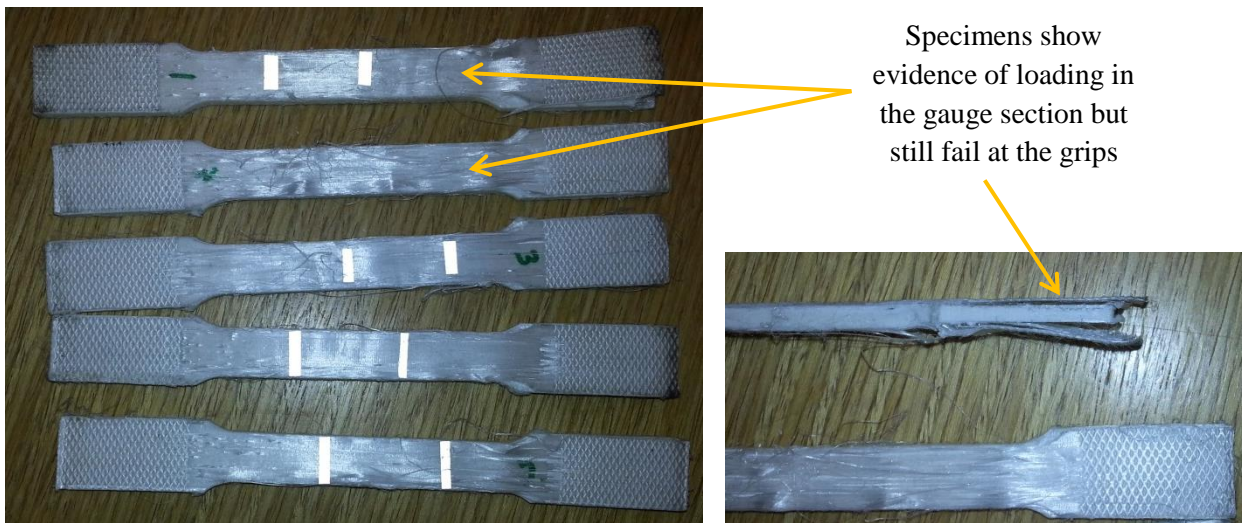


Figure 7 – Dog Bone Specimens

Data were analyzed from this round of tests regardless of the failure mode. Force was measured by a load cell and normalized by the cross sectional area of the specimen in order to calculate stress. Axial strain was directly measured using a laser extensometer. The calculated stress strain curves for the dog bone specimens can be seen in Figure 8.

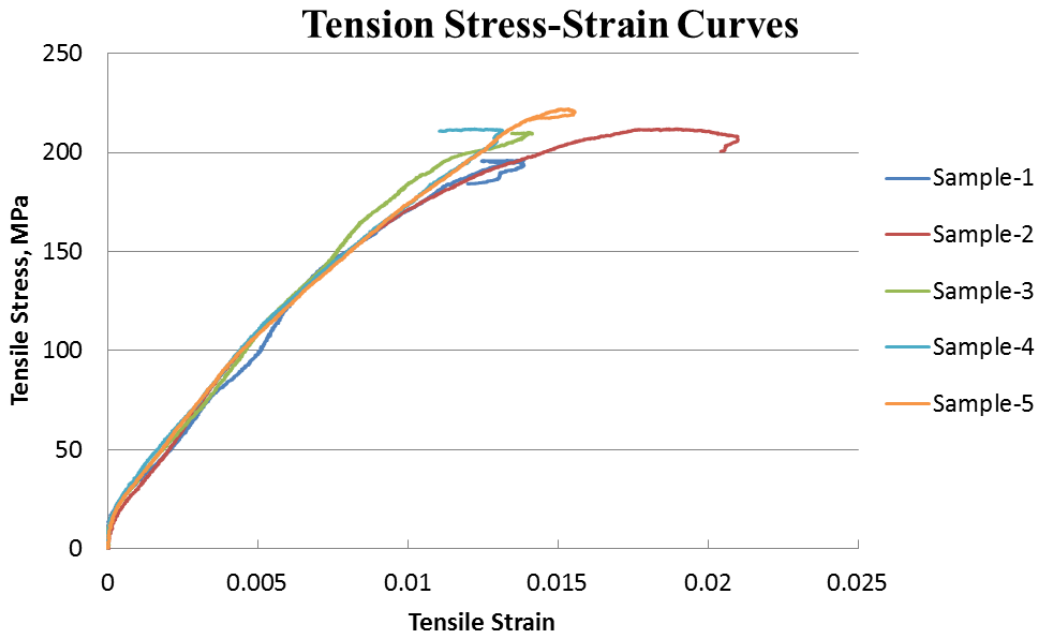


Figure 8 – Tensile Test Results

The stress strain curves exhibit a relatively tight grouping in the linear elastic region of loading (below 1% strain). When examining the failure region of the specimens, it was clear that two main modes of failure occurred. Sample 2 seemed to exhibit delamination of the outer layers, resulting in little to no additional load for increasing strain. The remaining specimens looked as though they experienced a decrease in strain. This can be attributed to the gripped layers ripping as was seen with the previous specimens. Since these failures were within the grip area, concern was raised as to the validity of the results.

The stiffness for each of these specimens was calculated by extracting the change in stress and strain for a small chord between 0% and 0.5% strain. This data can be seen in Table 2.

| Specimen | Cross-Section Area (mm ²) | $\Delta\tau$ (MPa) | $\Delta\varepsilon$ | Modulus (GPa) |
|----------|---------------------------------------|--------------------|---------------------|---------------|
| 1 | 45.085 | 65.847 | 0.004 | 16.408 |
| 2 | | 75.810 | 0.004 | 20.326 |
| 3 | | 71.653 | 0.004 | 17.943 |
| 4 | | 73.519 | 0.004 | 18.366 |
| 5 | | 79.137 | 0.004 | 19.976 |
| Average | | | | 18.604 |
| STD | | | | 1.302 |
| CV | | | | 0.070 |

Table 2 – Tensile Test Data

The stiffness results are fairly similar to one another with the exception of specimen 1 which seems to experience slipping through the grips at relatively low strains (see Figure 8). The standard deviation is 1.3 GPa which indicates a relatively tight grouping. This indicates that the loading is repeatable and uniformly distributed at least at low strains. However the gripping interface is also experiencing loading hence the failure occurring in this region for all specimens. Undoubtedly the effect of inter-laminar stresses is affecting the stress-strain response leading to decreased accuracy. Additionally, the ultimate stress is ~33% of the ultimate stress obtained during the characterization of a similar UHMWPE composite (Dyneema) by Russell et al. [17].

An additional tensile specimen was fabricated to ensure that the response being obtained during the characterization is purely a function of the material and not of the gripping scheme. The gauge section was very small when compared to the gripping area in order to ensure that the stress is localized through the gauge section and not through the bond line of the gripped layer. The specimen geometry was used based upon the recommendation from the Russell study mentioned above. The geometry of the specimen can be seen in Figure 9.

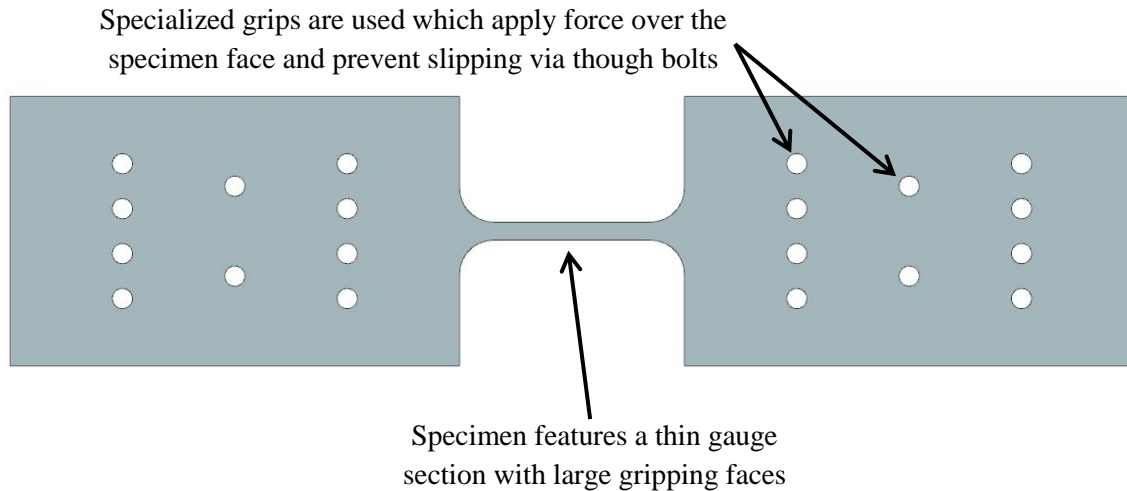


Figure 9 – Tensile Specimen from Russell Study

Results from initial tests have shown an increase in the ultimate stress to ~410 MPa. This indicates that the results seen in Figure 8 are experiencing reductions in load carrying capacity due to failure initiating at the gripped area. Unfortunately, further difficulties with strain gauge mounting prevented strain measurements. The specimen in Figure 9 is currently being redesigned to allow easier mounting of the strain gauge, in order to determine the stiffness more accurately.

Polypropylene Reinforced Carbon Fiber

An additional material was also selected to show the versatility of the hydroforming process. A consolidation technique was devised for this material for characterization and forming of the material. The carbon fiber used in this study is a 5x5 6k satin woven fiber using HTS40 E-13 carbon fibers from Toho Tenax. The matrix constituent is block copolymer polypropylene film from Bloomer Plastic Incorporated. Film of thickness 0.008” is used to target a fiber volume fraction of 50% in the final composite. The process used to consolidate the composite is referred to as resin film infusion (RFI) and will be described below.

Blank Consolidation

The consolidation technique of the carbon fiber-polypropylene composite (CF-PP) differs from SR-3136 due to the lack of concern regarding fiber degradation at elevated temperatures. The

consolidation temperature exceeds the melting temperature of the matrix, allowing intimate fiber-matrix contact and the elimination of voids. Ensuring these two criteria lead to a composite with predictable mechanical properties. The main difficulty in consolidation above the matrix melting point is preventing matrix squeeze out. This occurs as the platens exert force on the composite during consolidation and the molten composite is forced out of the woven CF fabric. The best way to prevent this is to fabricate a special mold which will allow high pressure to be exerted on the composite but prevent the liquid matrix from escaping. Such a device was fabricated and can be seen in Figure 10.

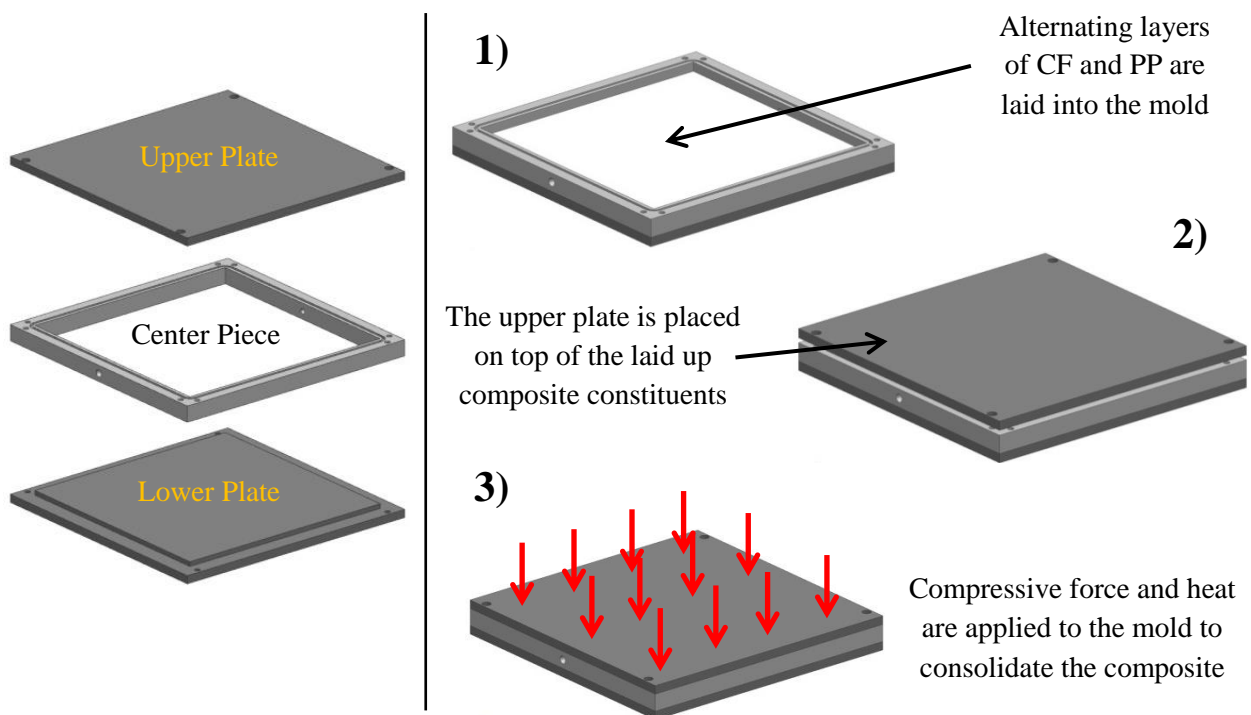


Figure 10 – CF-PP Consolidation Mold

This device consists of three components; a lower plate, center piece and upper plate. The composite is laid up within the cavity created by the lower plate and the center piece. The upper piece is then placed on top of the composite. As heat and pressure are applied to the stencil, the matrix melts but is prevented from escaping from the stencil. This device has been shown to significantly reduce matrix squeeze out and produce high quality consolidated plates with excellent surface finish.

The following procedure is used to consolidate the CF-PP:

1. Composite is laid up inside of the cavity created as the lower plate and center piece are attached. Care must be taken to ensure that the right amount of material is utilized as to avoid over packing or under packing the cavity.
2. The top plate is placed on the stencil, allowing the compression of the composite constituents.
3. The stencil is placed in the heated platen press and the press is closed in order to initiate contact between the heated platens and the stencil but also to ensure that very little pressure is applied.
4. The heating elements of the heated platen press are activated and the platens are raised to the desired consolidation temperature.
5. Once the platens reach the desired temperature, an additional heating period is utilized in order to ensure that the composite within the stencil has reached the specified temperature.
6. Once heating is complete, the desired consolidation pressure is applied via the heated platens. This pressure is applied for an extended period of time to allow the molten polymer to fill the gaps in between the woven fabric structure and to “wet out” the fiber tows.
7. A second stage of higher pressure can be applied if desired.
8. Once pressure and heat have been applied for a sufficient time period as to eliminate voids, the heating elements are deactivated and cooling measures can be implemented (active platen cooling, forced convection via fan, etc.)
9. The stencil is held under pressure during the cooling phase. Cooling continues until the composite within the stencil reaches a temperature sufficiently lower than the melting temperature of the polymer.
10. Release pressure from stencil and remove from the press. Allow additional cooling time once the stencil is removed from the press if necessary.
11. Disassemble the stencil and recover the consolidated laminate.

The above procedure is very general and can be used with any thermoplastic matrix constituent. It is very important to ensure that the cavity of the consolidation mold is not grossly over packed or under packed. Over packing involves putting more material in the cavity than can be housed in its fully closed

position. This will undoubtedly lead to matrix squeeze-out. Under packing the mold involves placing too little material in the cavity. Under packing can lead to excess void content in the consolidated composite and poor mechanical properties. It is preferable to slightly over pack the stencil (less than 5% over the volume capacity of the cavity) in order to generate pressure within the matrix. This matrix pressure forces the polymer to fill any voids in the fabric structure leading to a lower void fraction. It is not always possible to slightly over pack the cavity because the number of layers used in both the RFI and prepreg CF must be an integer. The best way to ensure that the cavity is sufficiently packed is to layup the composite constituents so that the total volume of constituents is within $\pm 5\%$ of the closed cavity volume.

The consolidation mold features through-passes on the centerpiece which allow thermocouples to be imbedded within the composite during trial consolidations. These sensors allow the actual temperature at the core of the composite to be taken in order to establish the additional heating and cooling times mentioned in the procedure above. Once these times are determined, composites without thermocouples can be consolidated while still giving confidence that the composite has reached the desired consolidation temperature.

Pressure is applied in two stages per the recommendation of Zampaloni [8]. The consolidation baseline conditions and other experimental conditions can be seen in Table 3.

| Specimen | PP plys | CF plys | Temp (f) | P1 (psi) | Time at P1 | P2 (psi) | Time at P2 |
|----------|---------|---------|----------|----------|------------|----------|------------|
| RFI-1 | 6 | 5 | 335 | 150 | 20 minutes | 350 | 5 minutes |
| RFI-2 | 6 | 5 | 375 | 150 | 20 minutes | 350 | 5 minutes |

Table 3 – Consolidation Conditions

Consolidation Properties Tool

A tool was developed to determine the appropriate number of layers of woven carbon fiber and polypropylene film in the layup of the RFI composite. The main goal of the tool is to determine the number of alternating layers of PP and CF that will fit into the cavity of the stencil when it is fully closed.

The tool operates on the assumptions that the final composite will have no voids once consolidated. The volume of the mold when it is fully closed is easily computed since it is perfectly rectangular. Calculating the volume of the film is also easy as it has constant thickness and is cut to fit tightly in the 10.5”x10.5” cavity. Calculating the volume of the woven carbon fiber is not necessarily as trivial. The areal density is used to compute the mass of each ply. This quantity is commonly used in the composite industry and is given as

$$\rho_{areal} = \frac{mass}{area} \quad (1)$$

The mass is then multiplied by the number of CF plies used, then the volumetric density is applied to calculate the total volume of CF to be used in the composite. Knowing the volume of both constituents is necessary in obtaining the volume fraction. Several other useful parameters are calculated using this tool as well. An example of the output can be seen in Table 4.

| RFI specimen | | |
|-----------------|-------------|-----------------|
| area of pp ply | 110.25 | in ² |
| | 0.071129032 | m ² |
| area of cf ply | 110.25 | in ² |
| | 0.071129032 | m ² |
| n carbon plies | 5 | plys |
| n polymer plies | 6 | plys |
| mass carbon | 0.134647258 | kg |
| mass carbon ply | 0.026929452 | kg |
| Vol. carbon | 7.65041E-05 | m ³ |
| | 4.668564706 | in ³ |
| Vol. polymer | 5.292 | in ³ |
| | 8.67204E-05 | m ³ |
| Vol. total | 0.000163225 | m ³ |
| | 9.96 | in ³ |
| V.f. | 0.469 | |
| Vol. mold | 10.3359375 | in ³ |
| | 0.000169376 | m ³ |
| Vol. voids | 0.38 | in ³ |
| specimen t | 0.09375 | in |

Table 4 – CF-PP Layup Tool

The tool allows the user to manually input the number of CF and PP plies as well as the area of the plies. Using this information, the tool also outputs the specimen's volume fraction, void volume, thickness, and other useful quantities.

Future Recommendations

Material characterizations are nearly complete for the SR-3136 samples. The specimen from the Russell study shows better results than the previously used specimens but the thin gauge section leads to difficulties mounting strain gauges. A similar specimen with a slightly thicker gauge section is being designed in order to mitigate this issue. Measuring the out of plane shear modulus is also desired but very difficult to achieve due to the thick laminate needed for the specimen. Machining a specimen of this thickness was not possible, but the recent discovery of excellent results via water jetting may make characterizing this property a possibly in the future. Additionally traction separation properties need to be determined. A double notch shear beam specimen can be used to determine these properties and was devised by Liu et al. [21].

Mechanical properties during this study have all been measured at room temperature. In order to obtain the most realistic forming response, the material must be elevated to its forming temperature when the properties are being measured. Additionally, the CF-PP material properties need to be obtained. This phase was abandoned to pursue other endeavors within the study. Characterization of this material will likely be much easier due to the increase in bond strength between the fiber and matrix constituents, allowing the easier machining of specimens and fewer issues with gripping.

Experimental Methods

The main focus of this project was to show that scaling up the thermo-hydroforming manufacturing process produces good results and can be used to make functional pieces. The punch used in this study was designed for forming Advanced Combat Helmets (ACH). The helmet punch was obtained through a partnership with BAE systems and is the first functional piece to be made with the composite hydroforming process. The geometry of the helmet requires deep drawing of the composite blank and present many difficulties.

In the past, methods used to form deep drawn parts using composite materials typically rely on hand layup techniques coupled with matched die tooling. This process has difficulty forming the parts without excessive wrinkling. One method used to mitigate the wrinkling issue is darting or cutting away blank material in high shear regions [37]. This method has been shown to significantly reduce wrinkling in deep drawn parts but also has many drawbacks. By darting the blank, continuous fibers are cut which reduces the overall strength of the composite. Complex darting also requires extended blank preparation time, increasing the part cycle time and decreasing manufacturing efficiency. Ideally simple blank shapes should be used with minimal trimming required before and after the part is formed.

Thermo hydroforming has shown the ability to reduce wrinkling in deep drawn parts and allows significant draw depths to be obtained [28]. The promise of high quality formed parts coupled with significantly reduced cycle times has attracted the attention of industry and prompted the acquisition of the 300 ton press, which is capable of forming full scale parts. Many modifications were made to the press to bring it to full operational capacity. This chapter will explain the modifications made to the press as well as the process used to form composite parts. The formed parts will be discussed as well in addition to future recommendations which will both increase quality and decrease process time.

Experimental Setup

The 300 ton thermo hydroforming press was delivered to MSU in the summer of 2011 in a partially completed state. Almost every aspect of the press was either only partially operational or not operational at all. The die set was too small to accommodate the blank of sufficient size to form the ACH and seal housings were designed in such a way that the seals were impossible to install. A single punch was delivered but was quickly broken due to a poor ram attachment mechanism. The pressure producing skid (PPS) was only able to operate in one of the three fluid zones designed into the tooling due to a lack of pressure regulation hardware. The high pressure pumps used in the PPS were also in danger of becoming damaged due to a lack of filtration and adequate heat removal from the fluid reservoir.

These issues and several others were discovered shortly after delivery of the press. This resulted in several key systems having to be either modified or completely replaced. This chapter will not only describe the modifications made to the press but also explain their functions in order to give the reader a better understanding of the operational capabilities of the 300 ton thermo-hydroforming (THF) press.

High Pressure System (HPS)

The high pressure system consists of the hydraulics and hardware that actuate the dies and punch of the press. This system was not heavily modified but contains several design flaws that limit the operational capacity of the press significantly. These flaws should be taken into account during the design of future THF presses. The main features of the HPS are a pressure producing and regulating system, the hydraulic rams that actuate the punch and clamp independently, and the mounting plate for the dies and hydraulic rams. The main components of this system can be seen in Figure 11.

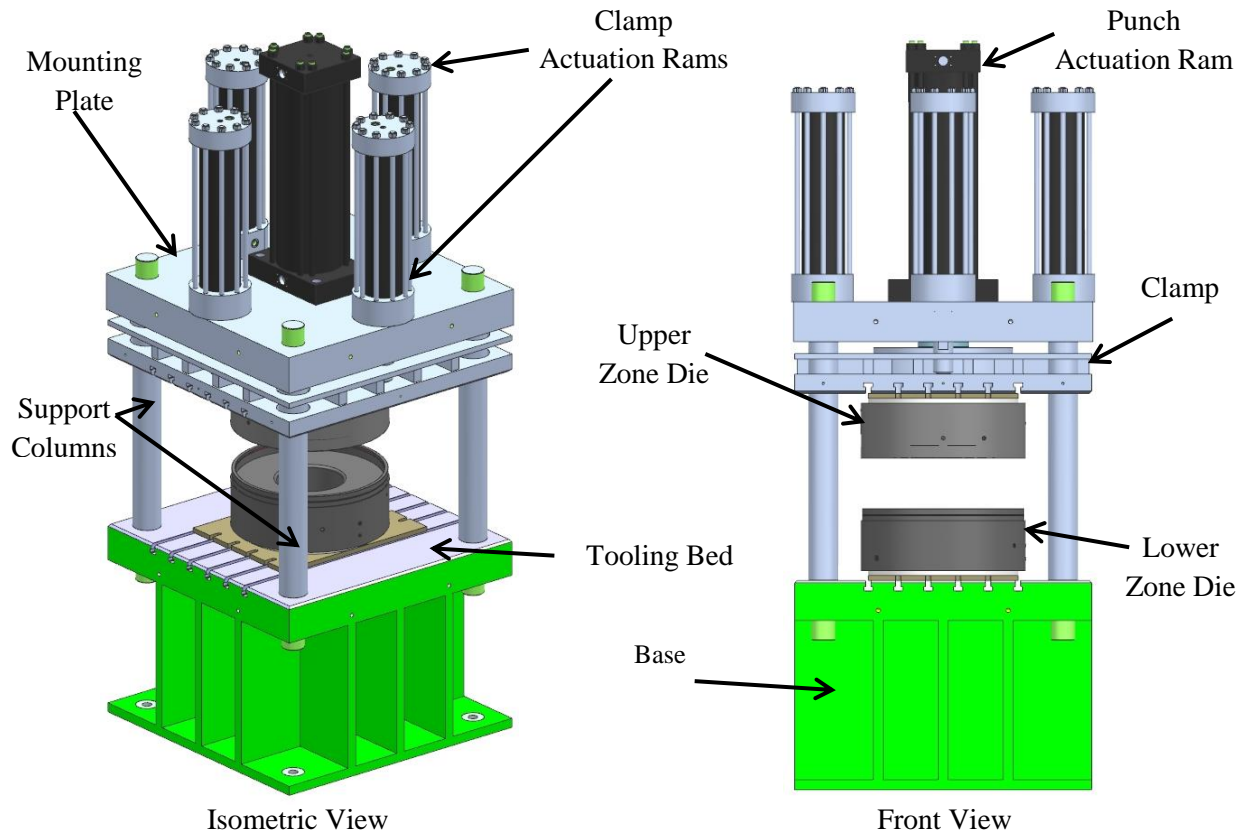


Figure 11 – HPS Components

Not pictured in Figure 11 is the pump and pressure regulators that control the rams. The pressurized fluid from these unseen devices is controlled and provided to the five rams seen mounted to the top of the mounting plate. The four outer rams actuate the clamp which houses the upper zone die. These rams can apply up to 135 tons of holding force to the composite blank as it is being formed. Even if the blank is not being actively clamped, the fluid pressure generated within the closed dies attempts to open the dies in order to alleviate the pressure within them. The rams apply a reaction force which holds the dies together under the high pressure forming conditions. A single ram in the center of mounting plate actuates the punch. This ram is actuated independently of the clamping rams making the press double acting.

The base is simply a heavy steel weldment with t-slots milled on the surface, allowing the lower zone die to be firmly attached to its surface. The support columns constrain the movement of the clamp and support the mounting plate to which the rams are attached.

The clamping rams are currently operating at 1300 psi, well short of the standard 3000 psi that most hydraulic equipment is designed for. By increasing the hydraulic pressure in the clamping rams, clamping force can be increased 230%. The lack of documentation and knowledge on these rams makes increasing their operating pressure risky as bursting a ram can lead to serious physical injury and extensive damage to the press. The problem is further explained in the Results and Discussion section of this chapter.

Pressure Producing Skid (PPS)

The primary function of the PPS is to provide high pressure hydraulic fluid to the lower zone die. This hydraulic fluid acts upon the composite blank forcing it to take the shape of the punch. A high pressure fixed displacement pump is used on the skid in order to pressurize the fluid up to 5000 psi. The fluid is fed to an array of air piloted pressure regulators. Three pressure regulators are used to independently control the fluid pressure in the top zone, side zone and bottom zone of the forming dies.

The forming fluid flows from the regulator array into the fluid cavity of the die through one port and out of the fluid cavity through a different port to the downstream pressure regulator. This regulator controls the pressure in the forming chambers of the dies. Excess fluid is constantly being allowed to enter the die from the upstream pressure regulator which is fed by the fixed displacement pump. This excess fluid is vented through the downstream regulator and returned to the fluid reservoir where it is cooled to 65°F and circulated through several filtration units. In the event that the oil in the forming chamber is heated and rapid cooling is desired, the operating point of the downstream pressure regulator can be reduced which allows the hot fluid to escape to the reservoir while cold oil is injected into the die. This operating condition is used to cool composite parts immediately after forming in order to drive process time down. A simple hydraulic schematic highlighting the components and fluid path through the PPS can be seen in Figure 12. It is important to note that there is only one path leading from the PPS to the forming dies. In reality there are three paths leading from independently controlled pressure regulators to separate forming zones of the system. These features were omitted in order to simplify the diagram.

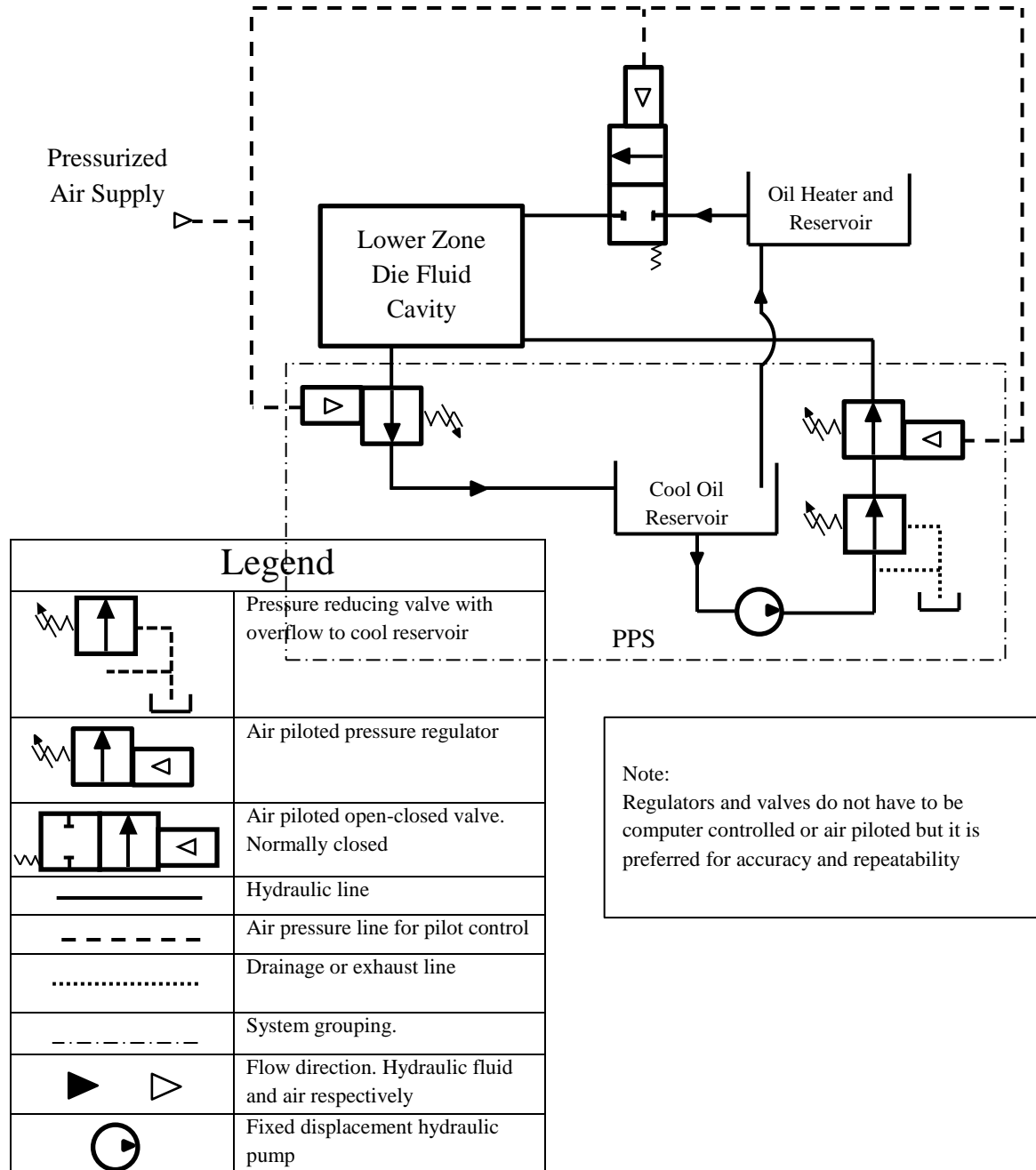


Figure 12 – Simplified Hydraulic Schematic of PPS and Forming Die

Filtration of the forming fluid is critical as high pressure pumps and regulators are very sensitive to debris and can be damaged by even the smallest particulate suspended in the oil. During early forming simulations many difficulties were experienced with the bladder system used to prevent the composite from coming into contact with the oil. Original bladders consisted of 1/8" rubber sheets and were prone to tearing and bursting under high forming pressures and clamping loads. Once the bladder was

compromised, the composite made contact with the oil, causing two major problems. The composite is ruined when it contacts the oil and the oil accumulates fibrous debris after contacting the composite. This debris can restrict flow in high pressure lines, prevent valves from sealing and damage high pressure pumps and regulators. A new bladder system was devised which consists of nylon vacuum bagging and Teflon release film which is sealed using vacuum bagging tacky tape. A schematic of this bladder system can be seen in Figure 13.

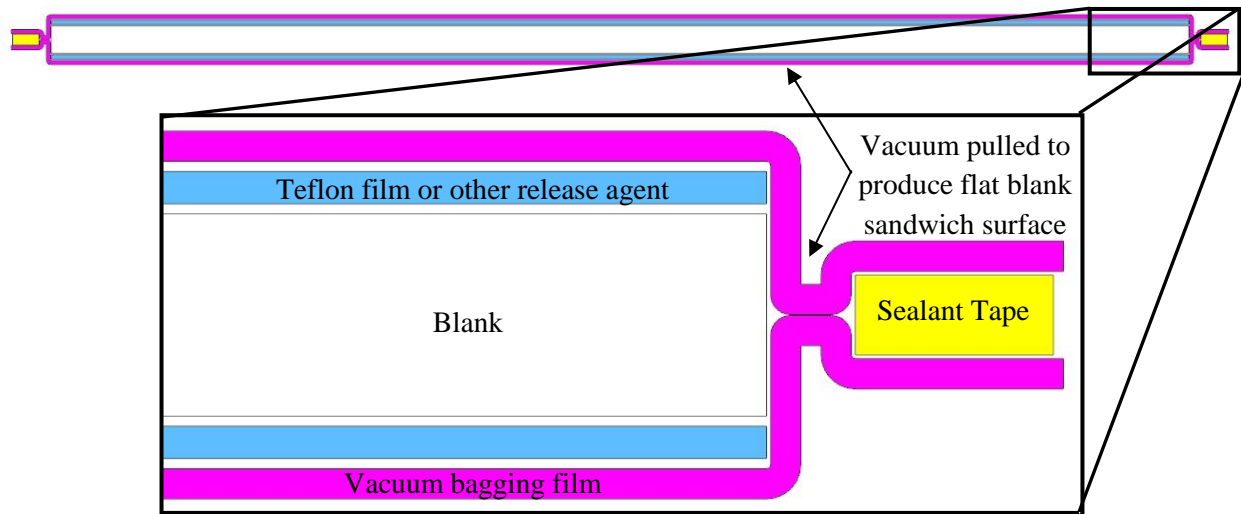


Figure 13 – The Blank Sandwich

This bagging system proved to be far more reliable than the previous rubber bladder and eliminated the threat of oil coming into contact with the composite. This drastically reduced the rate at which debris accumulated in the oil.

An additional heat exchanger was added to the system in order to reduce the temperature of the oil in the reservoir. The heat exchanger was implemented through a cooling loop which draws oil from the reservoir, passes it through the heat exchanger, then through a filter before it is returned to the reservoir. An example of this cooling/filtration loop can be seen in Figure 14.

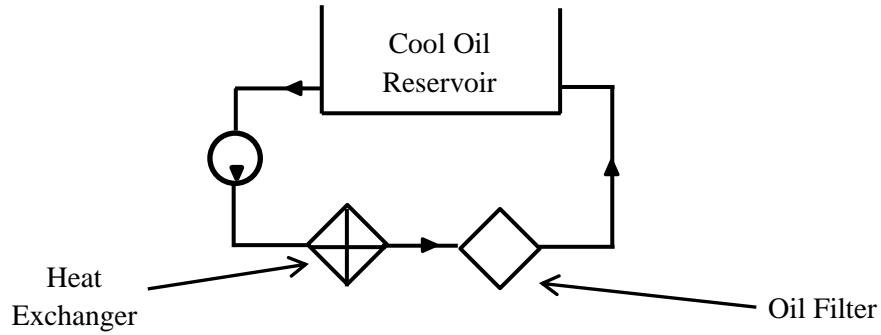
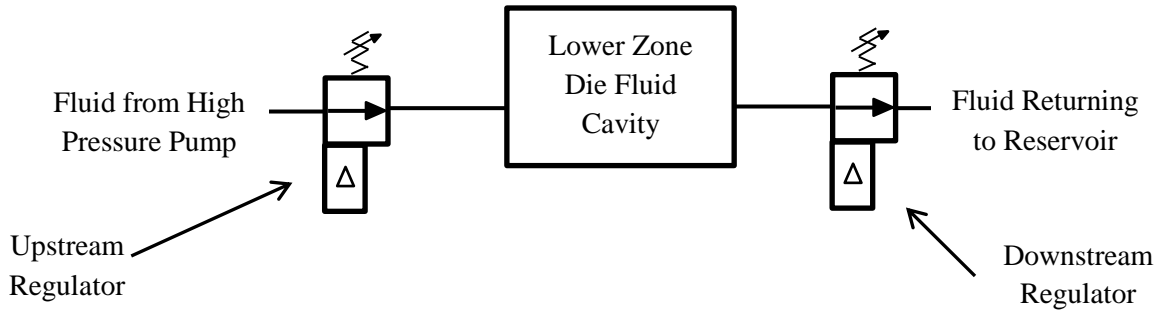


Figure 14 – PPS Cooling Loop

An additional feature was added to the cooling loop. By incorporating additional valves and fluid lines, the fixed displacement pump used in the cooling loop can be temporarily repurposed to pump fluid out of the forming dies and return it to the cool oil reservoir.

The last and perhaps most important modification to the PPS was the implementation of the downstream regulator. The addition of this regulator allows the pressure chamber of the forming dies to operate under several different conditions. Originally the forming dies did not feature a downstream regulator. The only means of pressure control was an open\closed pneumatically actuated valve which did not provide accurate control of the forming fluid pressure.

By implementing the downstream pressure regulator, pressure in the chamber can be raised or lowered to any desired set point. Examples of several operating conditions can be seen in Figure 15.



| Condition | Deadheading | Pressurized Circulation | Oil Flood |
|---------------------|--|--|--|
| Pressure Set Points | $P_{US} < P_{DS}$ | $P_{US} > P_{DS}$ | $P_{US} > P_{DS} ; P_{DS} = 0$ |
| Die Cavity Pressure | P_{US} | P_{DS} | ambient |
| Result | Pressure supplied by US reg. cannot overcome DS reg. | Fluid is circulated through the die cavity under the pressure P_{DS} | Fluid is circulated through the die cavity at ambient pressure |

Figure 15 – Regulator Operating Configurations

The ability to operate at several different conditions make the hydroforming press versatile and help drive down process time. The ways in which these different operating conditions are used will be discussed in the Forming Process section.

Forming Dies

The hydroforming dies are the most critical components in the hydroforming process. The other systems of the press are made of generic components where the dies are the first tooling of their type. Since there is no bench-mark for these types of dies, design has gone through several iterations. The initial tooling was designed to allow for rapid reconfiguration, allowing different forming conditions to be implemented.

The first iteration of the hydroforming dies was the prime example of this. These dies were designed with three separate pressurized fluid zones which ideally could be controlled independently of one another. A cut section of these dies can be seen in Figure 16.

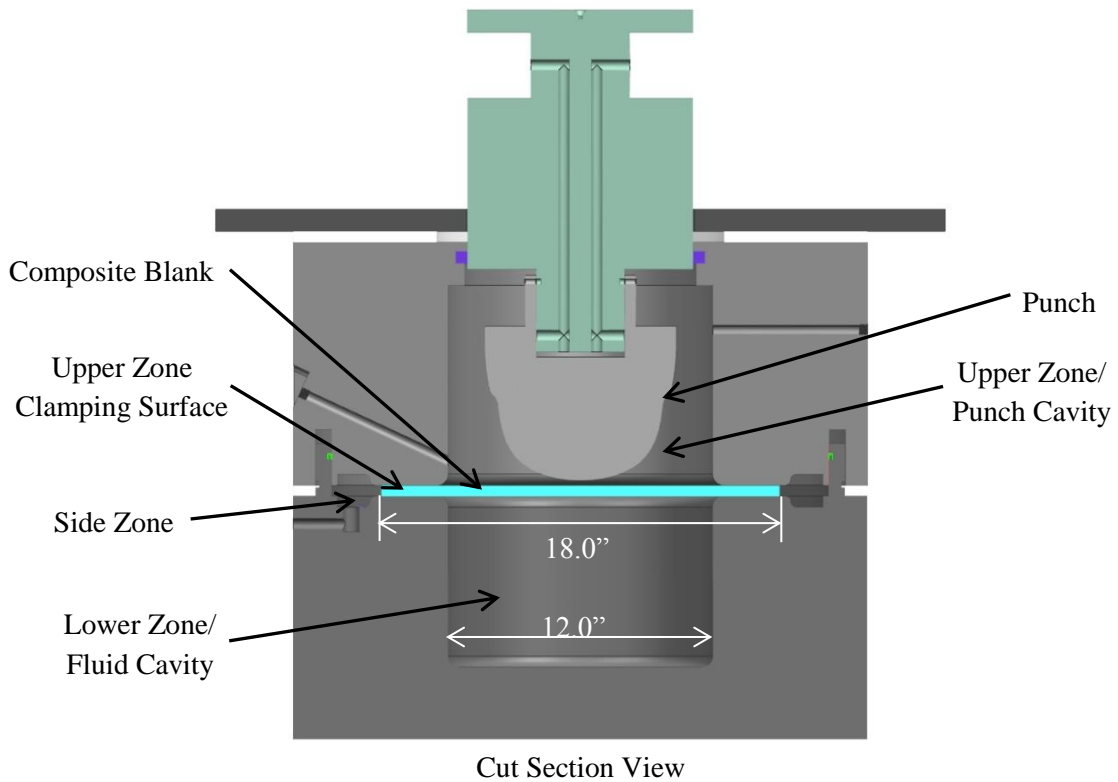
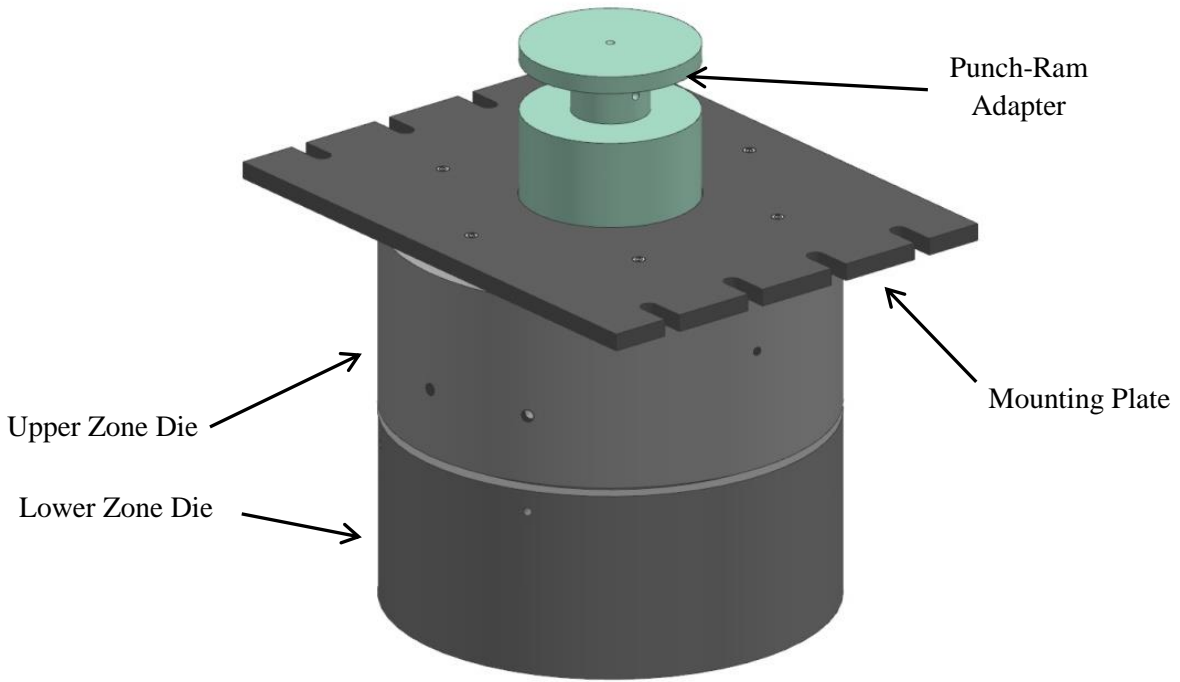


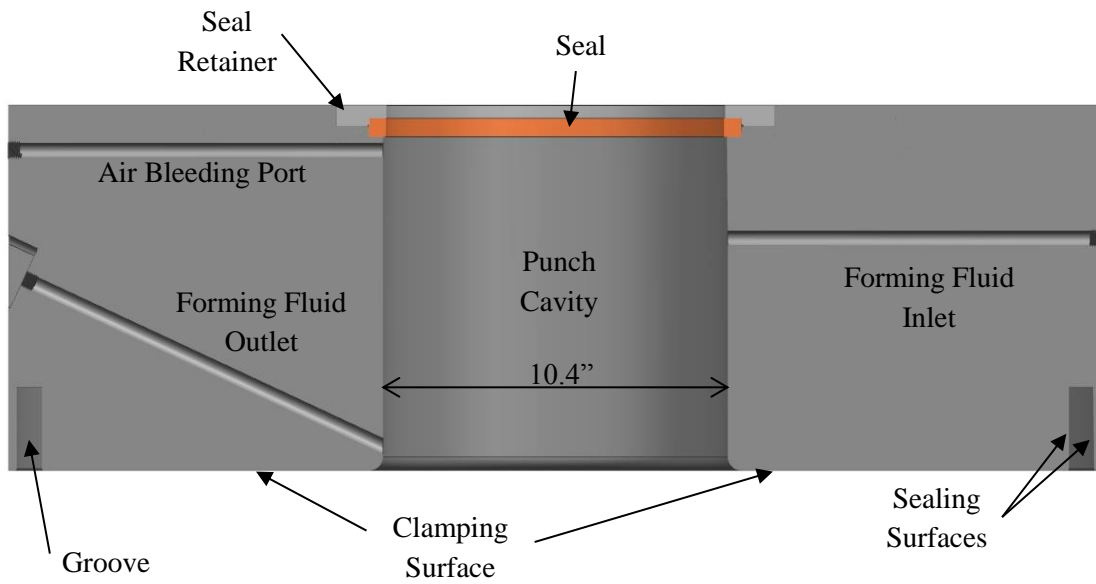
Figure 16 – Original Hydroforming Dies

The lower zone/fluid cavity is designed to allow fluid pressure to act against the composite blank and conform it to the punch. The composite blank is clamped between the upper zone die and the lower zone

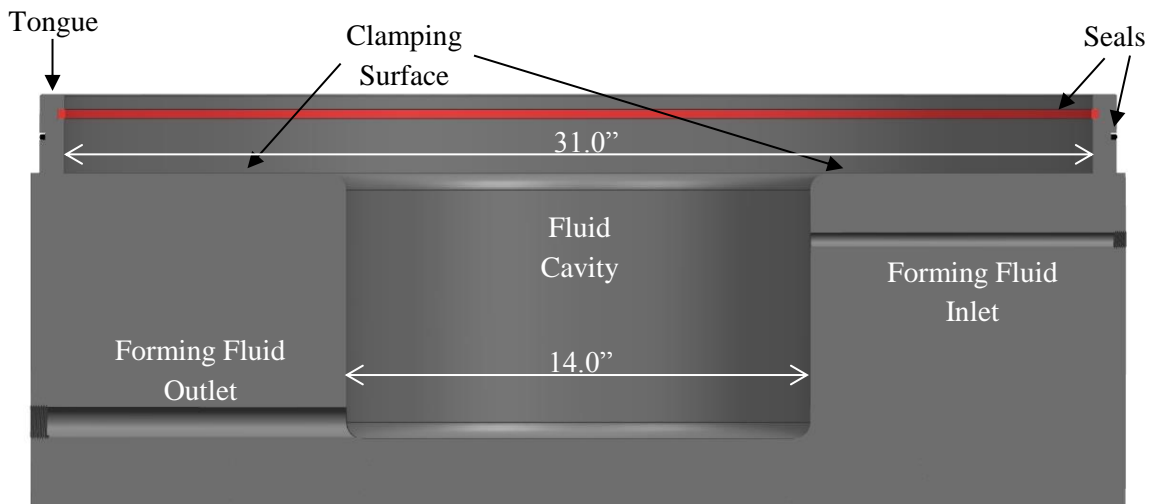
die clamping surfaces. This effectively separates the bottom zone from the side zone as is seen in Figure 16. The side zone is designed to apply pressurized fluid to the sides of the blank in order to apply force which promotes the blank drawing in if high clamping loads are used. The side zone was never used and was phased out in future designs.

The upper zone/ punch cavity houses the punch and the punch adapter. Pressurized fluid can be used in this chamber to balance the pressure exerted on the composite blank from the bottom zone. In the event that pressurized fluid is utilized from the lower zone alone, the blank acts as a diaphragm which contains the pressurized fluid. Before the punch is traversed downward through the material a gap will exist between the portion of the blank that is supported by the punch and the portion of the blank that is supported by the clamping surfaces. This area of the blank will bulge into the upper zone punch cavity and possibly rupture if the forming pressure becomes too high. Pressurized fluid can be added to the upper zone to help support this gap in blank support area and reduce the severity of the bulge. Unfortunately, applying pressure in the upper zone directly resists and cancels out the forming pressure in the lower zone. Additionally, the side zone severely reduces the outer diameter of the blank holding area, limiting the size of blanks that can be used to a circle with a diameter of 18”.

This die set was re-machined once in order to fill the side zone cavities in on both the upper zone and lower zone dies. This increased the clamping area, allowing circular blanks as large as 21.0” to be utilized. This would still prove to be slightly too small to form deep drawn components. For these reasons and several others, new dies were designed and fabricated. In the next design iteration, the side zones were removed and blank holding area was increased all the way to the edge of the tongue and groove. The redesigned upper and lower zone dies can be seen in Figure 17.



Redesigned Upper Zone Section View



Redesigned Lower Zone Section View

Figure 17 – Redesigned Hydroforming Die Set

The most obvious of these changes is the significant increase in the outer diameter of the clamping surfaces. The largest blank that can be clamped with these dies is a circle with 31” diameter. A new feature called the seal retaining ring was implemented in the redesigned upper zone die. This feature allows a third seal (colored orange in Figure 17) to be easily replaced and inspected if necessary. The flaw

with the original design is that the seal could not be inserted or removed without damaging the seal. With the implementation of the retaining ring, this seal can be inserted and removed several times without damage occurring.

Not pictured but also implemented in this design was the use of quick disconnects between the fluid cavity and the punch cavity. When connected, these two cavities are linked through flexible tubing which allows equal fluid pressure. Several experiments were performed with equal pressure in the upper and lower zone but, as stated above, this canceled out the forming pressure that forms the composite blank to the punch. With the quick disconnects removed, the fluid cavity is isolated and single side pressurization is engaged.

Since equal pressurization is abandoned as a viable option to reduce the blank bulging into the upper zone punch cavity, reduction in the gap between the unsupported portions of the blank is utilized. This gap is significantly reduced and can be seen in Figure 18.

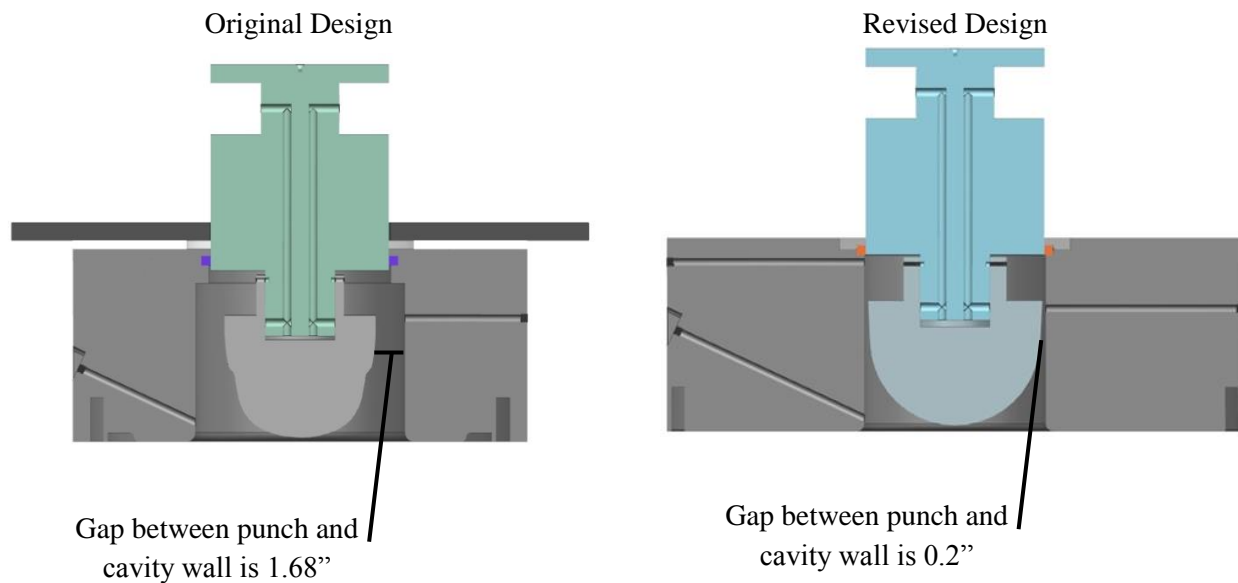


Figure 18 – Reduction in Punch Cavity Gap

There are several other important design changes to be noticed in the second revision of the hydroforming dies. The fluid cavity has been expanded to a diameter of 14.0\" while the punch cavity has been reduced to a diameter of 10.4\". The cavities of the original die set had the same diameter at 12.0\".

This change was made in order to take advantage of a specific type of blank clamping called hydrostatic clamping. Hydrostatic clamping relies on pressurized fluid to clamp the composite blank to the upper zone die clamping surface. Instead of applying the clamping force by pressing the two dies against one another, the pressurized fluid forces the blank against the upper zone blank holding surface. This style of clamping is implemented to reduce the probability of the bladder system tearing. Figure 19 shows a free body diagram that highlights the forces that are used in hydrostatic clamping.

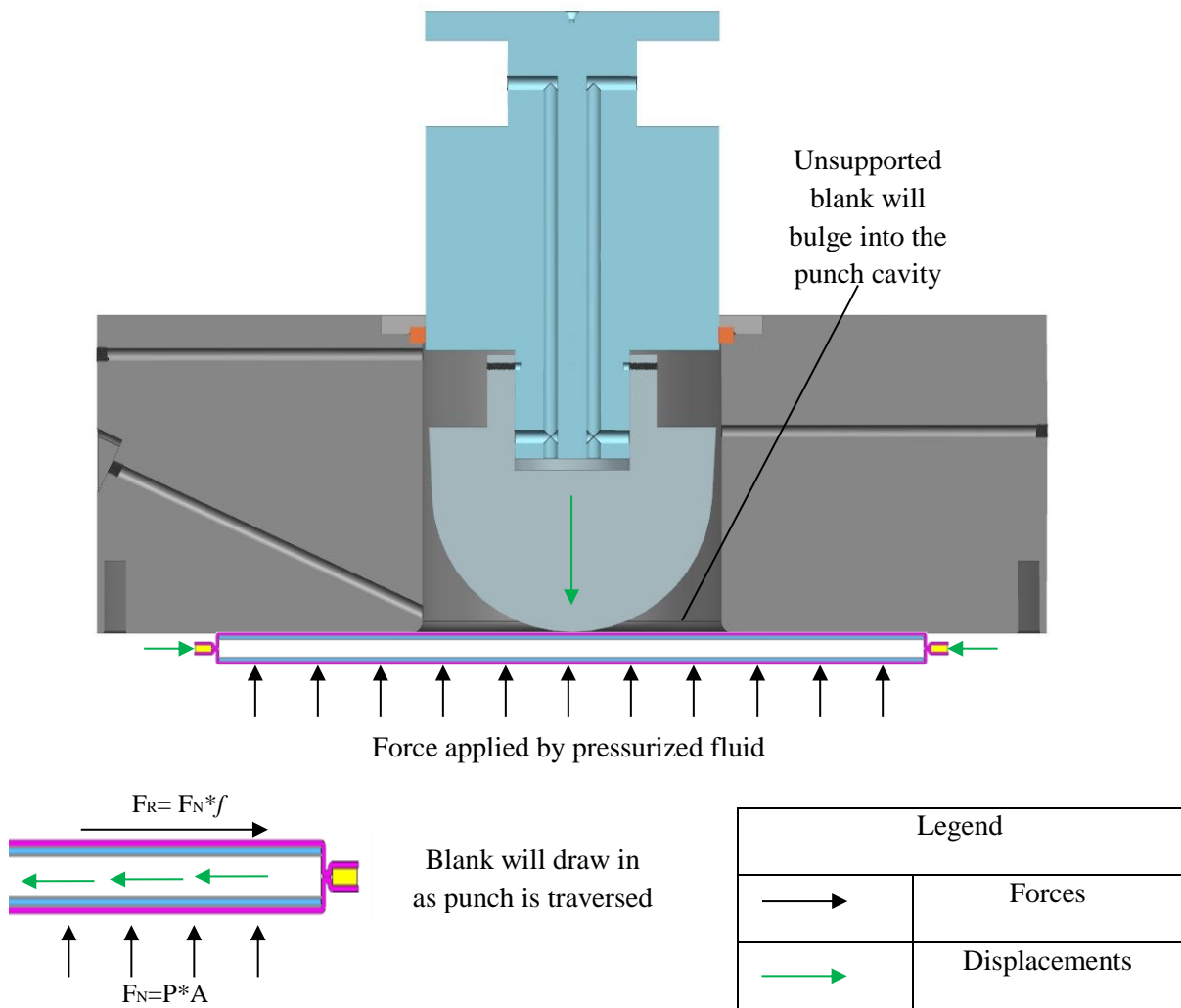


Figure 19 – Hydrostatic Clamping

The tongue and groove features of the dies are also modified to allow for a greater gap between the upper zone and lower zone die clamping surfaces. The tongue and groove features were adopted from the original die design. Seals are contained within grooves of the tongue which contact the sealing surface

of the groove, forming a seal. The tongue and groove are aligned in such a way that the gap between the upper and lower zone die clamping surfaces is variable as long as the seal contacts the grooves sealing surfaces. A schematic of this interface can be seen in Figure 20.

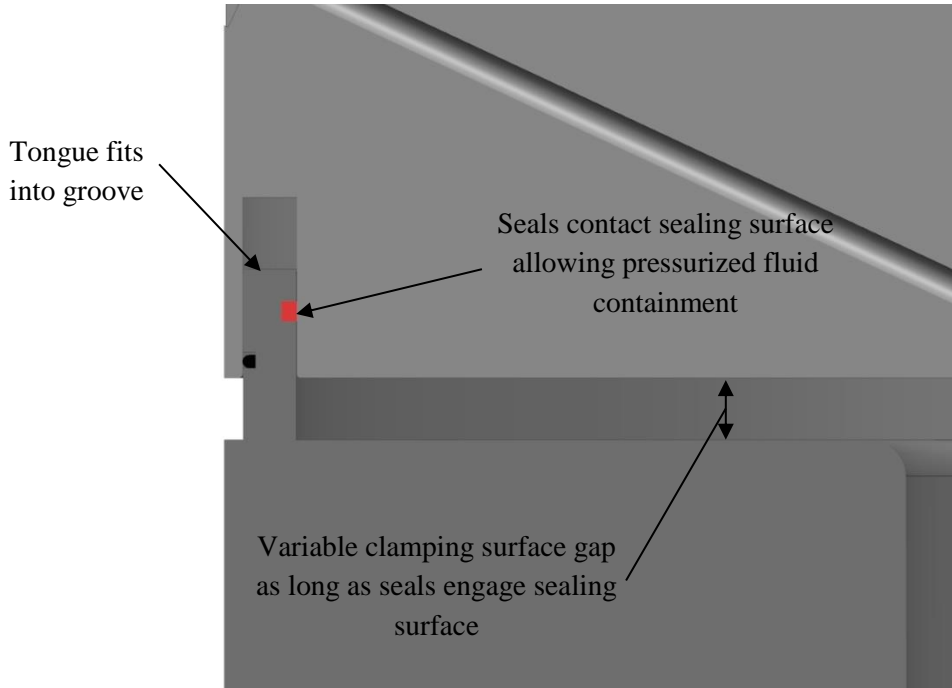


Figure 20 – Tongue and Groove Feature

The design of this feature was changed from the first die set. The seal grooves are raised to a higher position on the tongue, allowing the gap between the clamping surfaces to be larger while still maintaining a sealed fluid cavity.

Punches

The function of the punch is to provide the geometry to which the composite blank will be formed, similar to the function of the punch in sheet metal stamping. Since the materials formed in this process are much softer than metals, there is little concern over the punch becoming fatigued. The punch is connected to the punch-ram adapter by an opening that receives a cylindrical boss from the ram adapter. Several screws pass through the cylindrical opening into holes on the cylindrical boss that locks the punch in place. In order to prevent these screws from being sheared off, a ring is used to transfer load

from punch directly to the punch-ram adapter. The screws are used only to prevent the punch from rotating about the adapter. A schematic of the punch and the punch ram adapter can be seen in Figure 21.

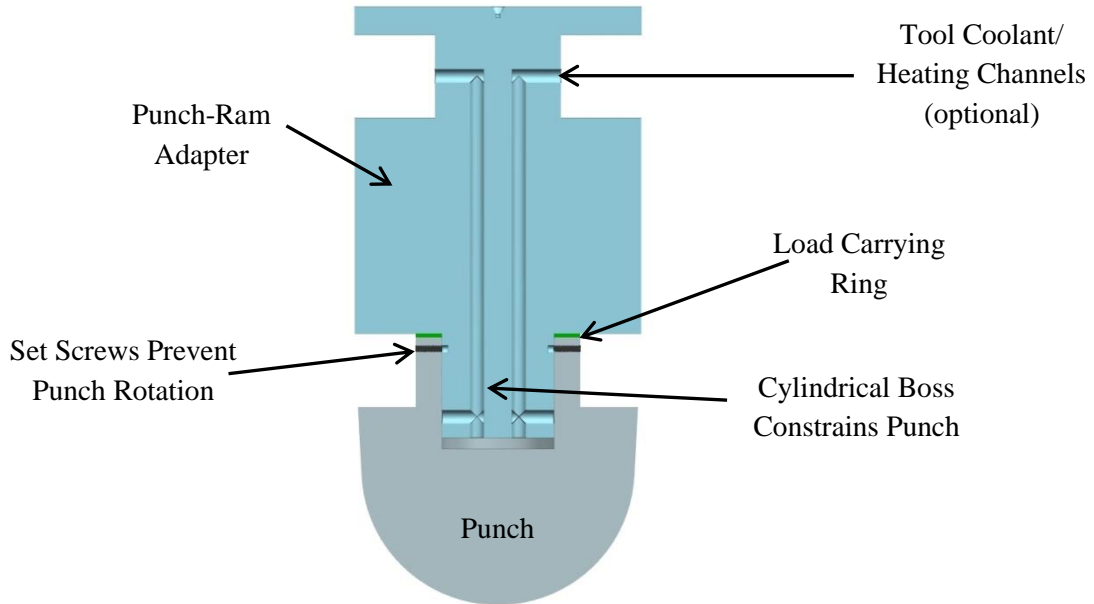


Figure 21 – Section View of Punch-Ram Adapter Interface

Two separate punches were designed and machined for the hydroforming press. Both of the punches are male plugs that require the material to be wrapped around them in order to form the desired shape. The ACH punch was provided by BAE Systems through a partnership that provided the hydroforming lab with the punch and Dyneema composite blanks.

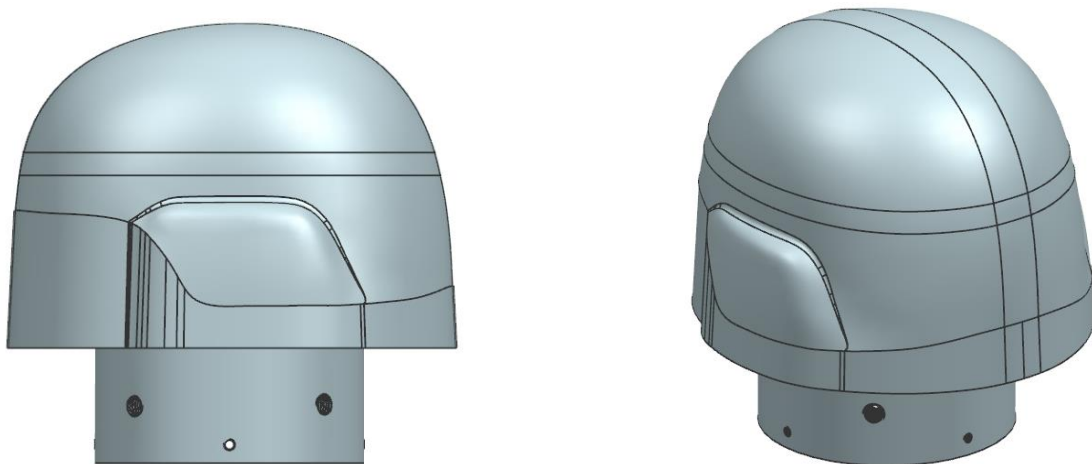


Figure 22 – ACH Punch

The other punch is a simple hemisphere. It was sized to create as small of a gap as possible between the blank holding surface and the punch. It can be seen in Figure 23.

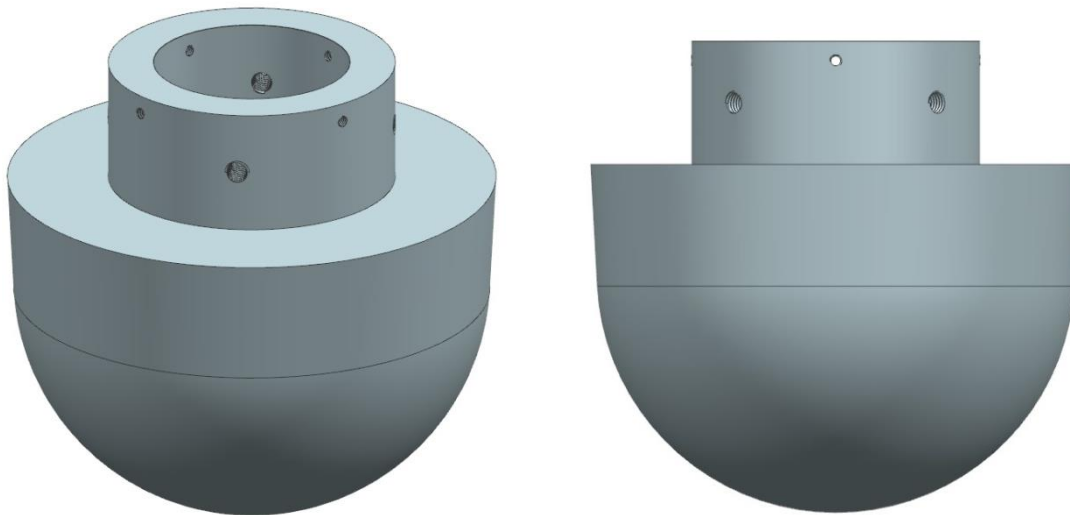


Figure 23 – Hemispherical Punch

The isometric view in Figure 23 provides a good view of the cavity that accepts the cylindrical boss from the punch-ram adapter in order to constrain the punch. Both punches feature positive draft angles when viewed from the side. This prevents the formed parts from locking onto the punches and becoming difficult to remove.

Oil Heater

Heating of the forming oil is necessary for the thermo-hydroforming process. The use of heated oil reduces the cooling rate of the composite, allowing sufficient time for the press to close, raise the forming fluid pressure and form the part before it solidifies. A Mokon oil heating unit is utilized to provide forming dies with heated oil. This unit heats the oil within an internal heat exchange loop and uses a low pressure pump to pump hot oil into the dies. This heater has the ability to raise the forming oil to temperatures in excess of 500°F. The oil is pumped directly into the room temperature dies and begins to cool rapidly. For this reason the hot oil should be flooded into the dies immediately before the preheated blank is loaded. Typically the commanded temperature is at least 50°F hotter than what is desired in the die in order to compensate for this cooling.

The oil pump used on the heater unit is not able to build fluid pressure higher than 50 psi. In order to raise the pressure past this point cool oil from the PPS must be utilized. The addition of this cool oil lowers the temperature of the fluid within the fluid cavity, reducing the amount of time that the composite will remain in its formable state. Typically this is not an issue as fluid pressure is built immediately prior to the forming of the blank to its final shape. In the case of thermoset composites the ability to flow hot oil at high pressures is needed to catalyze the curing process. Since the thermo-hydroforming process currently only deals with thermoplastic materials the inability for the heater to pressurized hot oil before send it to the forming dies is of little concern.

Infrared Heater

An infrared heater array was acquired by the lab in order to preheat the composite samples before forming them in the hydroforming press. This is a common industrial practice as heating within the tooling requires complex heating elements and increases the time that the part spends within the die. Experiments were performed where heated oil was circulated through the forming dies for over an hour in an attempt to bring the composite to its forming temperature. Even this extended period of time was not sufficient to bring the composite to the appropriate forming temperature. Direct temperature measurements of the composite when it is within the closed die are also quite difficult further prompting the abandonment of this preheating technique.

A 18.8 kW IR heater array was purchased from Radiant Energy Systems as an alternate to in-die composite heating. A simple gantry was constructed that allowed the IR elements to be raised and lowered over the composite to allow efficient heating of the specimen as well as easy recovery. This IR heating array is only able to apply heat to a single side of the composite. This resulted in a significant thermal gradient developing during the preheating of the composite. In order to mitigate this issue, a ceramic stone is utilized as a platform for the heated composite. Prior to the heating of the composite blank, the IR heaters directly heat the stone to approximately 20°F above the desired forming temperature of the composite. Once the stone is preheated, the composite is placed on top of the stone. The stone

remains hot for some time and help heat the composite surface that is not exposed to the IR heaters. This practice has been shown to significantly reduce and even eliminate the thermal gradient throughout the composite during preheating. A picture of the IR heating device can be seen in Figure 24.



Figure 24 – IR Heating Array

The IR heating elements have been shown to localize heat at the exposed surface of the composite. The first heating experiments resulted in the top layers of the composite becoming overheated and charred while the interior layers barely increased temperature at all. In order to prevent this from happening, a 1/8” rubber pad is placed over the composite to protect the surface layers during preheating. This method prevents the top layers from becoming overcooked and allows sufficient protection for the top layer while heat is being conducted through the thickness of the blank.

Initially, a blank was prepared with embedded thermocouples in order to investigate the severity of the temperature gradient within the composite during the preheating process. Results obtained with this test setup gave exact times and temperatures for heating a blank of a certain thickness. Comparable results were easily obtained by a far simpler method.

1. First the stone is preheated for 30 minutes until a thermocouple at the surface of the stone reads ~20°F above the desired forming temperature for the composite. Place 2 1/8" rubber sheets on top of the heating stone and the thermocouple during this process.
2. Place the composite within its bladder on top of 1 rubber sheet on the stone. Place one thermocouple between the rubber pad and the composite. Place another thermocouple on top of the composite and the other rubber pad on top of this.
3. Lower the IR heaters to within 0.5" of the rubber pad covering the composite.
4. Set the IR heater temperature ~100°F above the desired forming temperature of the composite.
5. Monitor both thermocouples. Make adjustments to the IR element temperature until both thermocouples read $\pm 10^\circ\text{F}$ of the desired forming temperature.
6. Maintain this thermocouple temperature for 30 minutes. Adjust the element temperature if necessary.
7. Once 30 minutes has elapsed, raise the heater elements and remove the rubber sheet. Using heat shielded gloves, move the composite from the heating platform to the forming dies.

This process has been shown to uniformly heat the composite to the appropriate forming temperature. Monitoring the through thickness temperatures using the blank with embedded thermocouples showed that the thermal gradient using this procedure is negligible.

Computer Control System

The entire press including the PPS, HPS, oil heater and die set is controlled using a computer system. The program used to control the system is UniTest and is programmed by Interlaken Technology Incorporated. This system has the ability to control each aspect of the press manually including the displacement of the punch and clamping mechanisms as well as their applied loads, the pressure applied to the separate pressurization zones and the valves which allows hot and cold oil to enter and leave the

die. This system can be programmed to automatically implement the desired forming conditions but, since forming is still in a highly experimental phase, commands are delivered manually.

The UniTest program interprets the data from numerous sensors around the press and uses this data to seek the inputted set-points through PID control. The data from these sensors can be output to a .csv file in order to analyze the data acquired during an experiment. Data from nearly any system of the press can be outputted including forming fluid pressure and temperature, punch and die displacement, pressure provided to the clamping and punch rams, and the forces applied by the clamping and punch rams just to name a few. These data provide a large amount of information but one piece of data was missing.

Since the punch and the ram can act independent of one another it is not useful to know the displacement of these two systems independently. The composite blank always remains in contact with clamping surface of the upper zone die. Therefore, the distance that the punch has been drawn through the composite material has to be related to the clamp displacement since the upper zone die is mounted to the clamp. By simply subtracting the displacement of the punch from the displacement for the clamp and adding an offset factor it can be determined how far the punch has penetrated the original plane that comprises the blank surface. This information is important to know for two reasons. First when the die is closed there is no visual confirmation of how far the punch is above the blank surface. By being able to calculate and display the displacement between the punch in the ram allows the operator to know how far the punch is from the composite once the upper and lower zone initiate clamping of the composite blank. Secondly, it is important to know when the punch has been traversed far enough to completely form the part. Calculating the punch to clamp (PtoC) displacement allows the operator actuate the press appropriately in order to ensure that the part is completely formed.

Forming Process

Even though several pieces have been formed successfully with the thermo-hydroforming process over the past decade, the process has not been well documented. Even if the process was well documented for the 40 ton press, it is likely that this process would not work well with the 300 ton press due to changes in tooling design and increases in thickness of the composite blank. The forming process has undergone numerous changes from the first attempt at forming the helmet. Many of these changes were made by simply altering the forming pressure or temperature. Others were more complex in nature such as application of single or double side forming pressure and either physically clamping the blank or hydrostatically clamping it. The more complex changes often required changes to the forming dies or the PPS.

The forming procedure presented below is the latest iteration on a forming process that is constantly changing. With each additional blank formed the process is further refined with the hope of increasing the part quality or decreasing process time. What is presented has given the best results so far.

Prior to forming, the composite is laid up inside of a bagging system referred to as the blank sandwich (see Figure 13). A vacuum is pulled within the blank sandwich, smoothing any wrinkles on the outer surfaces on the flat surfaces of the blank. The blank is then heated to its forming temperature while inside of the bagging system by any number of methods. As mentioned above, an IR heating system has been shown to work well. Unconsolidated composites can be laid up and consolidated while within the blank sandwich if the consolidation temperature does not exceed the service temperature of the bagging film. This method was not investigated during this study but is presented as an additional way to reduce processing time.

As the blank is heating, the lower zone fluid cavity is flooded with hot oil from the oil heater. This can be seen in Figure 25.

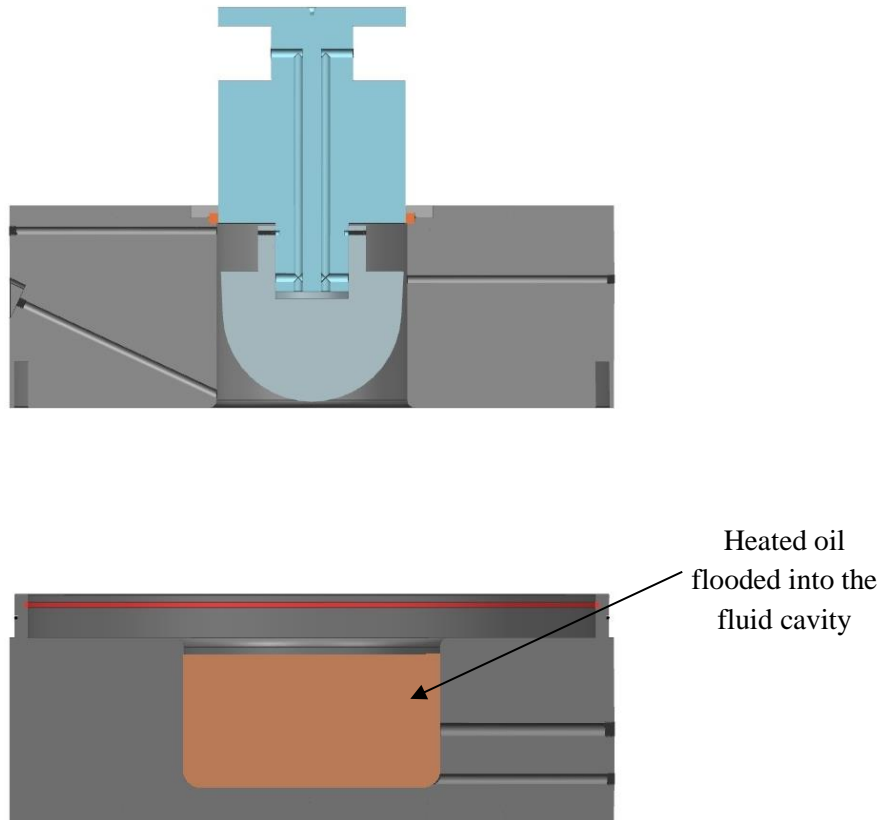


Figure 25 – Forming - Step 1

The temperature of this oil is typically 50°F above the forming temperature to reduce the effect of the die cooling the oil as described above. It is preferable to heat the upper clamping surface, lower clamping surface and punch as well in order to maintain the temperature of the blank sandwich. This requires heating elements built into the blank or some sort of external heating system. Tool heating was not utilized during this study.

Once the blank sandwich has been raised to the appropriate forming temperature, it is laid flat on the lower zone die clamping surface. In this step, it is important to properly align the blank sandwich with the punch so that the part forms properly. This can be seen in Figure 26.

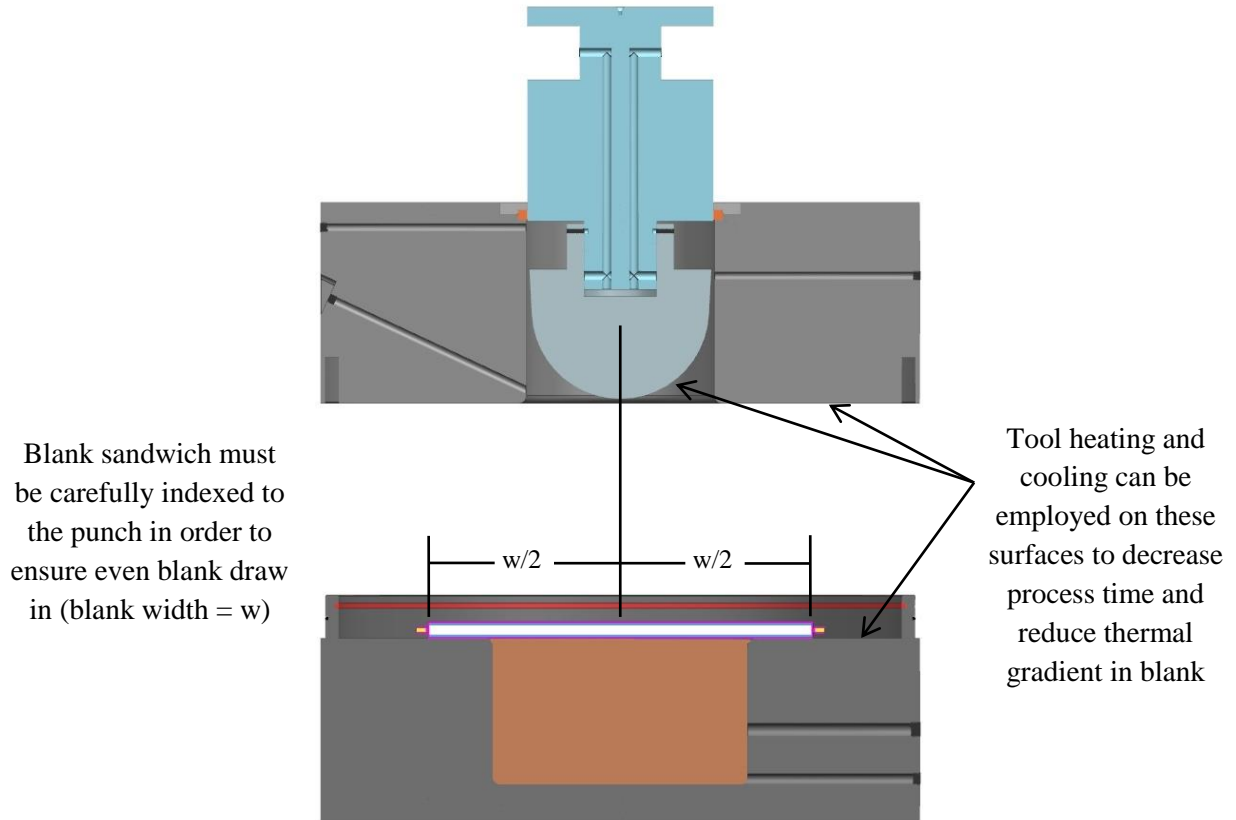


Figure 26 – Forming - Step 2

Next, the upper zone die is lowered onto the blank until a light clamping force is generated to firmly grip the blank sandwich between the upper zone and lower zone clamping surfaces. The punch is also brought down simultaneously until it is very close (approximately 0.040”) from the blank surface. This step can be seen in Figure 27.

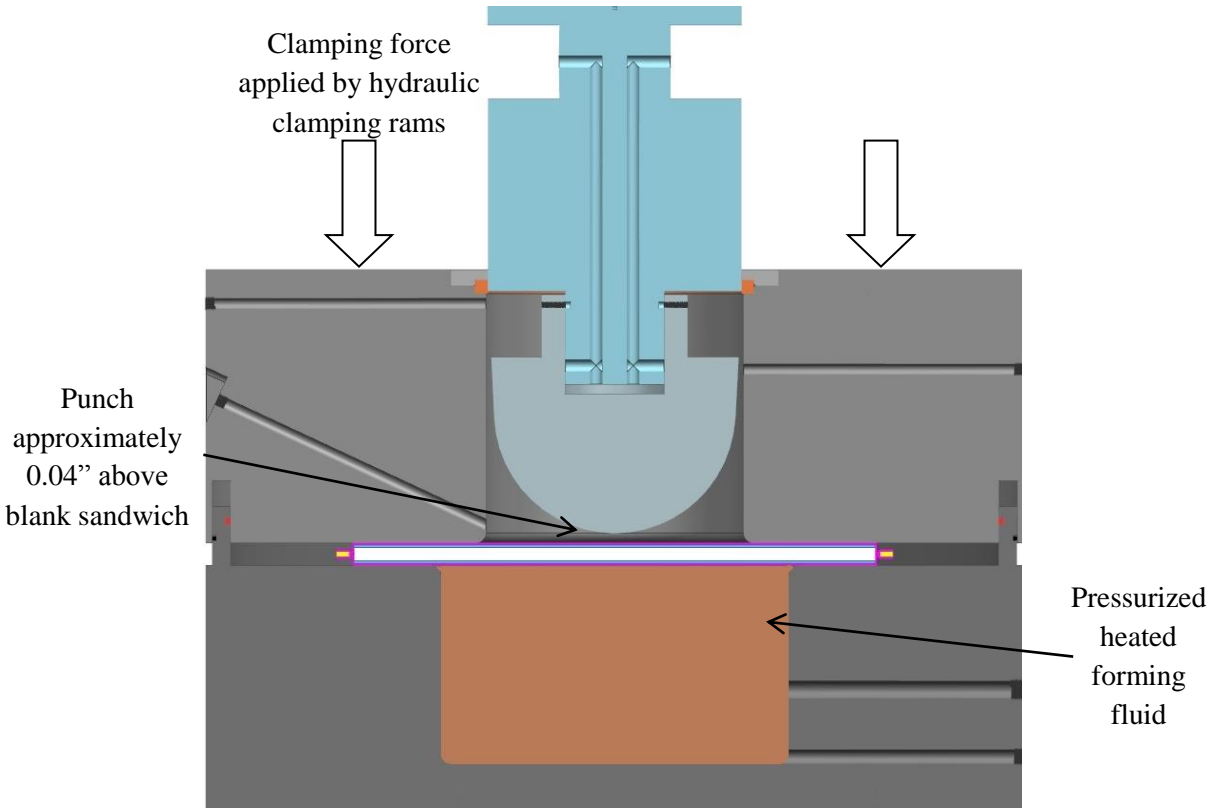


Figure 27 – Forming - Step 3

Depending on the thickness of the composite sheet, a relatively low pressure (e.g. about 10-100 psi) is built in the fluid cavity. Pressure is built using cool oil from the pressure producing skid (PPS). It is preferable to build pressure using hot fluid from the heater. However, that is not necessary as the volume of the fluid required to raise the pressure of the fluid cavity is small compared to the total volume of fluid in the fluid cavity. Once the pressure is raised, the upper zone is slowly raised up about 0.040" to keep the blank hydrostatically clamped to the upper zone clamping surface. When hydrostatically clamped, the blank will no longer physically contact the lower zone die. Hydrostatic clamping can be seen in Figure 28.

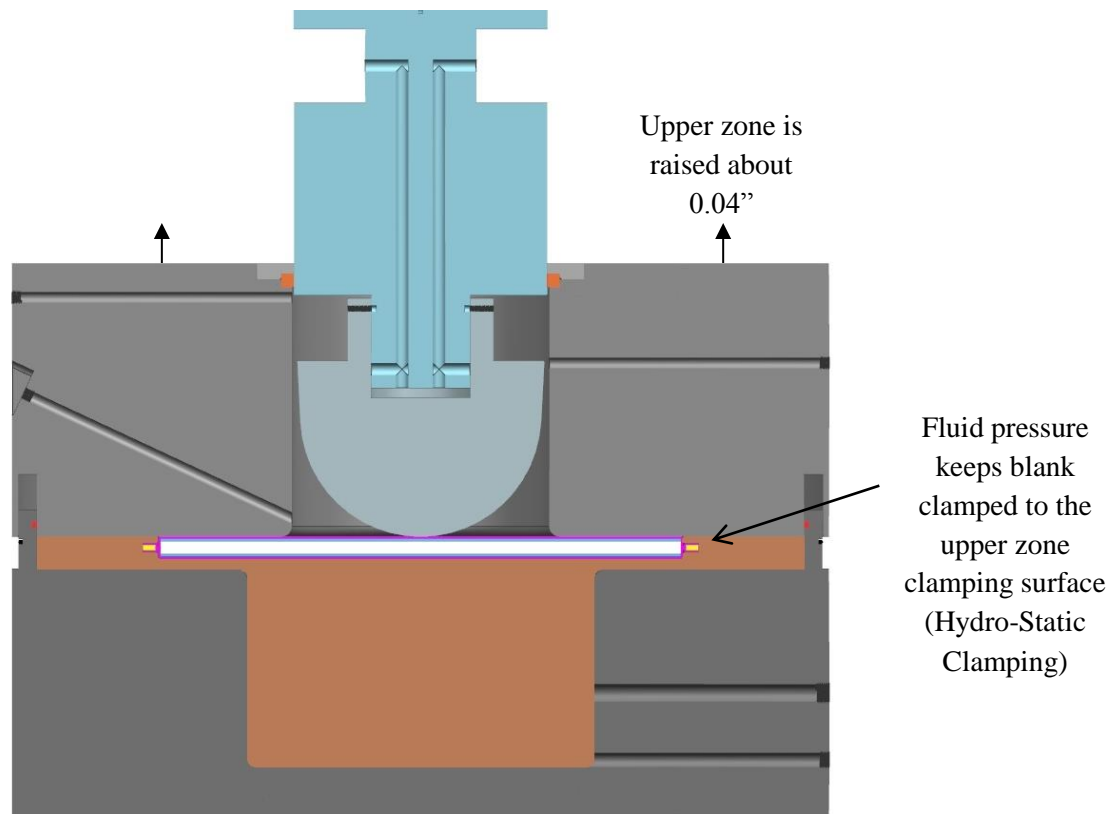


Figure 28 – Forming - Step 4

When hydrostatic clamping is being initiated, a portion of the blank is not supported by either the clamping surface or the punch. This section of the blank will bulge into the gap between the side wall of the punch cavity and the punch. As mentioned in the forming die section, care is taken to reduce the size of this gap in order to reduce the severity of the material bulge into the upper zone punch cavity. If an excessively large gap exists between the punch and the upper zone die clamping surface, the blank may be drawn too far into the upper zone leading to excessive wrinkling and the inability for the blank to form a seal and contain the pressurized fluid in the fluid cavity.

After the hydrostatic clamping has been accomplished, the punch is traversed down into the blank sandwich and eventually into the lower zone fluid cavity. As the punch is drawn into the lower zone, the blank conforms to the punch and is drawn across the upper zone clamping surface. This can be seen in Figure 29.

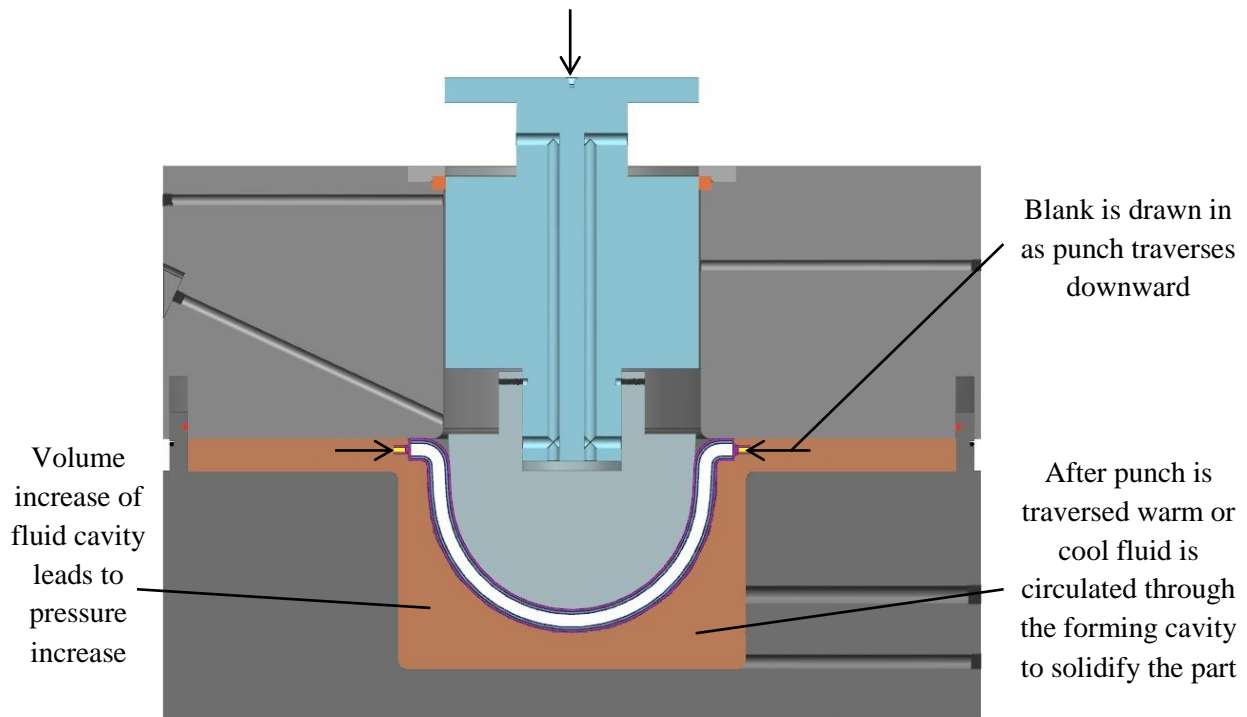


Figure 29 – Forming - Step 5

During this process, the volume of the fluid cavity is reduced leading to an increase in pressure. As the pressure increases and the blank draws across the clamping surface, the initial positioning of the blank becomes increasingly important. If the blank is off center before it is clamped then a discrepancy in contact area will exist when hydrostatic clamping is initiated. The side of the blank that engages more clamping surface will draw-in less due to a higher frictional force holding this section of the blank in place. This is why proper indexing of the blank to the punch and clamping surface before clamping is crucial. Having a clean smooth surface on the blank sandwich also helps ensure even draw-in of the blank.

As the punch is drawn through the composite material and into the fluid cavity, the rate of pressure increase can follow a predetermined profile which is controlled by the downstream pressure regulator. Once the punch has reached its fully traversed position, cool hydraulic oil is circulated through the forming cavity to solidify the thermoplastic resin. In the event that a composite uses a thermoset resin system, hot oil can be circulated through the die to accelerate the curing process. Once the part has

solidified, pressure from the lower zone can be relieved and the upper zone die and the punch can be traversed upward so that the finished part can be recovered and removed from the bladder.

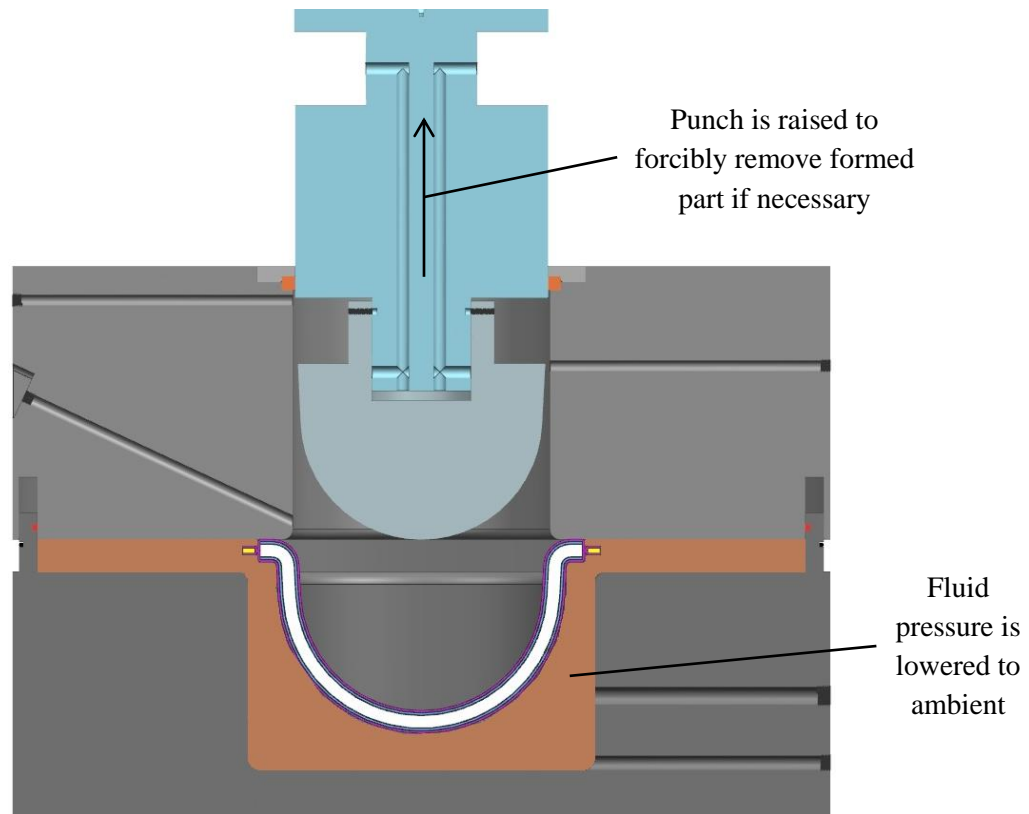


Figure 30 – Forming - Step 6

A passage for oil recovery is added to the lower zone which allows the hydraulic fluid to be returned to the oil reservoir. By integrating the plumbing with a cooling loop pump on the PPS, valves can be actuated that allow oil to be pumped at a high rate from the fluid cavity of the lower zone to the oil reservoir. An optional overflow passage from the reservoir can return excess oil back to the heater reservoir. This option has been implemented to eliminate the need to manually transfer oil from the PPS reservoir to the heater reservoir.

Results and Discussion

Many trials have been attempted to successfully form a part using the 300 ton hydroforming press. These experiments have helped shape the process described above as well as the tooling and

pressurization mechanisms of the press itself. This section will highlight the major discoveries that were made over the last two years as the process and the press itself has been refined. Pictures of the formed blanks will be displayed with the description of the discovery as well as the direction that this finding would have on the continuing development of the process and equipment.

Phase 1

The first hydroforming attempts were made with single layer polypropylene reinforced fiber glass. This material used is commercially available under the name TwinTex. It is a plain woven fiberglass that is comingled with strands of polypropylene. During consolidation these polypropylene strands melt and impregnate the woven glass structure. The fiber glass was sandwiched in between two rubber mats in order to protect the composite from the forming fluid. The upper zone was not able to contain pressurized fluid at this time so single sided pressurization was utilized. The blank and bladder system was clamped between the clamping surfaces of the upper zone die and the lower zone die. The method used to heat the composite to its forming temperature was circulation of hot oil in the fluid cavity using the oil heater. This method proved to be very ineffective and required over an hour to melt the polypropylene strands.

Single sided pressurization of the thin blank sandwich led to additional problems. At low pressures (~50psi) the blank sandwich would bulge excessively into the upper zone and burst, contaminating the composite and introducing glass fibers to the forming oil. It was determined that the main reason the blank sandwich burst was due to single sided pressurization. After this realization was made the upper zone die was redesigned. The design revisions allowed the die to contain pressurized fluid. Quick disconnects were used to connect the fluid cavity of the lower zone die to the punch cavity of the upper zone die, ensuring that the pressure on both sides of the die was equal. In reality, excess gap between the punch and the clamping surface played a large role in bursting the bladder as well. The punch used for this experiment is a double tapered cylinder. It can be seen in Figure 31.

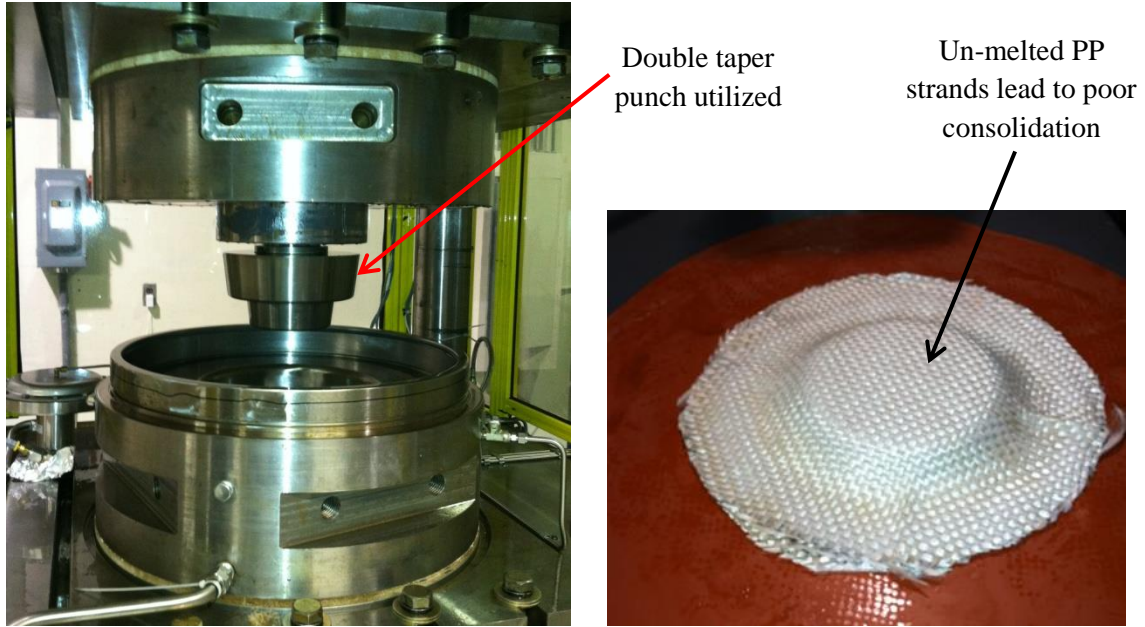


Figure 31 – First Hydroforming Results

Also in Figure 31 is a picture of a partially formed fiber glass blank. As mentioned above, the heating process used was very inefficient and did not completely consolidate the TwinTex material.

Several important lessons were learned during these initial experiments. Preheating the blank was required. Also, rubber bladders are prone to tearing and bursting. They would be abandoned in favor of the vacuum bag bladder system after the completion of this set of experiments. Finally, pressure regulation is critical. During these trials a downstream pressure regulator was not utilized which greatly hindered the operator's ability to control the forming pressure.

Phase 2

The second phase of forming trials saw several changes. The double taper punch was replaced by the ACH punch. The material used in this phase was an UHMWPE composite called Dyneema HB-80. This material is very similar to SR-3136 in laminated structure (4 unidirectional cross plys), fiber material and fiber volume fraction (~80%). The material is stacked 66 layers thick and consolidated to form a plate 0.5" thick. The blank shape used is a 19" circle.

The press was extensively modified as well. Filtration units were added in order to remove the fibrous material that contaminated the forming fluid in the previous phase of experiments. The upper zone die was also redesigned to allow the application of fluid pressure on both sides of the blank. A downstream pressure regulator was used to provide extra control over the pressure of the forming fluid. An IR heater was utilized to preheat the blank, significantly decreasing the time required to perform a single forming experiment. The vacuum bag bladder was also utilized instead of the rubber pad bladder.

The first experiments using this set up were performed using double sided pressurization. No compressive force was utilized to fix the blank during these experiments. A low forming pressure of 50 psi was utilized and the punch was drawn to a depth of 5.0". The results at these conditions were poor. The blank did not conform well to the punch and excess wrinkling covered nearly the entire surface of the blank. A diagram of the forming parameters and images of the blanks can be seen in Figure 32.

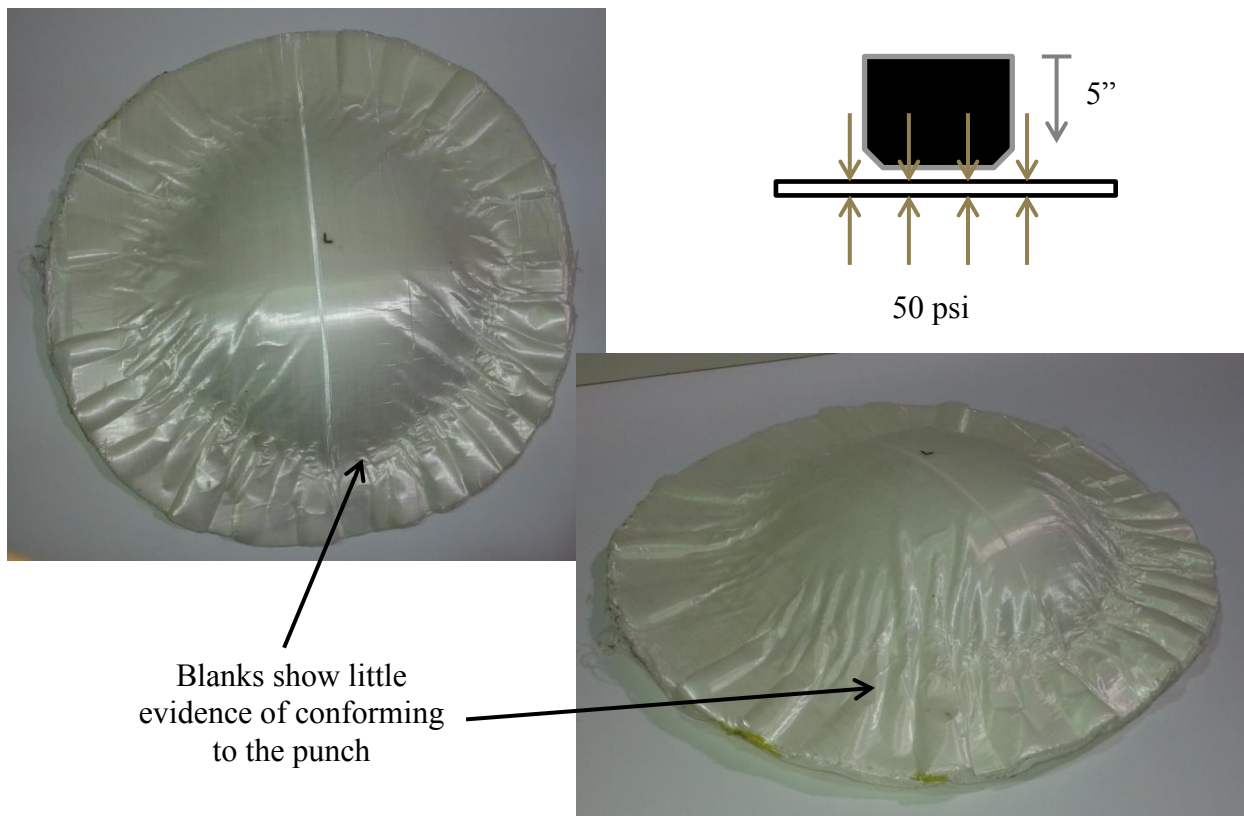


Figure 32 – Double Sided Forming Pressure on Dyneema Blank

The primary discovery made from this phase of experiments is that double sided pressurization of the blank essentially leads to the forming forces cancelling one another out and eliminating the forces that form the blank to the punch. Equal fluid pressure and no clamping load exerted by the clamping surfaces means that the blank is free to wrinkle, further reducing part quality. Finally, a draw depth of 5.0” is not nearly enough to form all of the features of the helmet. According to the geometry of the helmet and assuming that the punch starts by touching the upper surface of the helmet blank, a displacement of 7.5” minimum is required to fully form the helmet.

Phase 3

During the next phase of experiments, the choice was made to abandon double sided pressurization in order to form the composite to the punch as tightly as possible. Hydrostatic clamping is utilized to clamp the blank in order to reduce the likelihood of bladder tearing.

The first few experiments proved that the 19” blank was too small to form the helmet. As the punch is drawn downward the volume of the fluid cavity is decreased leading to an increase in forming pressure. This increase in pressure indicates that the blank has been hydrostatically clamped successfully and that the fluid is being contained within the fluid chamber. Every blank formed under these conditions failed to have the punch drawn to the desired depth of 7.5” before the fluid chamber experienced rapid decompression along with a loud pop. Data acquisition was used to acquire the forming parameters as this phenomenon occurred and can be seen in Figure 33.

Forming Pressure and Punch Displacement

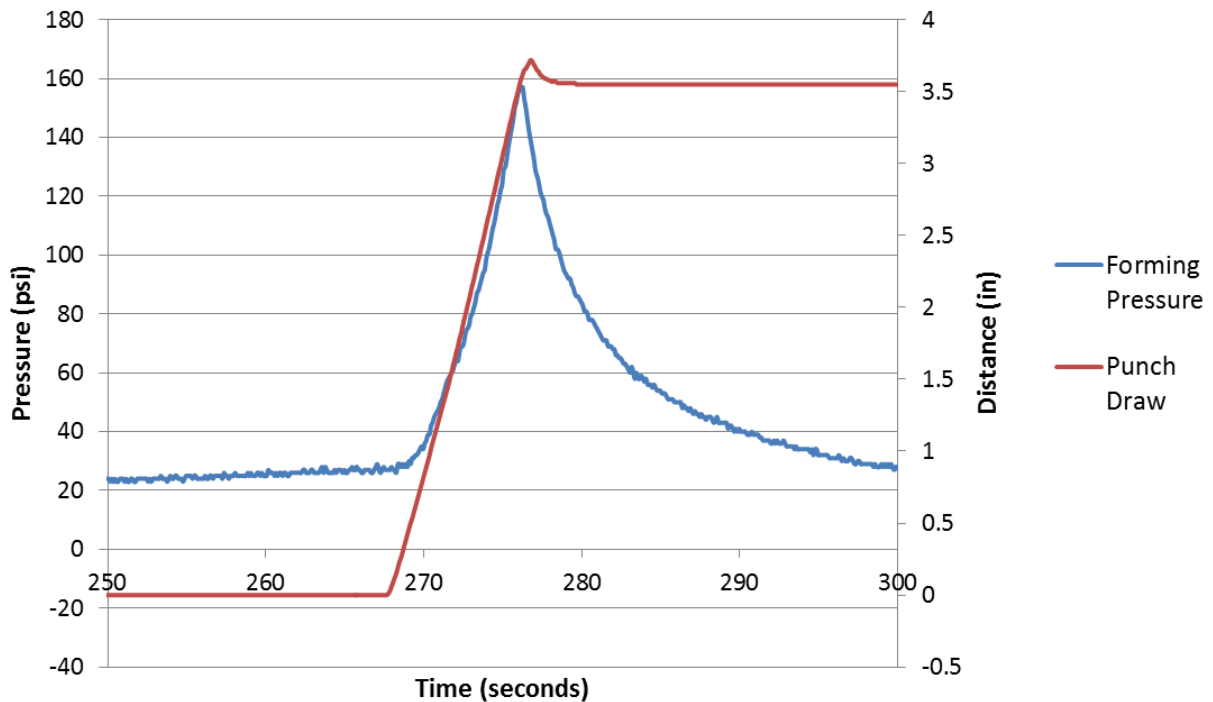


Figure 33 - Rapid Decompression of the Fluid Cavity

Upon recovery of the blank, it became clear what has happened. As the punch was drawn downward, the blank conformed to the punch and was drawn downward as well. A large portion of the blank was not directly acted on by the punch and was drawn along the clamping surface of the upper zone die. The increasing fluid pressure kept this portion of the blank tightly pressed against the clamping surface and maintained the seal that kept the pressurized fluid within the fluid cavity. The material continued to be drawn across the clamping surface until the edge of the blank reached the edge of the clamping surface. Since a large gap existed between the clamping surface and the punch, the blank was no longer able to contain the pressurized fluid. The blank was rapidly pushed into the upper zone die (punch cavity) which released the pressurized fluid, creating an audible pop. Once this has occurred, additional forming was not possible and the part had to be removed. This phenomenon was termed “popping through”. An example of a blank that popped through can be seen in Figure 34.

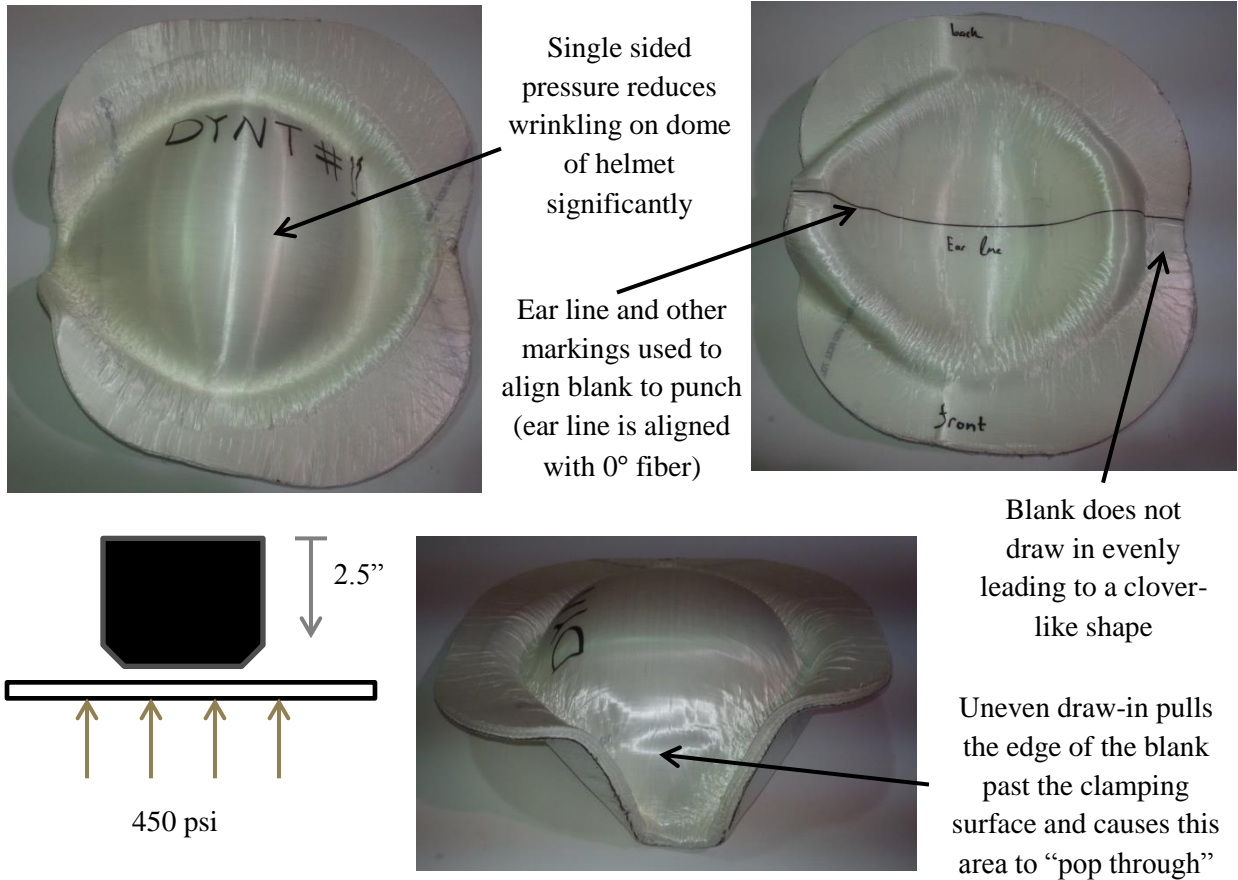


Figure 34 – Blank Formed with Single-Side Forming Pressure

It can clearly be seen in Figure 34 that even though the blank only popped through in one location, the blank was traversing a large gap around the entire circumference of the punch cavity. This gap can be seen on the blank as the trench that forms between the formed part and the clamped region. In these experiments, the maximum pressure obtained before decompression varied from ~150 psi (seen in Figure 33) all the way to above 450 psi. The depth the punch is drawn also varies between 2.5” and 3.5”. These relatively wide variances were the cause of changes in blank size and poor alignment of the punch to the blank.

It was observed that the blank appeared to draw-in the most along the orientations of the fiber reinforcements. This is expected because the fibers are stiffest in their axial direction and most compliant in the transverse direction. Since the blank is a laminate consisting of a layers oriented [0/90/0/90], we

expect that the in plane stiffness along the 0° and 90° orientations will be the greatest. This is shown in Figure 35.

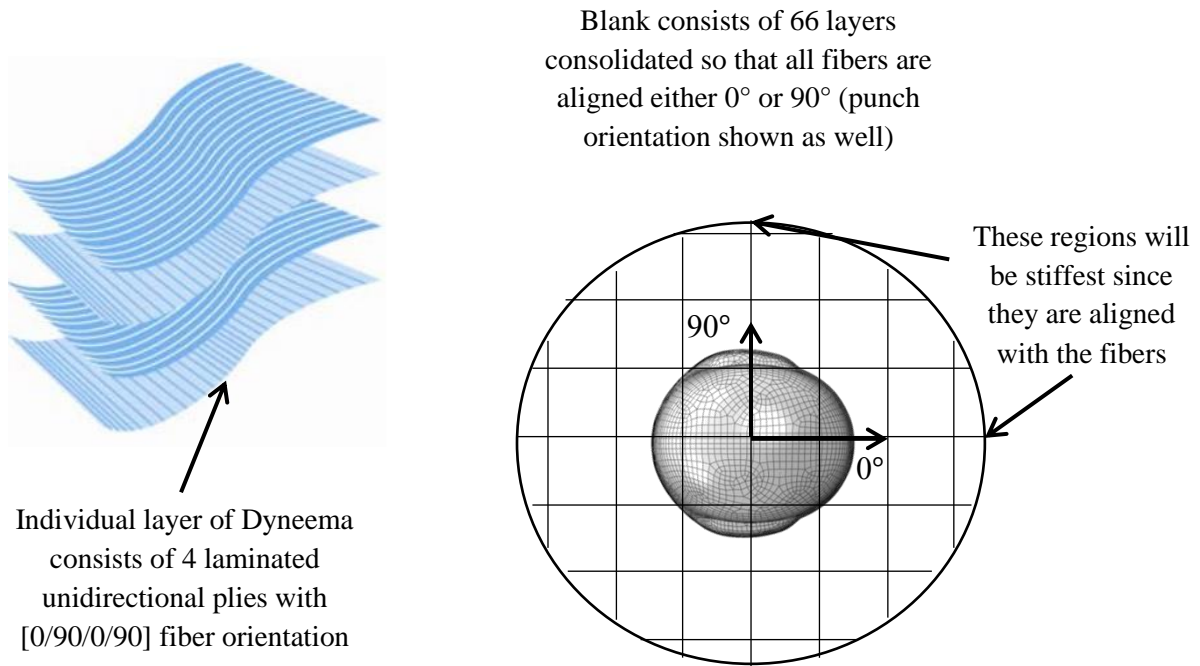


Figure 35 - Fiber Orientations of Dyneema Blank

Since the 0° and 90° orientations of the blank are the stiffest, we expect them to resist deformation during clamping the most, leading to greater draw-in around these areas. We would expect the material to be far more compliant in the 45° directions for two reasons. First, this direction is not aligned with the axis of the fiber. Second, the material has a tendency for the fibers to scissor over one another, leading to further increases in deformations. For these reasons we expect that the 45° orientations will draw-in very little.

This is exactly what we see in Figure 34. The ear line on the underside of the partially formed blank is aligned with the 0° fiber orientation leading to the blank popping through in this region. This also explains the clover shape that the circular blank takes on in the region that remains clamped. This continued to be an issue, even when larger 21.0" blanks were utilized.

Having identified the main issue as the blank drawing-in unevenly, an attempt was made to design a blank that would draw in evenly in order to maintain sufficient clamping area around the

circumference of the blank. A single blank was laid up using the stacking sequence $[0/45/0/45]_{16}$. Figure 36 shows the fiber orientations of this special blank.

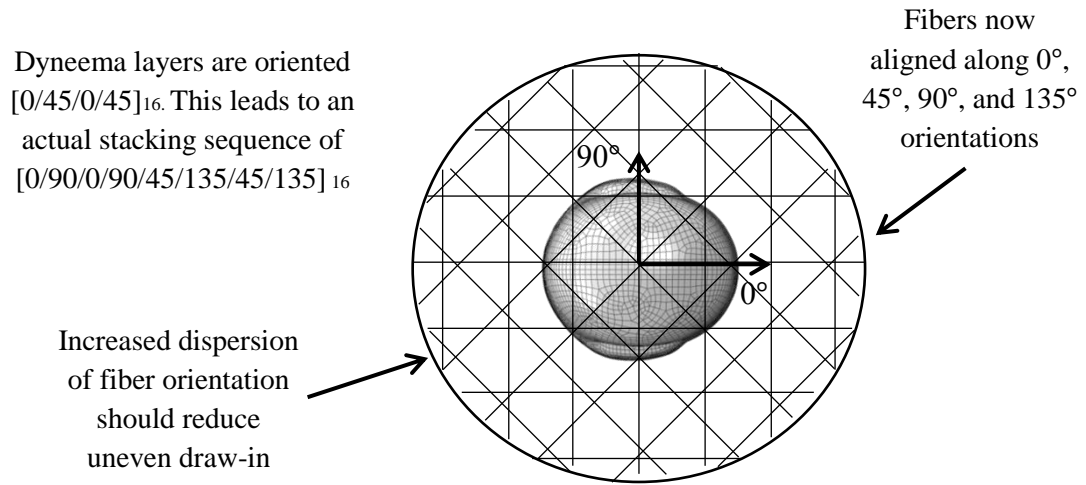


Figure 36 - Reducing Blank Anisotropy

The idea behind using this stacking sequence is to reduce the anisotropy of the blank in order to make it draw in more evenly. By reducing the unevenness of the blank draw-in, the hope was to increase depth of draw as well as forming pressure. The results of forming this blank can be seen in Figure 37.

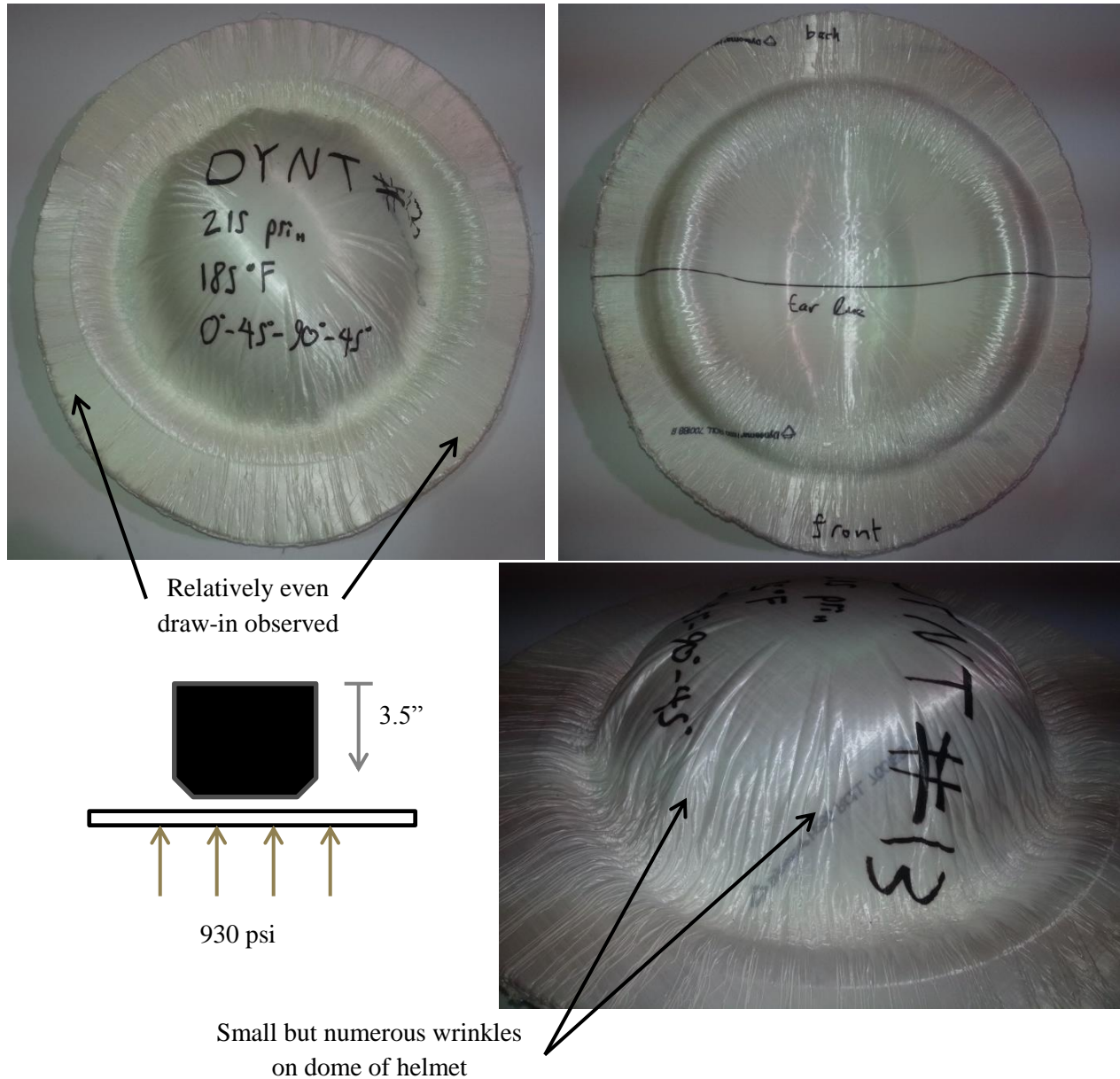


Figure 37 – Specialized Stacking Sequence

This blank was only drawn 3.5” to avoid popping the clamping arc of the blank into the upper zone. However, it appears that the punch could have been drawn further due to the large amount of blank clamping material remaining. It is because of this, that the forming pressure was able to be raised to its highest yet obtained value of ~930 psi. This exceptional forming pressure allowed the blank to be formed tight to the punch. This increased forming pressure is indeed necessary for forming parts of high quality and within tight tolerance.

This blank exhibited strange wrinkling patterns over the dome of the helmet that had not yet been previously observed. It was determined that these wrinkles were products of the abnormal stacking sequence used to form the blank. As the blank is formed to the shape of the punch, the adjacent material layers experience a similar deformation. However, due to their differing stiffness, stress levels are not the same. These differing stress levels do not satisfy force equilibrium and bend out of plane in order to do so. This out of plane bending is what we see all over the surface of the formed helmet. We do not see warping on the very top of the helmet because very little curvature is applied to the material in this area. Down the sides of the helmet we see increases in warping due to increases in both in plane strains and curvatures that are required to form the helmet to its final shape.

Several important discoveries were made during the experiments performed in phase 3. The most important discovery was that the gap between the punch and the clamping surface needs to be reduced in order to prevent the blank from popping through. It also appeared to be necessary to utilize larger blanks in order to prevent the loss of the pressurized fluid. This would lead to a complete redesign of the forming dies for the next phase of experiments. It was also discovered that the blanks will not draw in evenly due to their anisotropic material behavior. Additionally, the blank must be designed in a way that it allows the containment of the pressurized forming fluid as it is being drawn across the blank clamping surface.

Phase 4

This phase of experiments was performed on a completely new set of dies. These dies were designed to house circular blanks up to 30.0” in diameter. The gap between the punch and the clamping surface was drastically reduced and the lower zone die fluid cavity size was increased. These changes were made to the die design to reduce the amount of blank material that is bulged into the upper zone by the forming fluid and to increase the ease with which hydrostatic clamping can be initiated. The new die designs can be seen in Figure 17 and Figure 18.

The material used in this set of experiments is SR-3136 instead of Dyneema. The blank shape is also altered during this phase. CMA is used to predict the blank shape required for the helmet. The

stacking sequence was not altered due to fear of wrinkling behavior seen in Figure 37. The entire blank stack was rotated in order to see what orientation allowed for the smallest flat pattern. It was found that a 45° rotation minimized the overall blank shape. The blank shape predicted can be seen in Figure 38.

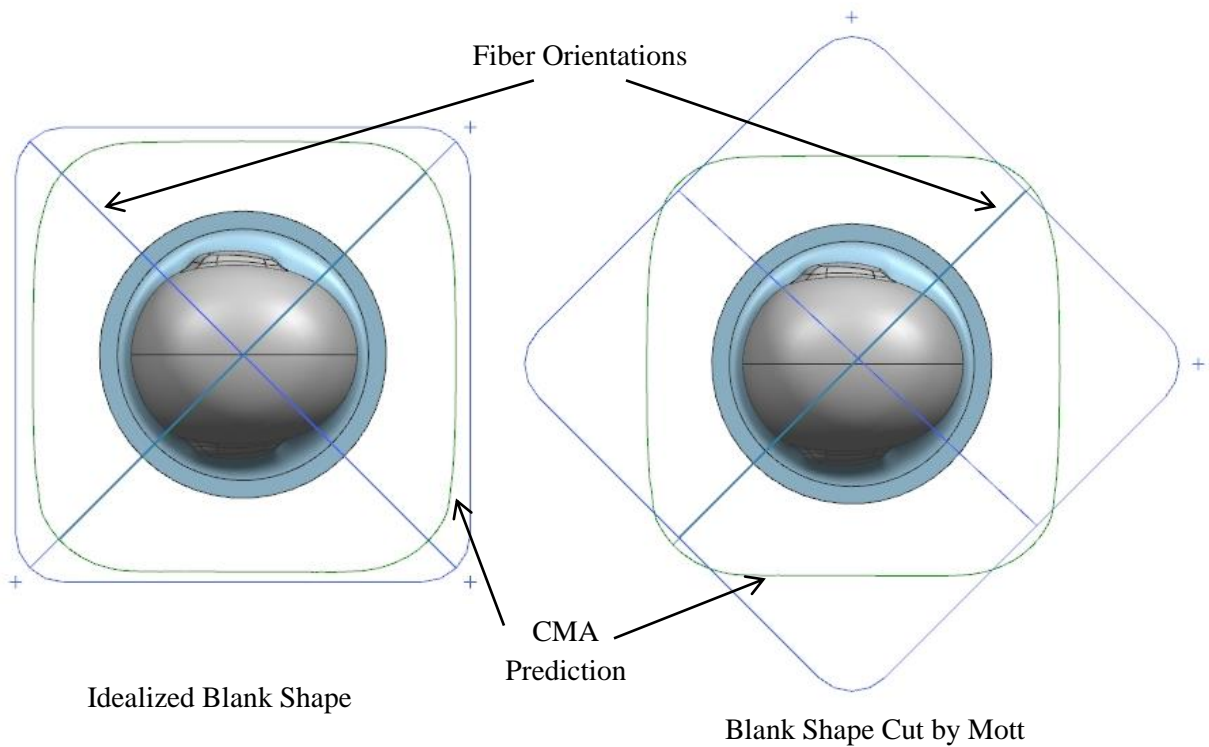


Figure 38 – CMA Predicted Blank Shape

The blank’s shape predicted by CMA is the inner rounded square seen in the figure above. The outer square represents the simplified blank shape that is easy to cut. The blank shape on the right is used due to difficulties with the cutting system utilized.

The leading issue experienced in this phase of forming is the difficulty to build pressure in the forming cavity when hydrostatic clamping is used. This has proven to be the leading issue in the thermo-hydroforming process. Pressurized fluid in the dies exerts force over every interior surface of the forming dies. The surface of concern is the upper zone die clamping surface. The pressure acting on this surface produces a force in the upward direction. This force must be matched by the 4 clamping rams on top of the press. If these rams cannot match the force applied to the upper zone die by the forming fluid pressure then they will be back driven causing the dies to open and relieving the forming pressure. If the applied

forces are not in equilibrium with one another, the upper zone die will be moved away from its desired location. This comparison can be seen in Figure 39.

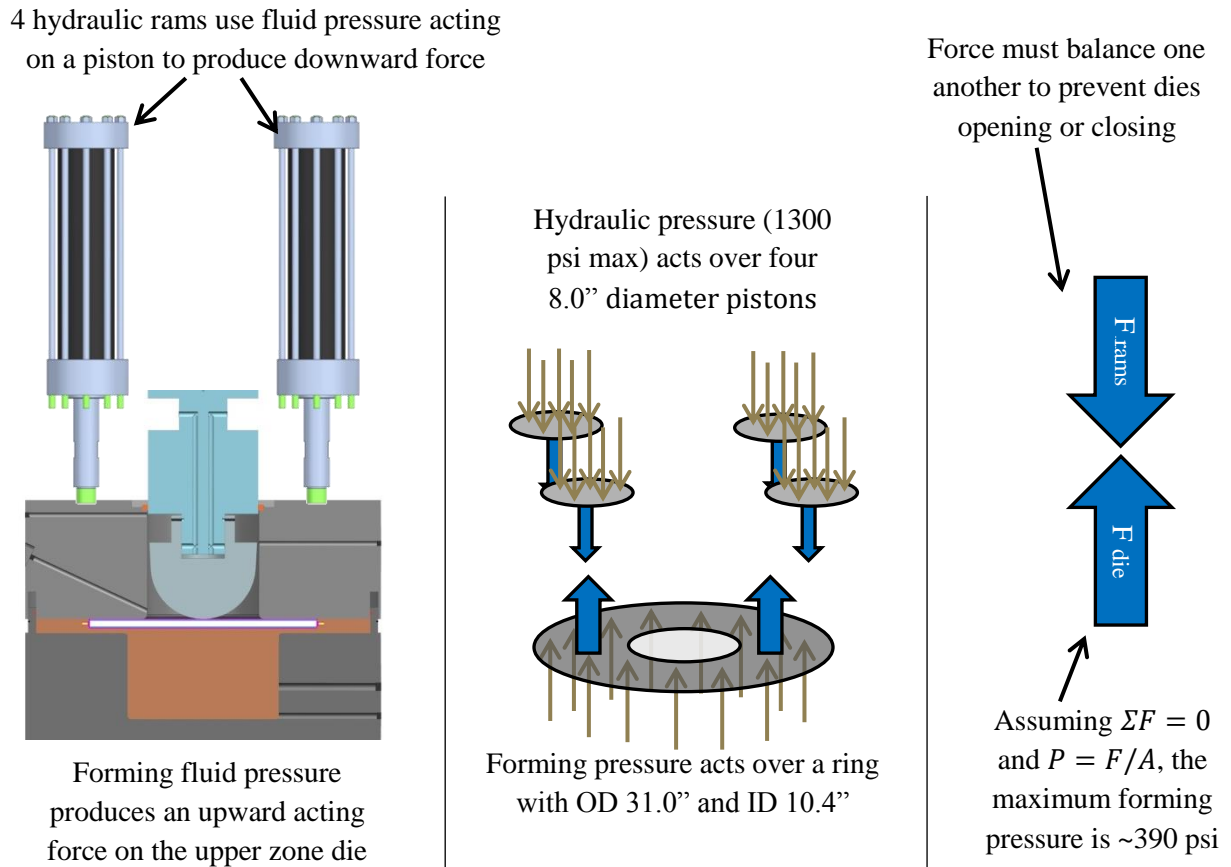


Figure 39 – Limited Forming Pressure

There are a few methods that can be used to increase the forming pressure. The easiest one is to increase the maximum operating hydraulic pressure that is supplied to the forming rams. As mentioned previously, the clamping rams used are not marked in any way and the maximum operating pressure is not known. If standard hydraulic equipment from a reputable company would have been used, the operating pressure of the rams would be around 3000 psi, increasing the maximum forming pressure to ~900 psi. Rams with larger pistons can be utilized, which allow the hydraulic fluid to act over a larger area. Similarly, a smaller upper zone die can be utilized in order to decrease the area that the forming pressure is acting over.

The forming experiment in this phase once again relies on the punch traversing downward to increase the forming pressure. As the calculation in Figure 39 indicates, this pressure produces an upwards force on the die that is far too great for the clamping rams to resist.

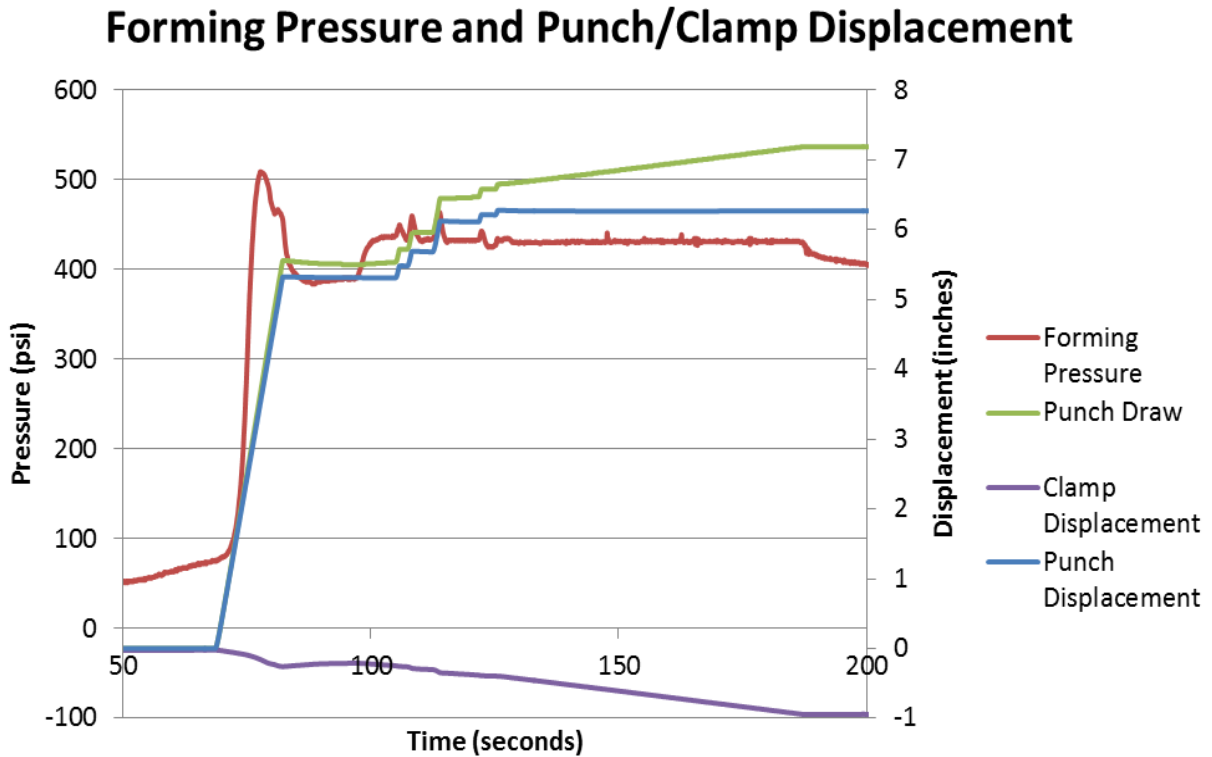


Figure 40 - Forming Pressure and Punch/Clamp Displacement

As we can see in Figure 40, the forming pressure peaks out at approximately 500 psi. After this, the clamp begins to displace since the rams cannot contain this high pressure. Around the 80 second mark, the pressure reduces to around 390 and the clamp does not displace any further. This is exactly what was predicted by the calculation performed in Figure 39, indicating a decent level of understanding of the systems hydraulics and limitations. Around the 100-second mark, the operator adjusted the downstream pressure regulator to not allow any fluid to escape, leading to a steady state pressure increase to around 430 psi. The punch displacement was then continued to around the 6.5” mark. At his point the pressure is held as well as the punch displacement. In can be seen that the clamp rams cannot resist this forming pressure and are slowly back driven as the experiment progresses (negative displacement is upwards).

Throughout the remainder of the experiment, the upstream pressure regulator is deadheading into the fluid cavity leading and driving the upper zone die upwards. The punch draw parameter appears to be creeping as well. The punch draw parameter (P to C) is calculated as the difference in displacement between the punch and clamp. Since the clamp is being driven backwards, the apparent displacement between the separate components appears to be increasing even though the punch is not moving within its own reference frame. Also important to note is that all displacement plots are normalized to 0 at the beginning of the forming experiment. So, Zero displacement for the clamp indicates the clamps displacement after hydrostatic clamping is initiated just prior to drawing the punch. Zero punch displacement indicates the punch's position just above the blank within the punch cavity before it is drawn through the blank.

The data acquisition indicates there are still issues with the operation of the press. However, the result is that the formed part has increased in quality. An example of a part formed in this phase is shown in Figure 41.

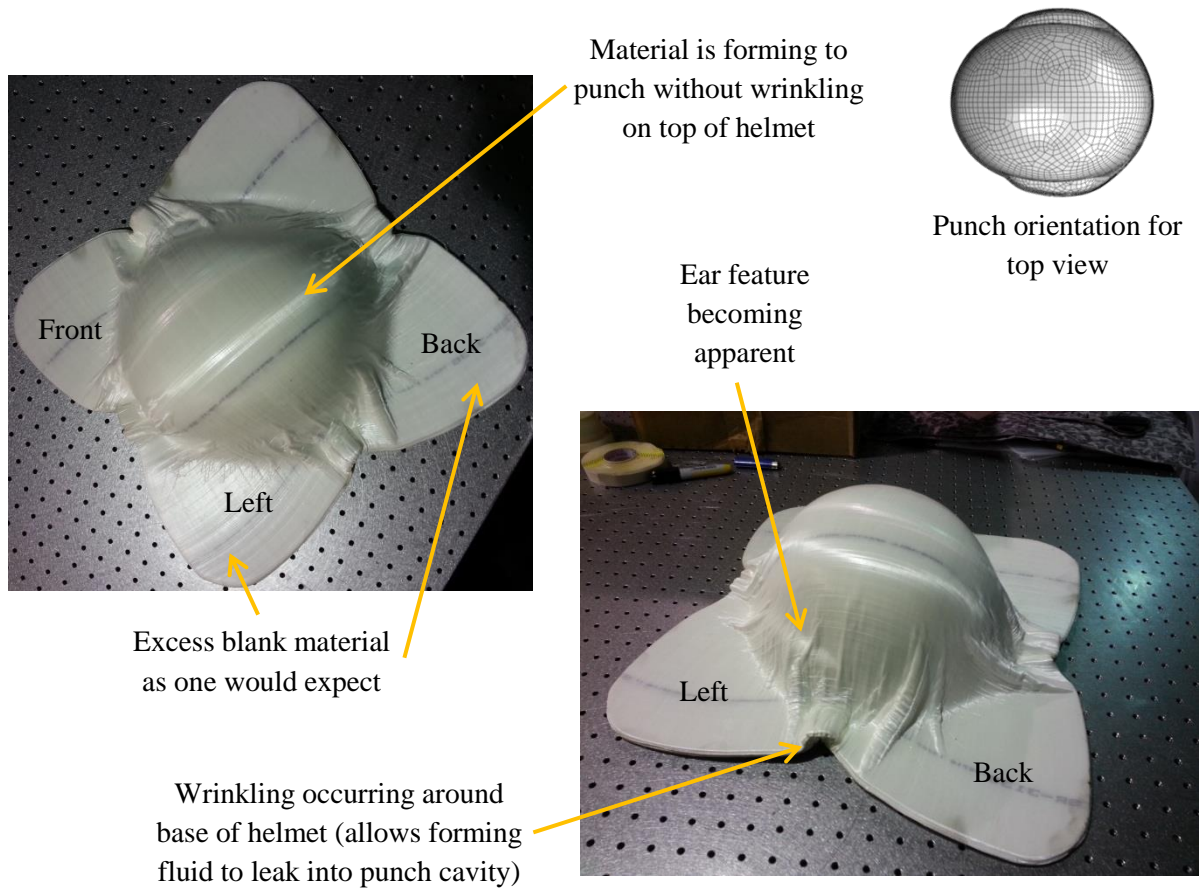


Figure 41 – Improvement in Results

The change in blank shape and orientation as well as the reduction in the gap between the clamping surface and the punch has allowed blanks to be formed at nearly the entire punch draw depth required (7.2” vs the needed 7.5”). This allows a more complete forming of the helmet where the finer features and details can be observed. Wrinkling around the base of the helmet is occurring where the blank has almost completely drawn to the base of the helmet. The more severe wrinkles lift the blank from the clamping surface and allow fluid to leak into the upper zone fluid cavity. Although the leak is not severe enough to cause a decrease in forming pressure, it does eventually starve the PPS reservoir. It is initially thought that these wrinkles could be ironed out with the use of greater forming pressure. However, these forming pressures cannot be obtained due to the issue with the clamping rams described above.

Additional experiments are performed with this clamping scheme. For the next trial the punch is drawn the full 7.5” to fully form the helmet. The results of this experiment can be seen in Figure 42

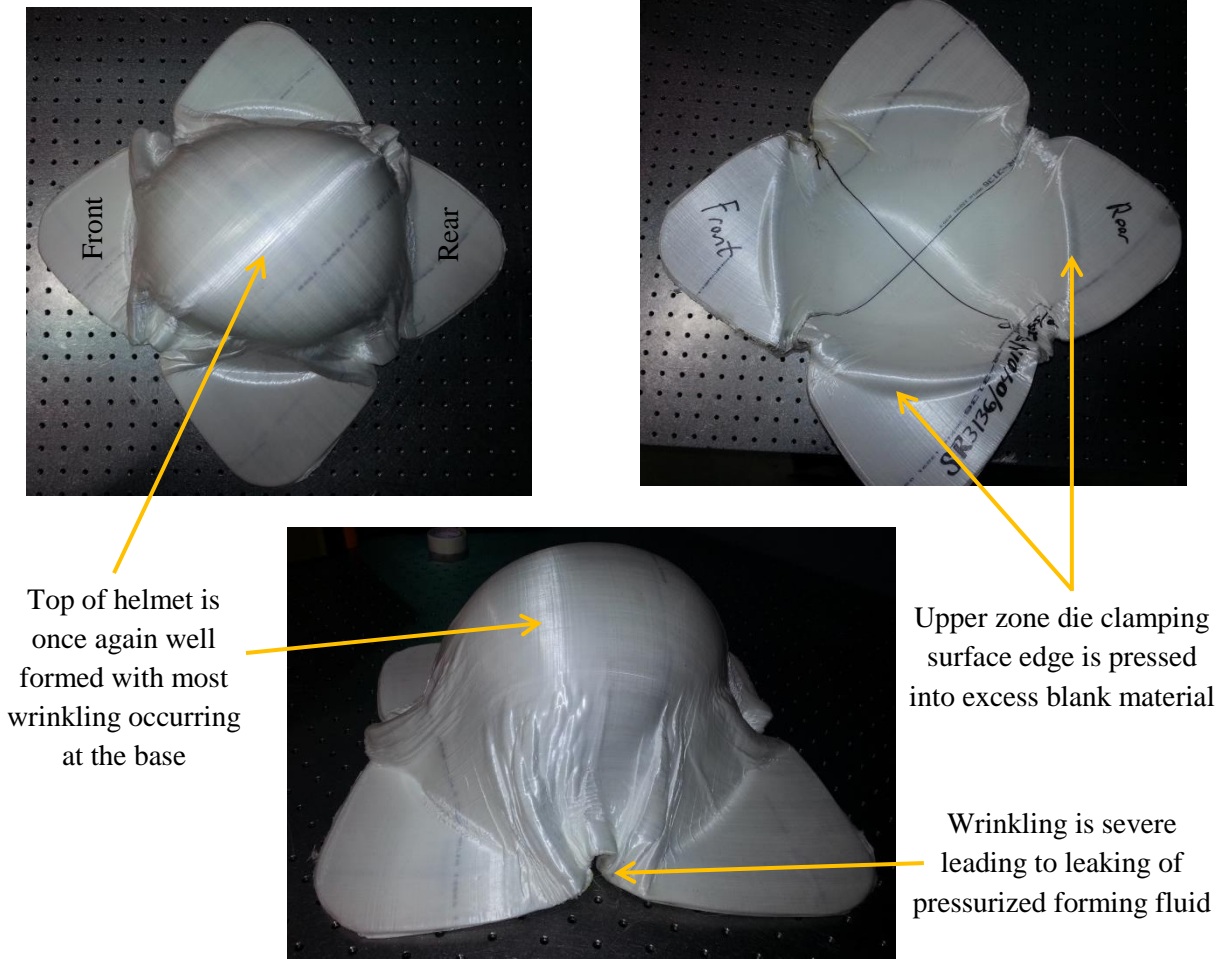


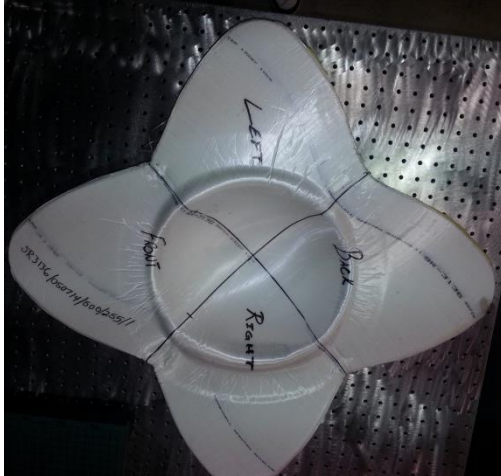
Figure 42 - Blank Lifting Problem

This blank was the first to be aligned using a laser alignment system. This helps ensure that the blank is perfectly aligned with the punch before forming it. This experiment reached a maximum pressure of ~430 psi. The material is conformed well to the top of the helmet, but once again, severe wrinkling occurs near the base of the helmet leading to the loss of fluid pressure. During this trial the circular edge of the upper zone die clamping surface can be seen. It is important to note that once the blank has been pulled past the edge of this circle, the pressurized fluid will not be contained within the fluid chamber any longer. This is exactly what we see in Figure 42, indicating that the blank is slightly undersized as was predicted earlier. It is also clear that hydrostatic clamping alone will not be able to prevent the blank from wrinkling especially at the base of the helmet where the critical seal that contains the pressurized fluid is formed.

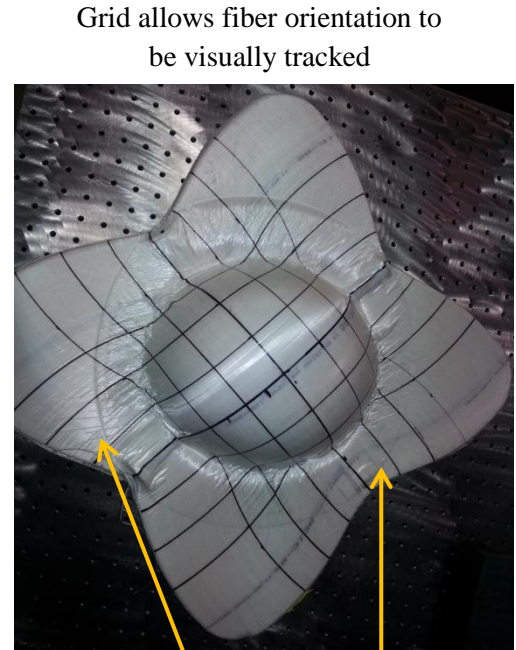
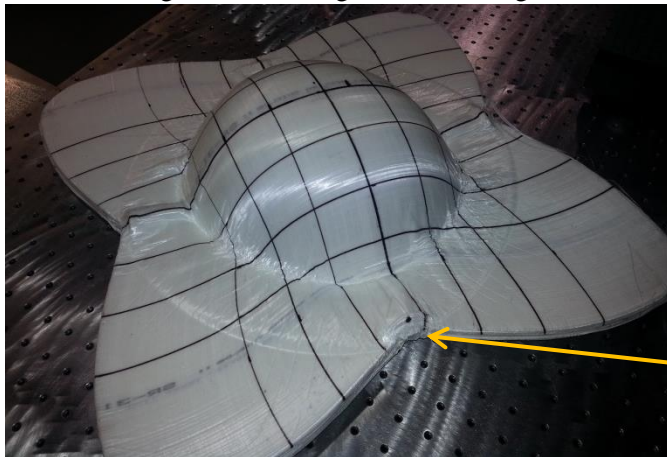
Physical clamping of the composite blank between the upper zone die and lower zone die was attempted in order to see if wrinkling at the base of the helmet could be eliminated. A slightly different forming procedure was used for this experiment and it is highlighted below.

1. The fluid cavity is filled with hot forming oil.
2. The pre-heated blank is placed in die and indexed to the punch using the alignment laser method.
3. The upper zone is lowered onto the punch and a 50 kip clamping load is applied. The punch is lowered until it is just above the blank.
4. The pressure in the fluid cavity is built to 150 psi. The downstream regulator is set to 100 psi to allow pressurized circulation.
5. The punch is drawn 6” through the material. Since the downstream regulator is set up to allow circulation, the decrease in the fluid cavity volume will not result in a pressure increase.
6. The forming pressure is increased to 1000 psi. The downstream regulator is set to 900 psi to continue pressurized circulation.
7. The punch is drawn the final 1.5” under this condition. This also stretches the blank helping to eliminate any wrinkles.
8. Pressurized circulation is continued until the part cools and solidifies.
9. Pressure is released and the part is recovered.

This process amendment is in the very early stages of development but it has already shown promising results as can be seen in Figure 43.



Blank is formed to upper helmet region with no signs of wrinkling



Grid allows fiber orientation to be visually tracked

Circle indicates boundary of fluid cavity and edge of clamped region

Blank barely drew in past lower zone fluid cavity

Figure 43 - Change in Clamping Scheme

Also, implemented during this stage of forming experiments is the grid on the top side of the blank. This grid is aligned with the fiber orientations of the blank. In the future, it will be used to track the amount of shear seen at different locations of the blank and compared to the results of the numerical simulations. As can be seen in the figure, the amount of wrinkling of the blank is significantly reduced. Only a few small areas of the blank show any wrinkling whatsoever. For this experiment, the punch was only drawn 4.5” to prevent the blank from drawing in past the punch cavity which would result in a loss of forming fluid. The maximum forming pressure was ~440 psi, well below the desired 1000 psi desired in the revised procedure. However, this pressure was able to conform the blank to the punch surprisingly well.

Ideally, the blank should not draw past the edge of the lower zone fluid cavity. If this can be accomplished, then the area being acted on by the pressurized fluid will be reduced to a circle of 14” in diameter. This significant reduction in area will allow increases in forming pressure with the rams being able to hold the upper zone die at a fixed position. As can be seen in Figure 43, a few small areas of the blank were pulled past this boundary allowing fluid to act over the full upper die clamping surface. This caused the upper die to be lifted which in turn initiated hydrostatic clamping. The operator was able to reduce the forming pressure, allowing upper zone to be traversed downward and reinitiate physical clamping.

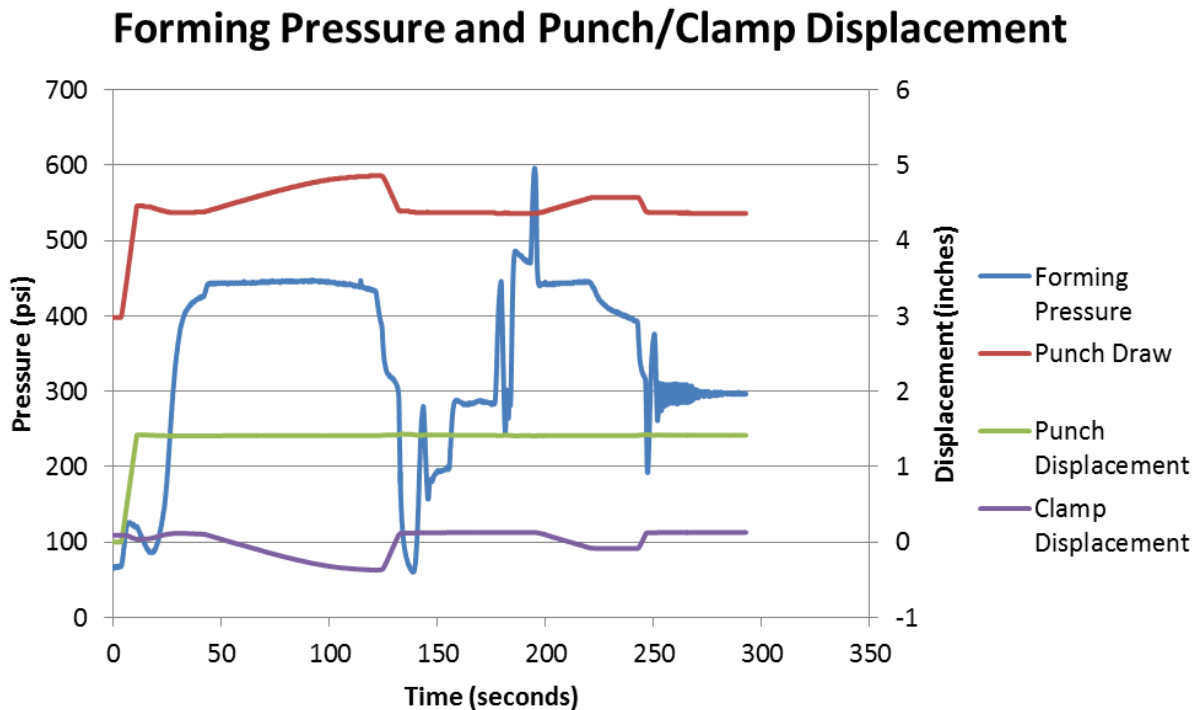


Figure 44 – Clamping Scheme Difficulties

It is hard to say whether physical clamping or coupled physical and hydrostatic clamping is the cause of the high quality results seen in the experiment. Further tests are required to determine the true reason for the success of this forming experiment.

Many important discoveries were made in this phase. Perhaps the most important discovery is that the use of physical clamping of the blank will not lead to tearing of the bladder system. It can also be

used to reduce the wrinkling of the blank over the clamping surface, eliminating the ability for the fluid pressure to leak into the punch cavity. It was also discovered that low forming pressures (around 450 psi) can produce high quality formed parts as can be seen in Figure 43. It was also discovered that the blank used is slightly too small for the helmet, at least in the press's current configuration. The ability to generate higher clamping loads can allow higher forming pressures to be used when hydrostatically clamping the blank. Increasing clamping load will more than likely require the replacement of the clamping rams.

Future Recommendations

The final sets of thermo-hydroforming experiments show that the process has the ability to form high quality parts. The helmet possesses complex geometry and is a very deep drawn structure. The abilities that the process has shown on such an advanced part indicate that this process can be used as a viable manufacturing method for parts with complex geometry. Forming parts of a simpler geometry can no doubt be accomplished seeing the results that have been produced initially.

The next set of forming experiments should investigate the effect of physical clamping as these were showing very impressive results after the first few attempts. Large blanks should be implemented for the initial forming experiments. Trying to form with an optimized blank before the process was well understood leading to several failed attempts that could have been surpassed. The hemispherical punch was not able to be used in this study but should be used in the future. This punch has a very simple geometry and allows for a simplified analysis of fiber shearing when comparing to numerical results.

The next round of modifications to the press should mostly be centered on the implementation of high pressure clamping rams. Additionally, a better computer controller needs to be implemented. During several experiments the operating pressure would differ drastically from the desired pressure producing a large error. During several experiments it would take up to 20 seconds before the regulators input voltage was adjusted, leading to long lag times and pressure oscillations. This issue appears to happen with the

downstream pressure regulator and could not be fixed by altering the PID parameter of the controller.
This issue should be fixed in the future for better pressure control.

Numerical Methods

Numerical simulations require a deep understanding of both the material properties of the laminated blank and the boundary conditions. The purpose of these simulations is to be able to develop a model which produces results that compare well with the experimental results. The goal of modeling the process is to be able to determine forming conditions and optimal blank shape so that the highest quality parts can be formed with minimal waste. First, a model of sufficient accuracy must be developed.

This chapter will summarize the material model and the changes made to it in order to improve its accuracy and increase practicality. The results of the simulations will be discussed and compared to experimental results that were obtained in the previous section.

Preferred Fiber Orientation (PFO) Material Model

The material model utilized in this study comes from the PhD dissertation of Mike Zampaloni [3]. This material model operates on the premise that a majority of a fiber reinforced composites stiffness comes from the fiber itself. A complex laminate or woven structure will possess many fiber orientations which all have an orientation in which they are stiffest and an orientation in which they are most compliant. The model tracks the orientation of these separate fibers and applies their stiffness to a global tensor in order to obtain the overall stiffness of the material. The model sets itself apart is its ability to update the fiber orientations as the body is deformed.

The Preferred Fiber Orientation (PFO) model uses a time marching explicit solver that calculates the change in fiber orientation for each time increment and updates the stiffness tensor accordingly. This model tracks the preferred fiber orientations and recalculates the stiffness tensor, allowing the materials response to be updated as the material deforms and fiber orientations change. Multiple fiber orientations can be tracked, allowing this material model to accurately characterize several types of composite materials, including biaxial weaves, triaxial weaves, unidirectional tapes, and even randomly oriented fiber mats.

Constitutive Model

Typically composite materials follow linear elastic deformation up to failure. UHMWPE composites are no different in this respect as is shown by Russell et al. [17]. This allows the individual fibers to be characterized as a linear elastic material. The stress-strain relation is given by Hooke's Law.

$$\sigma_{ij} = C_{ijkl}\epsilon_{kl} \quad (2)$$

When Hooke's Law is fully expanded, the 4th order stiffness tensor, C, contains 81 independent terms. Since the stress and strain are 2nd order tensors, the number of independent C terms is reduced to 36. The material stiffness is assumed to be symmetric, so the number of C terms is further reduced to 21 and can be displayed as such.

$$\begin{bmatrix} \sigma_1 \\ \sigma_2 \\ \sigma_3 \\ \sigma_4 \\ \sigma_5 \\ \sigma_6 \end{bmatrix} = \begin{bmatrix} C_{11} & C_{12} & C_{13} & C_{14} & C_{15} & C_{16} \\ C_{12} & C_{22} & C_{23} & C_{24} & C_{25} & C_{26} \\ C_{13} & C_{23} & C_{33} & C_{34} & C_{35} & C_{36} \\ C_{14} & C_{24} & C_{34} & C_{44} & C_{45} & C_{46} \\ C_{15} & C_{25} & C_{35} & C_{45} & C_{55} & C_{56} \\ C_{16} & C_{26} & C_{36} & C_{46} & C_{56} & C_{66} \end{bmatrix} \begin{bmatrix} \epsilon_1 \\ \epsilon_2 \\ \epsilon_3 \\ \epsilon_4 \\ \epsilon_5 \\ \epsilon_6 \end{bmatrix} \quad \text{where} \quad \begin{bmatrix} \sigma_1 \\ \sigma_2 \\ \sigma_3 \\ \sigma_4 \\ \sigma_5 \\ \sigma_6 \end{bmatrix} = \begin{bmatrix} \sigma_{xx} \\ \sigma_{yy} \\ \sigma_{zz} \\ \sigma_{yz} \\ \sigma_{xy} \\ \sigma_{xy} \end{bmatrix} \quad \text{and} \quad \begin{bmatrix} \epsilon_1 \\ \epsilon_2 \\ \epsilon_3 \\ \epsilon_4 \\ \epsilon_5 \\ \epsilon_6 \end{bmatrix} = \begin{bmatrix} \epsilon_{xx} \\ \epsilon_{yy} \\ \epsilon_{zz} \\ \epsilon_{yz} \\ \epsilon_{xy} \\ \epsilon_{xy} \end{bmatrix} \quad (3)$$

The stiffness tensor as it exists in this form can be further reduced by the assumption that the material is orthotropic. An orthotropic material contains 3 planes of elastic symmetry. This means that the material will have a unique stiffness in each of its three principal directions. This simplification dictates that when a normal strain is applied, only normal stresses will be generated (no shear-extension coupling). The application of shear strains within the planes of symmetry will only produces shear stresses within this plane and no normal stress (no shear-shear coupling). This allows the stiffness tensor C to be reduced even further.

$$\begin{bmatrix} \sigma_1 \\ \sigma_2 \\ \sigma_3 \\ \sigma_4 \\ \sigma_5 \\ \sigma_6 \end{bmatrix} = \begin{bmatrix} C_{11} & C_{12} & C_{13} & 0 & 0 & 0 \\ C_{12} & C_{22} & C_{23} & 0 & 0 & 0 \\ C_{13} & C_{23} & C_{33} & 0 & 0 & 0 \\ 0 & 0 & 0 & C_{44} & 0 & 0 \\ 0 & 0 & 0 & 0 & C_{55} & 0 \\ 0 & 0 & 0 & 0 & 0 & C_{66} \end{bmatrix} \begin{bmatrix} \epsilon_1 \\ \epsilon_2 \\ \epsilon_3 \\ \epsilon_4 \\ \epsilon_5 \\ \epsilon_6 \end{bmatrix} \quad (4)$$

Individual layers of composite materials are modeled, allowing a plane stress is assumption. Their thickness prevents out of plane stresses from becoming prominent and allows for their removal from the

stiffness tensor. Assuming the thickness of the composite is in the z-direction, this allows the removal of any z terms which correspond to the 3rd, 4th and 5th rows and columns of the C tensor in equation 4.

$$\begin{bmatrix} \sigma_1 \\ \sigma_2 \\ \sigma_6 \end{bmatrix} = \begin{bmatrix} Q_{11} & Q_{12} & 0 \\ Q_{12} & Q_{22} & 0 \\ 0 & 0 & Q_{66} \end{bmatrix} \begin{bmatrix} \epsilon_1 \\ \epsilon_2 \\ \epsilon_6 \end{bmatrix} \quad (5)$$

The formulation of the reduced stiffness tensor, Q , has, up to this point, assumed that the material reference frame (1, 2, 3) has been aligned with the structural reference frame (x, y, z). These reference frames do not always align which requires the use of distinct notation in order to avoid confusion. The 1-direction of the material reference frame is always aligned with the fiber orientation, while the 2-direction is transverse to the fiber direction but still within the plane of the material. The structural frame rotates with the body of interest while the material frame rotates with the fiber orientation. This can be seen in Figure 45.

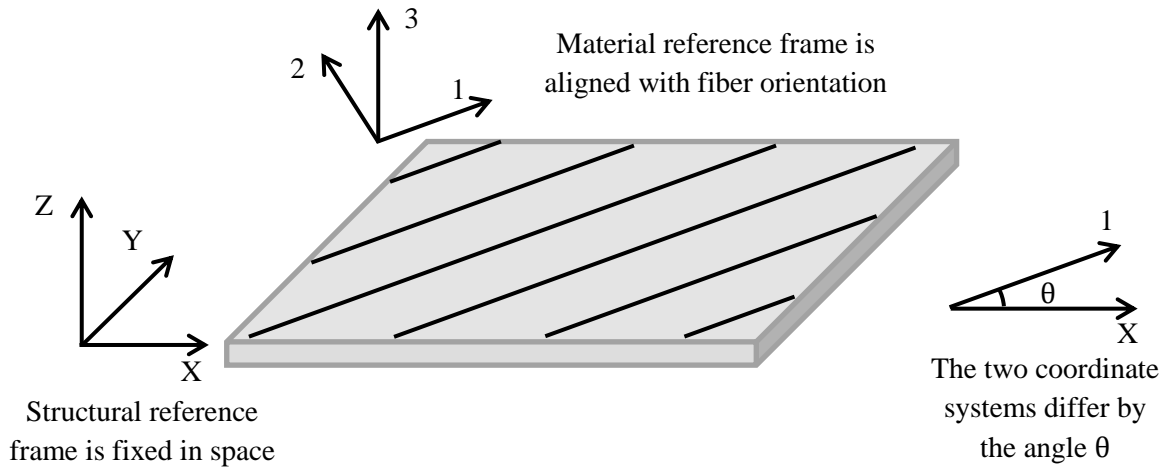


Figure 45 – Material and Structural Coordinate Systems

The best way to define stiffness components is to align them with the material coordinate system. By doing this, the material properties have a deeper physical meaning due to their alignment with the reinforcing fiber structures giving the following stiffness components.

$$Q_{11} = \frac{E_{11}}{1-\nu_{12}\nu_{21}} ; Q_{22} = \frac{E_{22}}{1-\nu_{12}\nu_{21}} ; Q_{12} = \frac{\nu_{12}E_{11}}{1-\nu_{12}\nu_{21}} ; Q_{66} = G_{12} \quad (6)$$

E_1 is the elastic modulus of the material measured along the fiber orientation. E_2 is the stiffness of the material measured transverse to the fiber orientation. ν_{12} is Poisson's Ratio based on the 1, 2, 3

coordinate system. G_{12} is the shear modulus based on this coordinate system as well. Based on this adjustment, equation 5 needs to be reformed in order to give the stresses and strains in terms of the material coordinate system and not the structural coordinate system.

$$\begin{bmatrix} \sigma_{11} \\ \sigma_{22} \\ \tau_{12} \end{bmatrix} = \begin{bmatrix} Q_{11} & Q_{12} & 0 \\ Q_{12} & Q_{22} & 0 \\ 0 & 0 & Q_{66} \end{bmatrix} \begin{bmatrix} \epsilon_{11} \\ \epsilon_{22} \\ \gamma_{12} \end{bmatrix} \quad (7)$$

The stiffness matrix can be condensed and written simply as Q_{ij} . Now that the constitutive relation has been related to the material frame, the stiffness needs to be able to be related back to the structural frame to provide a common reference point. A transformation matrix based on the stiffness tensor is used.

$$T(\theta) = \begin{bmatrix} m^2 & n^2 & -2mn \\ n^2 & m^2 & 2mn \\ mn & -mn & m^2 - n^2 \end{bmatrix} \text{ where } m = \cos \theta \text{ and } n = \sin \theta \quad (8)$$

The stiffness in terms of the structural frame can then be solved for by performing a change of basis operation.

$$\overline{Q}_{ij} = T Q_{ij} T^T = \begin{bmatrix} \overline{Q}_{11} & \overline{Q}_{12} & \overline{Q}_{16} \\ \overline{Q}_{12} & \overline{Q}_{22} & \overline{Q}_{26} \\ \overline{Q}_{16} & \overline{Q}_{26} & \overline{Q}_{66} \end{bmatrix} \quad (9)$$

\overline{Q}_{ij} is the stiffness of the material rotated to the global frame. T^T is the transpose of T . Now that the stiffness in the material frame is known, it is possible to calculate the stress in the global frame.

$$\sigma = \overline{Q} \epsilon \quad (10)$$

Similarly, the strain in the material frame can be found if the stress is known using the compliance tensor.

$$\epsilon = \overline{S} \sigma \text{ where } \overline{S} = \overline{Q}^{-1} \quad (11)$$

Obtaining Material Properties

Now that the constitutive model has been developed the stiffness matrix, Q_{ij} , must be populated. The constants E_{11} , E_{22} , ν_{12} and G_{12} are required in order to fully characterize the stiffness matrix in equation 8. All of these constants can either be measured directly (as was performed in the Material Characterization section) or can be calculated using accepted relations such as the various rules of

mixtures. This section will review the various ways in which the engineering constants can be calculated and discuss their shortcomings.

E_{11} is the Young's Modulus of the unidirectional composite measured in the direction of the fibers. The classical approach in determining this constant is to use the rule of mixtures.

$$E_{11} = E_f V_f + E_m (1 - V_f) \quad (12)$$

E_f and E_m are the Young's Moduli of the fiber and matrix components specifically. V_f is the fiber volume fraction of the composite it represents the percent volume of the composite that is fiber. The calculation $(1 - V_f)$ is used to calculate the matrix volume fraction V_m . This leads to a zero void assumption.

$$V_f + V_m = 1 \quad (13)$$

In reality, even the highest quality composites contain voids so equation 14 is highly idealized. This leads to inaccuracies when using equation 12 but generally they are small. Furthermore, equation 13 assumes perfect bonding between the fiber and matrix constituent. Equation 14 takes into account continuity of mass and is presented by Mohammed et al. [38].

$$V_f = \frac{V_{fo}}{\sin \alpha} \quad (14)$$

V_{fo} is fiber volume fraction prior to deformation and α is the angle between the a-fiber and the b-fiber assuming that they are orthogonal to one another prior to deformation.

Generally, these void free and perfect bonding assumptions introduce error but it is usually small enough to be ignored. In UHMWPE composites, void fractions have been reported in excess of 10% [39]. Additionally, the bond between UHMWPE fiber and a PE matrix is shown to be weak at best, leading to issues with the perfect bonding assumption. Nevertheless, the rule of mixtures gives a ballpark estimation as the longitudinal stiffness that should be expected.

E_{22} is the transverse Young's Modulus and represents the stiffness of the material when loaded transverse to the fiber axis. The simplest calculation to determine this constant is with the inverse rule of mixtures.

$$E_{22} = \left(\frac{V_f}{E_f} + \frac{1-V_f}{E_m} \right)^{-1} \quad (15)$$

This equation makes the same assumptions as the rule of mixtures of equation 12, leading to errors. Okoli developed an empirical relation based on the Halpin-Tsai equation for E_{22} [40]. This equation shows reductions in error when compared with experimental results.

$$E_{22} = E_m \left(\frac{1+ABV_f}{1-B\psi V_f} \right) \quad (16)$$

This equation contains several nested relations and values which can be seen in equation 17.

$$\psi = 1 + V_f \frac{1-\theta_m}{\theta_m^2} ; B = \frac{\frac{E_f}{E_m} - 1}{\frac{E_f}{E_m} - A} ; A = 0.5 ; \theta_m = 0.82 \quad (17)$$

These equations are configured to work with random fiber orientations reducing their accuracy when used with unidirectional tapes.

Poisson's ratio is found using a simple rule of mixtures as is presented by Mohammed [38].

$$\nu_{12} = \nu_f V_f + \nu_m (1 - V_f) \quad (18)$$

ν_{21} is found through a relation taking into account the longitudinal and transverse Young's Modulus.

$$\nu_{21} = \frac{E_{22}}{E_{11}} \nu_{12} \quad (19)$$

The shear modulus can be found via several methods. The simplest one involves a simple rule of mixtures approach.

$$G_{12} = \left(\frac{V_f}{G_f} + \frac{1-V_f}{G_m} \right)^{-1} \quad (20)$$

Halpin and Tsai propose another method to empirically determine the shear modulus [41].

$$G_{12} = G_m \left(\frac{1+\xi\eta V_f}{1-\eta V_f} \right) \quad (21)$$

Much like equation 16, equation 21 contains many nested variables and factors which can be seen below.

$$\eta = \frac{\frac{G_f}{G_m} - 1}{\frac{G_f}{G_m} - \xi} ; \xi = 5 + 10^5 V_f^{10} \quad (22)$$

The ξ term in equation 23 is presented separately by Okoli and Smith [40]. This term is once again based on a randomly oriented fiber structure and leads to errors when used with unidirectional tapes. Many of these empirical relations lead to poor predications of the engineering constants needed for the stiffness tensor Q_{ij} . They would be modified to fit the expected trends and would eventually be replaced by direct material characterization. This process will be further described in the Use of Material Characterization Data section.

Preferred Orientations

The constitutive relation developed in the previous sections is able to accurately characterize a unidirectional material. As seen in Figure 35, the UHMWPE composites utilized in this study (both Dyneema and Spectra Shield) consist of numerous layers of orthogonally stacked unidirectional composite layers. The stiffness tensor of the laminated composite can be assumed to be the sum of the stiffness tensors of the two separate fiber orientations. In this case the fiber orientations are oriented in the 0° and 90° directions (classified as the a-fiber direction and the b-fiber direction respectively). These orientations are orthogonal to one another in the undeformed setting. It is not necessary that these orientations remain orthogonal to one another as the laminate is deformed. Figure 46 shows the summation of the a-fiber and the b-fiber to yield the laminated material stiffness.

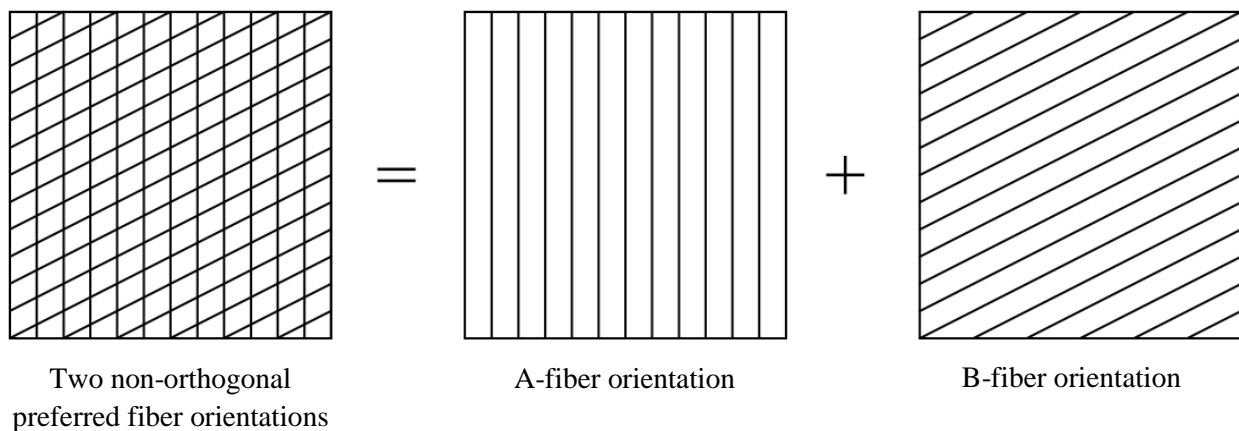
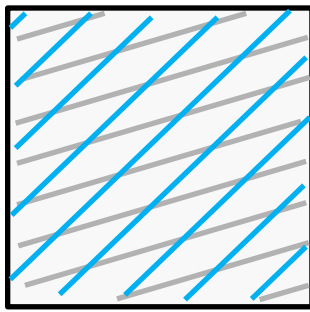


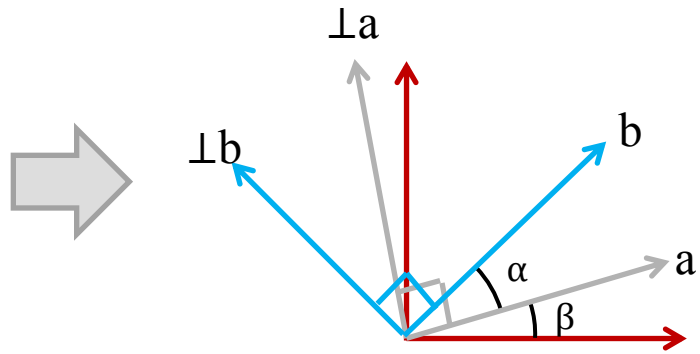
Figure 46 – Stiffness Summing Used in PFO Model

Additional fiber orientations may be utilized if the material cannot be adequately characterized by two preferred orientations. Randomly oriented fiber mats, tri-axial weaves and unidirectional layups where the fibers have three or more orientations in the stacking sequence are examples of materials that can benefit from the use of additional PFOs. Determining the fiber orientations is an easy task when the materials used have highly regular and repeated orientations such as with woven fabrics and unidirectional layups with a repeated stacking sequence. With other materials, the PFO's may not be obvious such as with random mat orientations. A squeeze flow test was developed by Zampaloni that can be used to determine the preferred orientations [3].

The materials in order to sum the stiffness of the individual PFO's, a common structural frame must be utilized. The stiffness tensors of the individual fiber orientations in the structural frame are obtained using equation 7. The stiffness tensors are then rotated to the common structural frame with equation 8. Once the individual PFO's have been rotated to the common structural frame they can be summed in order to determine the materials stiffness. This method is highlighted in Figure 47.



Composite material with two obvious fiber orientations



Each fiber orientation is assigned its own material coordinate system and a common structural coordinate system is set (red)

$$\bar{Q}_{ij} = \bar{Q}_{ij}^a + \bar{Q}_{ij}^b$$

Laminate stiffness is found by summing rotated stiffness tensors

$$\bar{Q}_{ij}^a = T(\beta)Q_{ij}T(\beta)^T$$

$$\bar{Q}_{ij}^b = T(\alpha + \beta)Q_{ij}T(\alpha + \beta)^T$$

Stiffness is calculated for each PFO and rotated to the material frame

Figure 47 – Rotation of PFO’s to the Structural Frame

The method highlighted in Figure 47 is used to find the stiffness of a composite laminate. The fiber orientations are typically known at the beginning of a numerical simulation, allowing the stiffness to be updated throughout the simulation.

As one would expect, changes to the angles α and β will change the transformation matrix T . Alteration of the transformation matrix results in the alteration of the laminate stiffness \bar{Q}_{ij} leading to a changes in behavior of the laminate such as increased stiffness in a particular direction or the introduction of shear-extension coupling. These changes have a profound effect on how the material will deform and therefore must be taken into account. Consider a small differential element of laminated composite material with a-fiber and b-fiber directions as well as its own structural coordinate system. This material

is acted on by an arbitrary deformation gradient tensor. Polar decomposition of the deformation yields a stretch tensor and a rigid body rotation tensor.

$$F = RU \tag{23}$$

F is the deformation gradient tensor, R is an orthogonal tensor representing a rigid body rotation and U right stretch tensor. This deformation gradient acts on the differential element by stretching and rotating it. The structural coordinate system is acted on by the rotation tensor (R) in order to remain aligned with the element and still provide an orthogonal coordinate system. The a-fiber and b-fiber directions are acted on by the stretch tensor and the rotation tensor (RU), which alters the angles that these fiber directions make with respect to the material coordinate system. This can be seen in Figure 48.

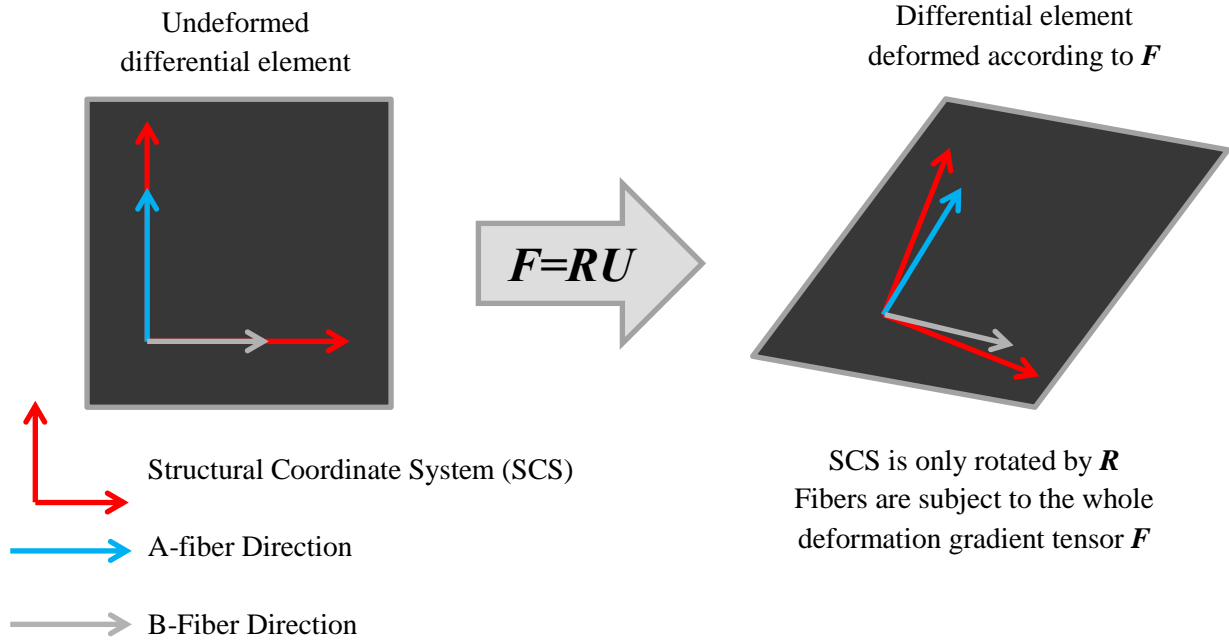


Figure 48 – Modification of the Structural Coordinate System and Fiber Orientations

In this example the fibers are aligned with the SCS in their undeformed configuration. The deformation gradient tensor alters their alignment with the SCS, which in turn alters the stiffness of the differential element.

Implementation in Abaqus

This scheme is implemented in Abaqus explicit through a user subroutine. The explicit solver uses a time marching scheme allowing the strain increment, deformation gradient tensor to be fed into the subroutine during each step. The user subroutine uses the deformation gradient tensor to determine how the SCS and the fiber orientations are changed during the current time step as was shown in Figure 48. Once this is determined, the stiffness (Q_{ij}^a) of the PFO is determined. Next, the stiffness is rotated to the structural frame, giving \bar{Q}_{ij}^a . This is repeated for each PFO. Once all the PFO stiffness are rotated to the material frame, they are summed to obtain \bar{Q}_{ij} . The strain increment is then multiplied by the stiffness giving the stress increment for the time step. This information is fed back into the Abaqus solver. A flow chart of this process can be seen below.

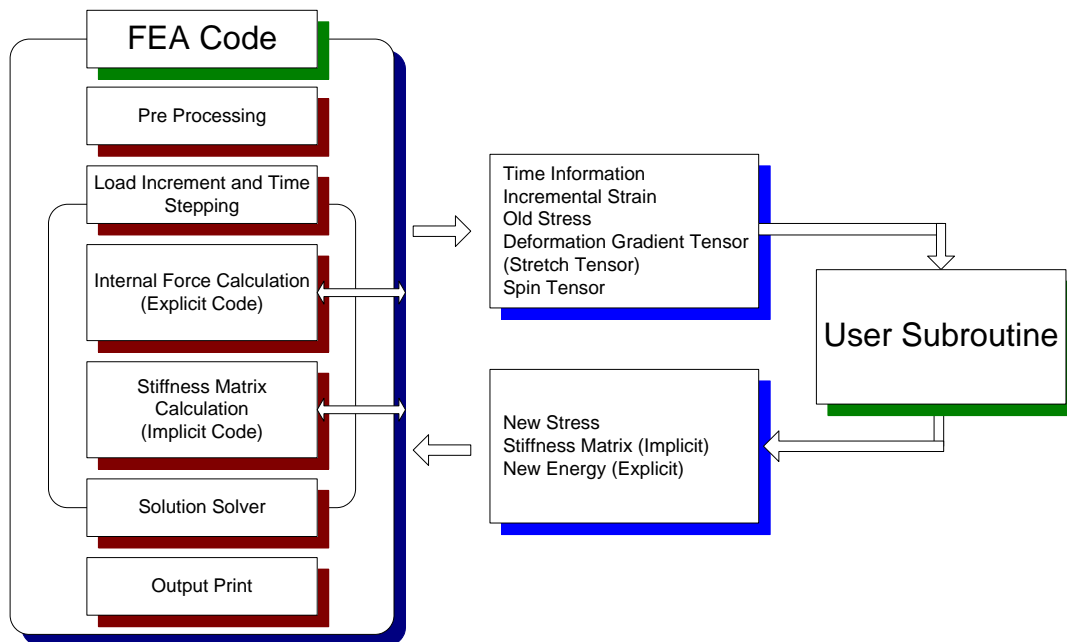


Figure 49 – User Subroutines Within Abaqus/CAE

The elements of the hydroforming press are implemented as rigid bodies. The blank is comprised of 6 layers of shell elements tied together by cohesive interactions.

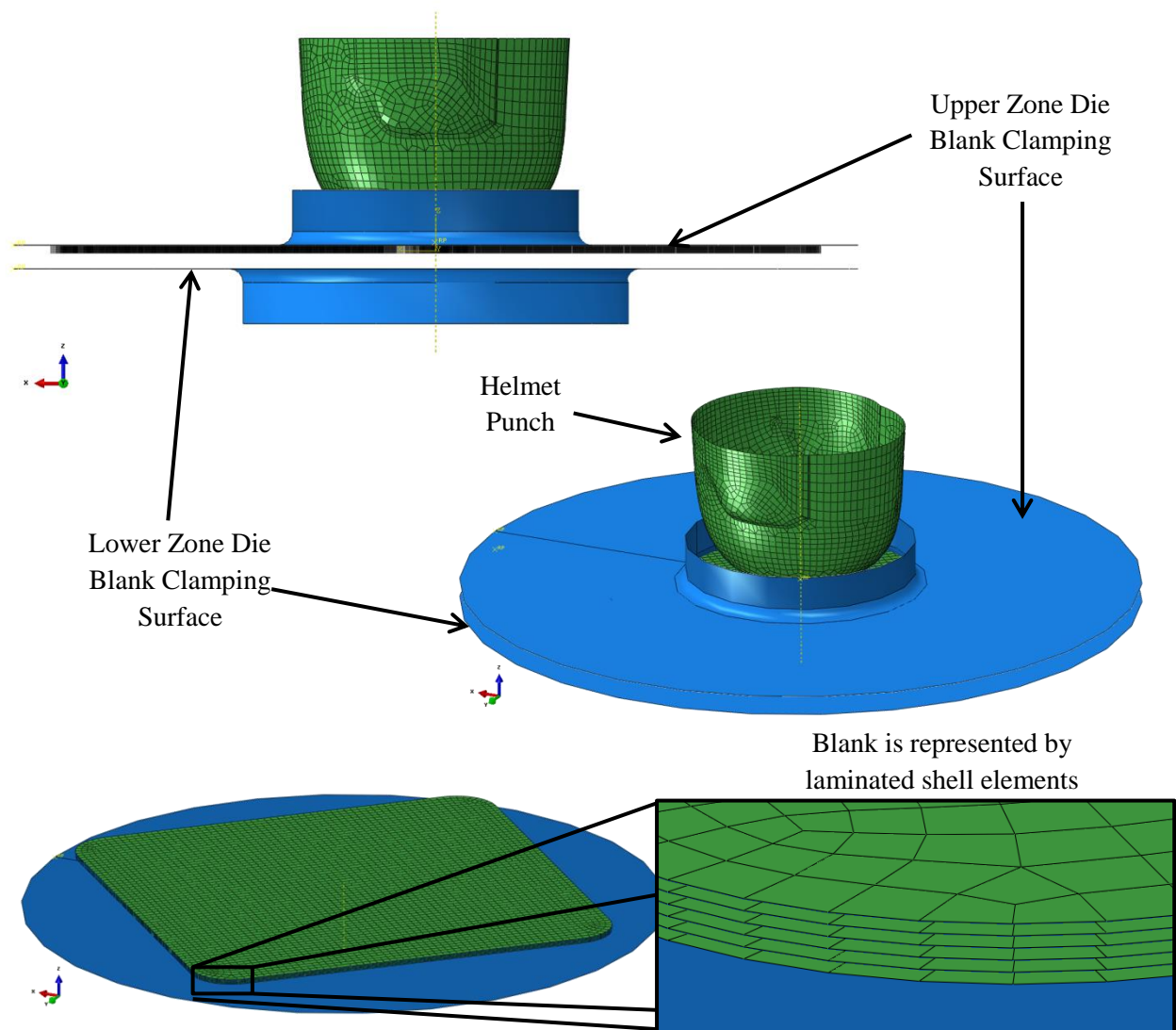


Figure 50 - Model Setup

Simulation Changes and Adaptions

The model displayed several short comings at the beginning of the study, the most prominent of which was its inability to simulate a blank of thickness required for the helmet forming project. The transverse shear stiffness was incorrectly defined and it was also found that the transverse Young's

modulus and the shear modulus were significantly over-predicted. This led to the numerical simulation giving poor results.

Originally, the composite materials simulated using this model were one or two layers thick and could be idealized as a single layer with minimal voids. This allowed the use of many of the rules of mixtures equations to predict the response of the composite relatively accurately. In this study increased blank thickness as well as a different composite system do not allow the use of these simplifying assumptions.

Multiple Layer Simulation

The Spectra Shield blanks used in the forming experiments consist of 45 layers of SR-3136 which consist of 4 plies a piece. In actuality, the composite consists of 180 layers of unidirectional composite material with a layup sequence $[0/90]_{90}$. To simulate each one of these layers individually would be computationally expensive. Instead, the simulations utilize 6 layers of shell elements (plane stress elements) that are tied together using cohesive surface interactions.

One of the biggest problems when attempting to model this thick blank as a single layer is a very coarse mesh. In order to use the thin shell theory, the shell elements must have a length to thickness ratio of 10:1 or greater. By using a single layer of shell elements, a very coarse mesh would need to be utilized. Even if these large elements used quadratic shape functions, they would give very poor predictions for stress, strain and every other field variable. Therefore, multiple layers must be used, not just to simulate the effect inter-laminar separation but also to refine the mesh in order to obtain accurate results.

The cohesive surfaces interaction uses the fracture mechanics principal of traction-separation in order to take into the adhesive forces that hold the separate layers of the blank together. Similar methods have been used to simulate adhesive bonds in composites [42], [43]. Principals of elasticity and plasticity are utilized in order to determine crack growth along a predetermined path. An applied force can initiate crack growth in three ways as can be seen in Figure 51.

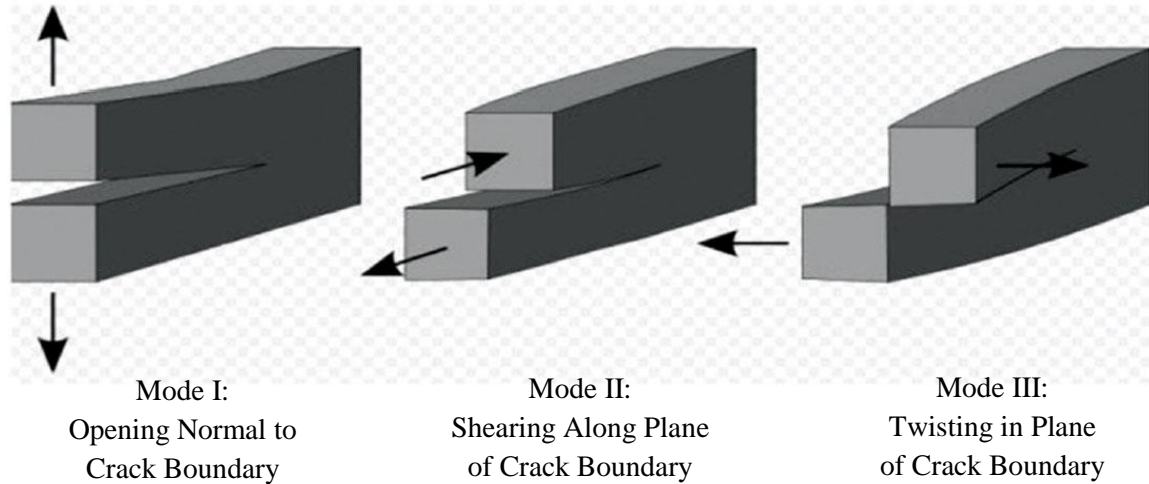


Figure 51 – Fracture Modes

As cracks open, a measurable separation between the two sides of the crack form. As the crack grows, traction attempts to return the crack to its initial closed position. This traction is a linear function of the separation and is represented in matrix form.

$$\begin{bmatrix} t_n \\ t_s \\ t_t \end{bmatrix} = \begin{bmatrix} K_{nn} & K_{ns} & K_{nt} \\ K_{ns} & K_{ss} & K_{st} \\ K_{nt} & K_{st} & K_{tt} \end{bmatrix} \begin{bmatrix} \delta_n \\ \delta_s \\ \delta_t \end{bmatrix} \quad (24)$$

The subscripts n , s and t refer to fracture modes I, II and III respectively. The K_{nn} , K_{ss} and K_{tt} terms refer to the terms that directly relate a traction with a separation of the same mode. Mixed mode stiffness (K_{ns} , K_{nt} and K_{st}) can be defined to implement coupling between the fracture modes or may be left as zero indicating that there is no coupling between the fracture modes.

This linear traction can be viewed as an elastic deformation (fully recoverable) between the two elements and represents the stretching of the adhesive bond between two elements prior to the initiation of damage. Eventually the adhesive bond will become damaged when a certain damage initiation criterion is met. This damage criterion can be based either on a critical traction or separation value. Additionally, the damage criterion can occur as a function of a single mode (equation 25) or as a quadratic function (equation 26) of all three modes. These criteria are expressed mathematically below.

$$\max \left\{ \frac{\langle \delta_n \rangle}{\delta_n^0}, \frac{\delta_s}{\delta_s^0}, \frac{\delta_t}{\delta_t^0} \right\} = 1 \quad (25)$$

$$\left\{ \frac{\langle \delta_n \rangle}{\delta_n^o} \right\}^2 + \left\{ \frac{\delta_s}{\delta_s^o} \right\}^2 + \left\{ \frac{\delta_t}{\delta_t^o} \right\}^2 = 1 \quad (26)$$

The angle brackets around the normal separation term mean that only tensile separations are taken into account since compression of the interface does not result in fracture. δ_i^o is the critical separation for mode i that will lead to damage initiation.

After the damage criterion has been met, the interfaces and their load carrying capacity deteriorate. With increased separation, the traction will gradually reduce to zero. Damage evolution is typically represented as linear softening of the interface but can be represented by exponential decay as well. This study will utilize linear damage evolution as it is the most commonly used. Linear damage evolution can be characterized in two ways; defining a failure separation (δ_i^f) or specifying the total fracture energy (area under the traction-separation curve). These specifications will yield a traction separation curves similar to the ones seen in Figure 52.

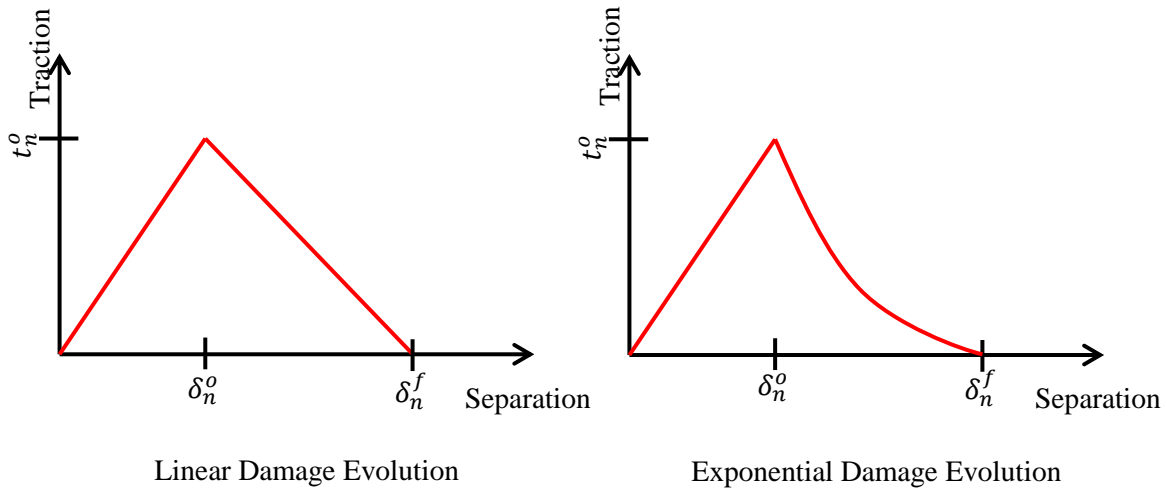


Figure 52 - Traction-Separation Curves

This traction separation behavior is implemented through the cohesive surfaces interaction. The interaction is implemented by attaching adjacent elements of the two bonded constituents. Methods for empirically determining the cohesive properties are not well documented or widely accepted. The best way to determine these properties is through a specialized material characterization. Liu et al. developed a method using a double notch shear beam to directly measure the mode II traction separation curve [21].

Time did not permit for these tests to be performed. Luckily, Liu characterized and published the traction separation behavior for Dyneema HB-26 UHMWPE composite. Since, this composite is similar in structure and materials to SR-3136 the properties were adapted for the cohesive surface interaction. Table 5 shows the properties utilized for this interaction.

| | |
|--|---------|
| $K_{nn} = K_{ss} = K_{tt}$ | 8 GPa/m |
| $\delta_n^o = \delta_t^o = \delta_s^o$ | 0.2 mm |
| $\delta_n^f = \delta_t^f = \delta_s^f$ | 0.4mm |

Table 5 - Traction Separation Properties

Transverse Shear Stiffness

The transverse shear stiffness has shown to be a critical property in forming simulations involving blanks of substantial thickness. The simulations performed by Zampaloni [3] were mostly concerned with thin composites mostly one or two layers thick. When working with materials this thin, transverse shear is negligible.

During this study, however, the blanks used did have substantial thickness (up to 0.5”) making the correct assignment of the transverse shear stiffness critical to obtain good results. When a user subroutine is used to evaluate the material properties of shell elements in Abaqus, the transverse shear stiffness must be manually defined according to the following equation.

$$K_{11}^{ts} = \frac{5}{6} G_{13} t ; K_{22}^{ts} = \frac{5}{6} G_{23} t \quad (27)$$

t is the thickness of the shell elements to which the transverse shear stiffness is being applied. The Scaling factor of $\frac{5}{6}$ is a shear correction term to account for the non-uniform shear stress distribution through the thickness of the element. The shear moduli directions are given assuming that the 1-2 plane represents the plane of the element. Figure 53 shows the orientation of transverse shears.

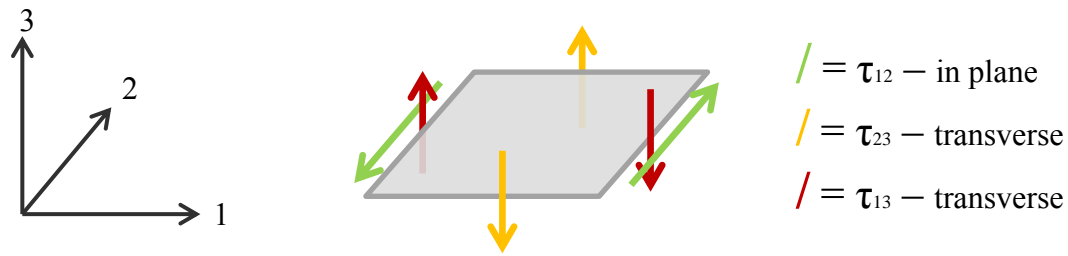


Figure 53 - Tansverse Shear

Prior to this study, hydroforming simulations were performed using properties similar to what can be seen in Table 6.

| | |
|-----------------------------|----------------------|
| Element thickness | 0.0002 m |
| G_{12} | $2.84 \cdot 10^6$ Pa |
| $K_{11}^{ts} = K_{22}^{ts}$ | 1000.0 Pa*m |

Table 6 – Original Transverse Shear Properties

At the time these simulations were performed, direct measurement of the out of plane shear modulus was not performed. Davalos et al. reported that materials similar to the ones used in these simulations showed a transverse shear modulus that was typically between 60% and 80% of the value of the in-plane shear modulus [44]. If we calculate the transverse stiffness under the assumption that the transverse shear modulus is 70% of the in plane shear modulus, then the value used should be 331 Pa*m as opposed to the 1000 Pa*m used in the simulation. Thanks to very small thickness of the composites being evaluated, this overestimation did not have a significant impact on the results of the simulation.

The transverse shear stiffness has proven to have an enormous effect on the deformation of the blank since the thickness has been increased for the forming simulations. The most prevalent effect that this property has on the deformation of the blank is in the amount of in plane shearing exhibited and the prevalence and realism of out of plane warping (wrinkling). The out of plane (OOP) shear modulus for SR-3136 was not measured and is estimated as 70% of the in-plane shear modulus. The results of varying this parameter will be discussed further in the Results and Discussion section.

Transverse Young's Modulus

Measuring the Young's Modulus for SR-3136 is relatively straightforward, but applying the data in a meaningful way is less obvious. Tensile specimens are loaded along the 0° direction meaning that approximately 50% of the fibers are aligned with applied load while the other 50% of the fibers are transverse to the applied load. Several publications have reported low bond strength between fiber and matrix as well as a lack of continuity when observing the microstructure of the composite [15], [17]. For these reasons it is assumed that the plies with fibers aligned with applied tensile load carry a vast majority of the load while the transverse fibers carry almost none of it. This assumption in terms of stiffness can be expressed as $E_{11} \gg E_{22}$. Since the material has the stacking sequence [0/90/0/90], there is no way to directly measure the transverse Young's Modulus (E_{22}).

The only way to obtain this quantity therefore is through an empirical relation. The rule of mixtures is chosen as the method to compute the properties. A fiber volume fraction of 80% and stiffness value for the matrix constituent (LDPE) is used (0.75 GPa). Using equation 12 and assuming that tensile test results give E_{11} , the apparent Young's modulus of the fiber is found (E_f). Using this same set of constants, E_{22} is found using the inverse rule of mixtures (equation 15). The Halpin and Tsai method to compute E_{22} can also be used, but the use of the inverse rule of mixtures yields a lower stiffness and complies better with the original assumption of $E_{11} \gg E_{22}$.

Use of Material Characterization Data

SR-3136 was characterized in order to obtain the Young's Modulus and the shear modulus as was. As mentioned above in the Transverse Young's Modulus section, the value obtained from these tests was assumed to be primarily from the fibers aligned with the load direction. Therefore, the modulus obtained from this test is assumed to be E_{11} and is applied to equation 7 in order to populate the Q_{11} and Q_{12} portions of the stiffness tensor.

The shear modulus is directly obtained from the Iosipescu test highlighted in the Consolidation of Flat Panels and Material Characterization section. Since the fiber alignment of the test specimen was aligned with the load applied by the test fixture, the modulus obtained by this test is taken as G_{12} . The implementation of this parameter requires additional insight. The Q_{66} parameter of each individual fiber orientation is G_{12} of a unidirectional composite. The specimen tested is a laminate of two unidirectional composites where the fiber orientations of the layers are 0° and 90° . Since two fiber orientations are used in the material model, applying G_{12} as the Q_{66} value will result in \bar{Q}_{66} for the laminate having the value $2 * G_{12}$.

$$\bar{Q}_{ij} = \bar{Q}_{ij}^{0^\circ} + \bar{Q}_{ij}^{90^\circ} = \begin{bmatrix} Q_{11} & Q_{12} & 0 \\ Q_{12} & Q_{22} & 0 \\ 0 & 0 & Q_{66} \end{bmatrix} + \begin{bmatrix} Q_{22} & Q_{12} & 0 \\ Q_{12} & Q_{11} & 0 \\ 0 & 0 & Q_{66} \end{bmatrix} = \begin{bmatrix} Q_{11} + Q_{22} & 2Q_{12} & 0 \\ 2Q_{12} & Q_{22} + Q_{11} & 0 \\ 0 & 0 & 2Q_{66} \end{bmatrix} \quad (28)$$

Seeing that the laminate value for the shear modulus has taken on a value of $2Q_{66}$, an easy correction is made by changing the individual fiber orientation to $\bar{Q}_{66}^a = \bar{Q}_{66}^b = G_{12}/2$. These properties are implemented in the user subroutine by adapting the FORTRAN input file to use them directly instead of using them as inputs to the various rules of mixtures.

Results and Discussion

Many simulations have been performed which utilize the modified PFO model described above. In order for the modeled laminate to take on a realistic thickness, many plies were needed which drastically increased the amount of time required to complete the simulation. For this reason, most simulations were conducted with 6 plies, giving the laminate a total thickness of $\sim 0.3''$. Several blanks were laid up to this thickness and experimentally formed so that good comparisons could be made with the numerical simulations.

The impact of the transverse shear stiffness of the results of the simulation, especially pertaining to wrinkling, was huge. This was determined to be the material property that had the largest effect on the outcome of the simulations. The effects of varying this property will be investigated as well.

Due to difficulties with the forming procedure and equipment, very few parts have been experimentally formed successfully at this time. This makes it difficult to compare the numerical results directly with the experimental results. Most of the evaluation of the numerical simulations has been based on the trends that are seen in the experiments for this reason. Several aspects of the model show good correlation with the experiments and others need to be improved.

Impact of Transverse Shear Stiffness

The impact of the transverse shear stiffness was noted early on. During this stage of the simulations, a circular blank was utilized. Additionally, material properties were inferred from the literature and ended up not being very accurate due to the issues with the empirical estimations of the properties, as was described above. Nevertheless these simulations show the important effect that correctly defining transverse shear has on wrinkling prediction and on the amount of in plane shear allowed.

As multiple layer simulations were began, interesting patterns in wrinkling began to be observed. The wrinkling observed was very tight and showed very little in plane shear occurring. Upon modifying the transverse shear stiffness, the wrinkling pattern changed entirely. The wrinkling observed was far less prevalent and took on realistic patterns. The in plane shearing also increased significantly and reflected more accurately what was seen in the forming experiments. Figure 54 shows a side by side comparison of the effect of under defining and correctly defining the transverse shear stiffness.

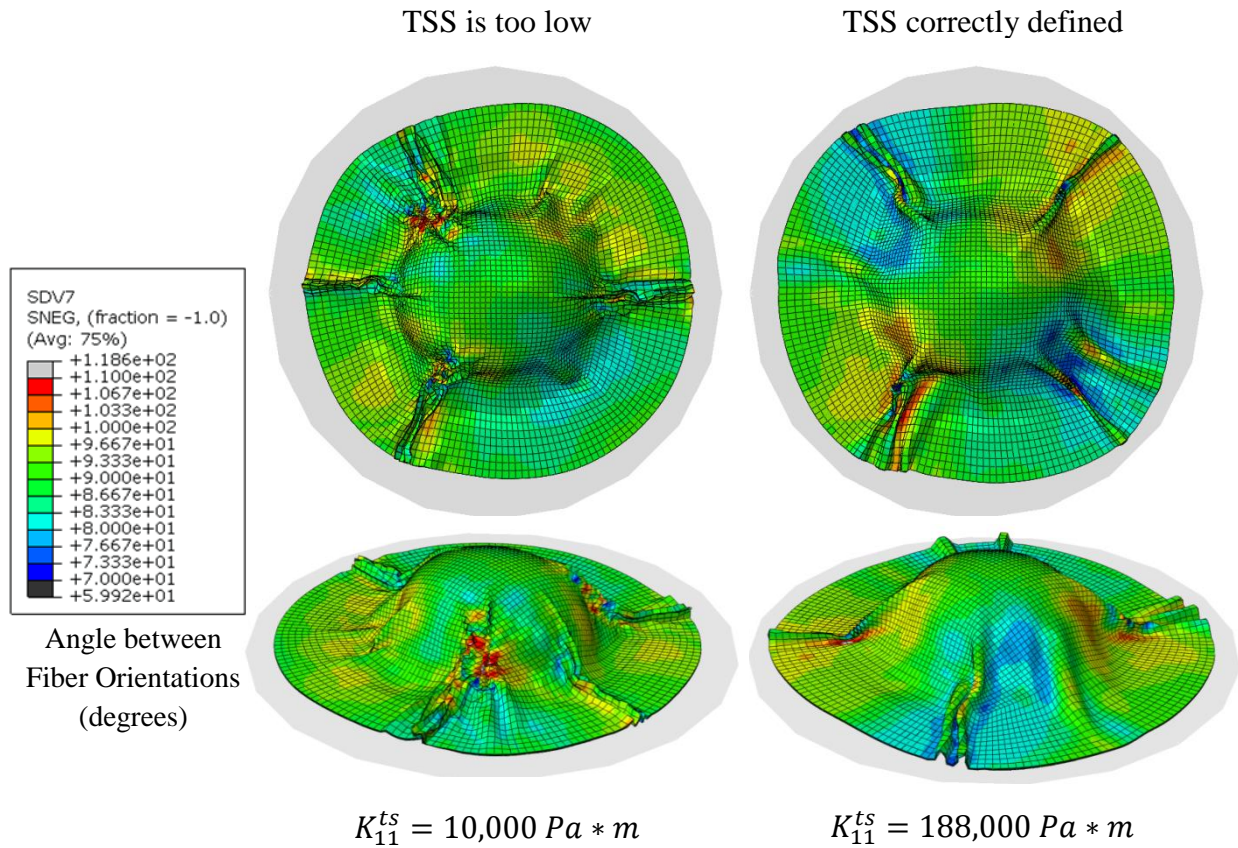


Figure 54 – Transverse Shear Stiffness Effects

The initial results on the left were obtained using the default value of the transverse shear stiffness (TSS) left over from the Zampaloni simulations. The simulations on the right are performed using the empirically obtained value from equation 27. The undeformed configuration of the fiber orientations is 90° , so the simulations with the correct TSS show more widespread values of fiber shearing which is closer to what is observed in Figure 43. The wrinkling severity is reduced and is more gentle than the sharp sporadic wrinkling seen in the simulation with the low TSS. This is similar to what we see in the forming experiments. Another benefit of correctly defining the TSS is the reduction in element warping which causes the simulation to fail. Prior to updating this parameter, many simulations ended prematurely due to excessive element warping in the areas of severe wrinkling. Updating the TSS has significantly reduced the occurrence of these problems.

The wrinkling in these forming simulations is occurring too soon and is occurring too far up the dome of the helmet. One reason for this is that these simulations utilize properties from the empirical relations which compare poorly to the measured values from the material characterizations. Upon the implementation of the measured material properties, simulation quality increases.

Square Blank Simulation Results

Most of the more recent simulations have been performed using boundary conditions and blank shapes that directly mimic the forming experiments being performed. The only substantial difference between the simulations and the experiments is in the application of forming pressure. In the simulations pressure increase is a linear function of time. In the forming experiments, pressure is largely a function of the punch displacement. Pressure also reaches a limiting value due to the limited holding capacity of the clamping rams described in Figure 39. Pressure is modeled for the ideal forming situation. Other than this discrepancy, the simulation inputs are set to reflect the exact properties of the blank and can be viewed in Table 7.

| | | |
|-----------------------------|-------------|--------------------------|
| E_{11} | 18.6 GPa | Characterization Results |
| E_{22} | 3.32 GPa | Equation 15 |
| ν_{12} | 0.46 | Equation 18 |
| G_{12} | 0.1264 GPa | Characterization Results |
| $K_{11}^{ts} = K_{22}^{ts}$ | 88,480 Pa*m | Equation 27 |
| Laminate Thickness | 0.3" | - |
| Number of layers | 6 | - |
| Cohesive Zone Properties | Table 5 | [21] |
| $f_{contact}$ | 0.1 | - |
| P_{max} | 1000 psi | - |

Table 7 – Simulation Properties

The blank shape utilized is shown in Figure 38. The latest results of the simulations can be seen below in Figure 55.

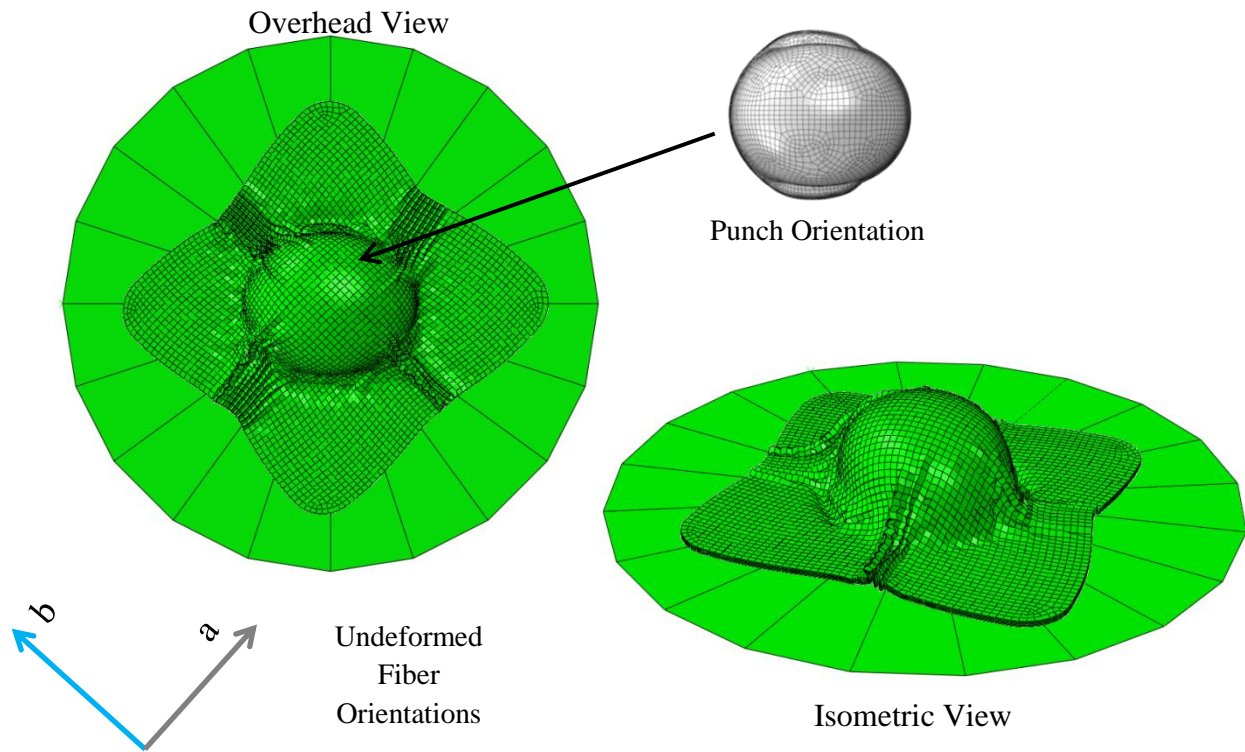


Figure 55 – Deformed Blank Shape

It can clearly be seen that the simulation results exhibits out of plane warping along the 0° and 90° orientations of the blank. Even though the extent of the warping is more than is seen in the experiments, it is occurring in the same regions seen in Figure 41 and Figure 42. In previous numerical simulations, warping occurs along the $\pm 45^\circ$ orientations which are directly conflicting with what was seen in the forming experiments. These results can be seen in Figure 56.

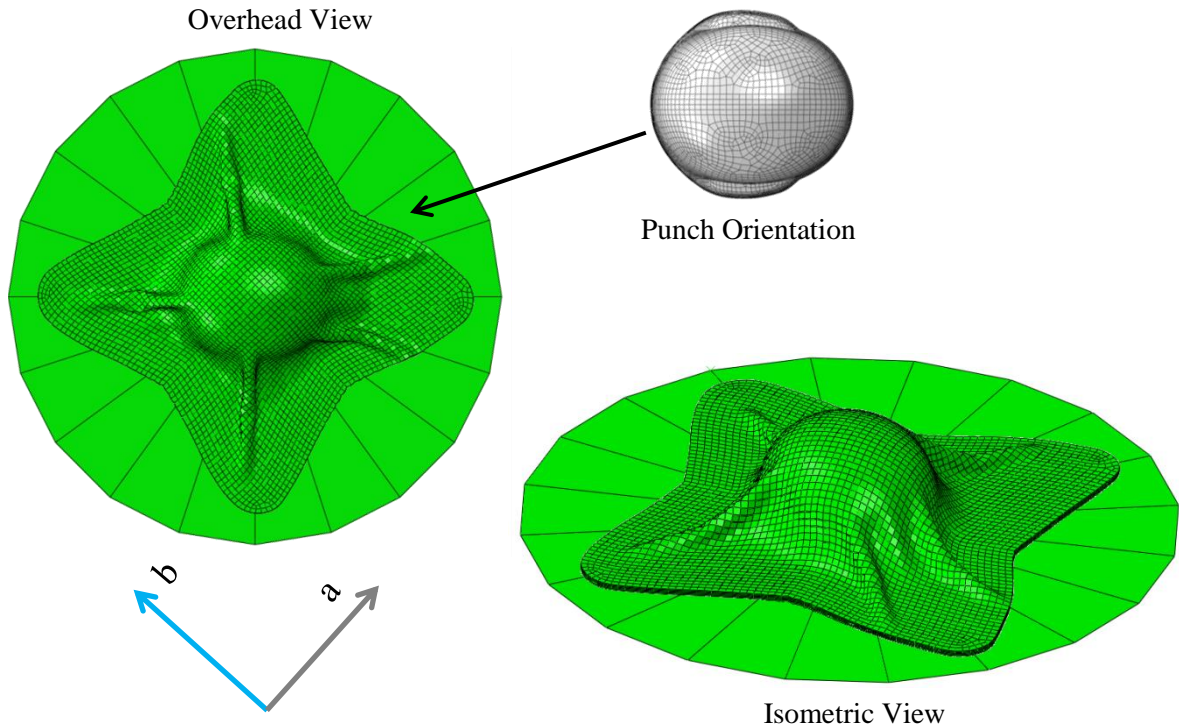


Figure 56 - Previous Simulation Results

It can be seen that the wrinkling in these simulations is along the $\pm 45^\circ$ direction of the blank. The main reason for out of plane warping in these areas is the over prediction of shear stiffness in these regions. This phenomenon will be further discussed in the next section.

The advantage of utilizing a user subroutine is that contour plots of any variable can be created. One of the most useful plots is the angle between the a-fiber orientation and the b-fiber orientation. This provides a physical quantity which can be measured and compared on the formed helmet blanks in order to compare the numerical results to experimental ones. The fiber shear plot can be seen in Figure 57.

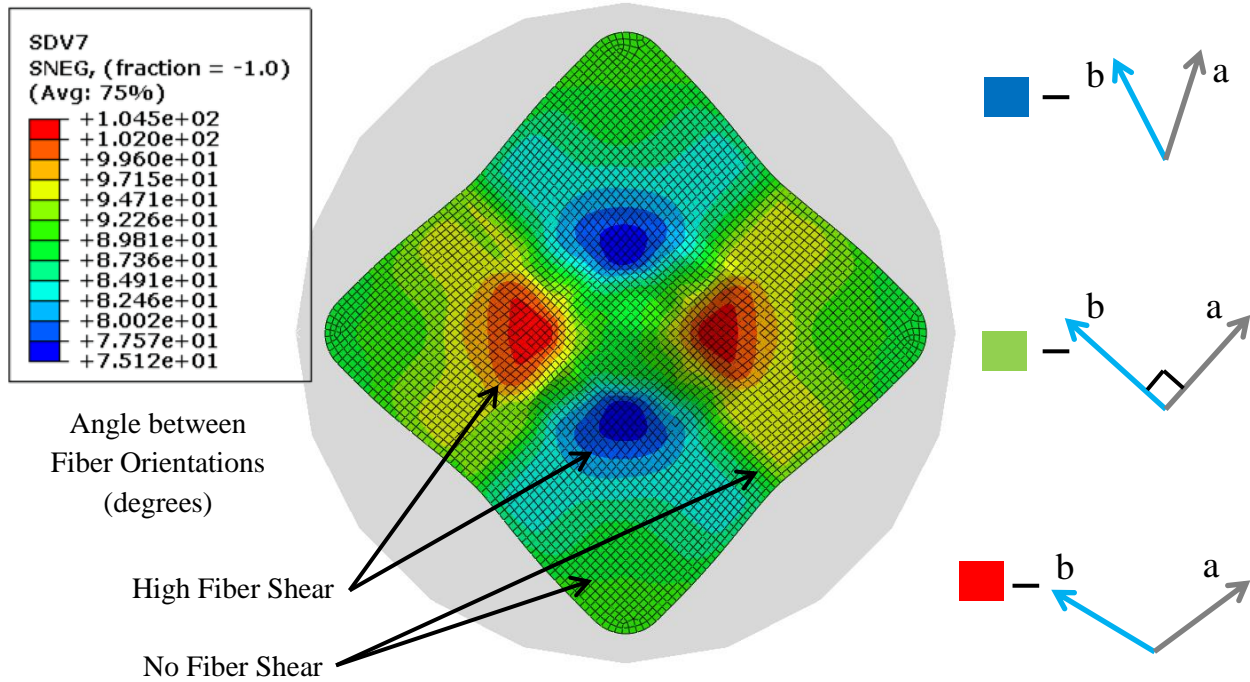


Figure 57 – Fiber Shear Contour Plot

The contour plot image is taken immediately prior to the wrinkling of the blank in order to show the distribution of the value of the shear stiffness. It can be seen that the composite experiences very little fiber shearing along the directions that the fibers are oriented. $\pm 45^\circ$ degree offset from these orientations the maximum value of fiber shear is seen.

The fiber shear angle as well as the angle that each PFO makes with respect to the structural coordinate system is plotted. The distribution of the fiber orientations is important due to their impact on the material properties. Another important material property is the shear stiffness, especially when evaluating parts to be deep drawn. The property is so important because the composite is required to undergo large shear strains in order to conform to the punch. The shear stiffness is updated during each step based on the fiber orientation of the PFO's. As the PFO's deviate from their initial orientation, the shear stiffness (\bar{Q}_{66}) increases due to the changes manifested in the transformation matrix (T). This effect can be seen in Figure 58.

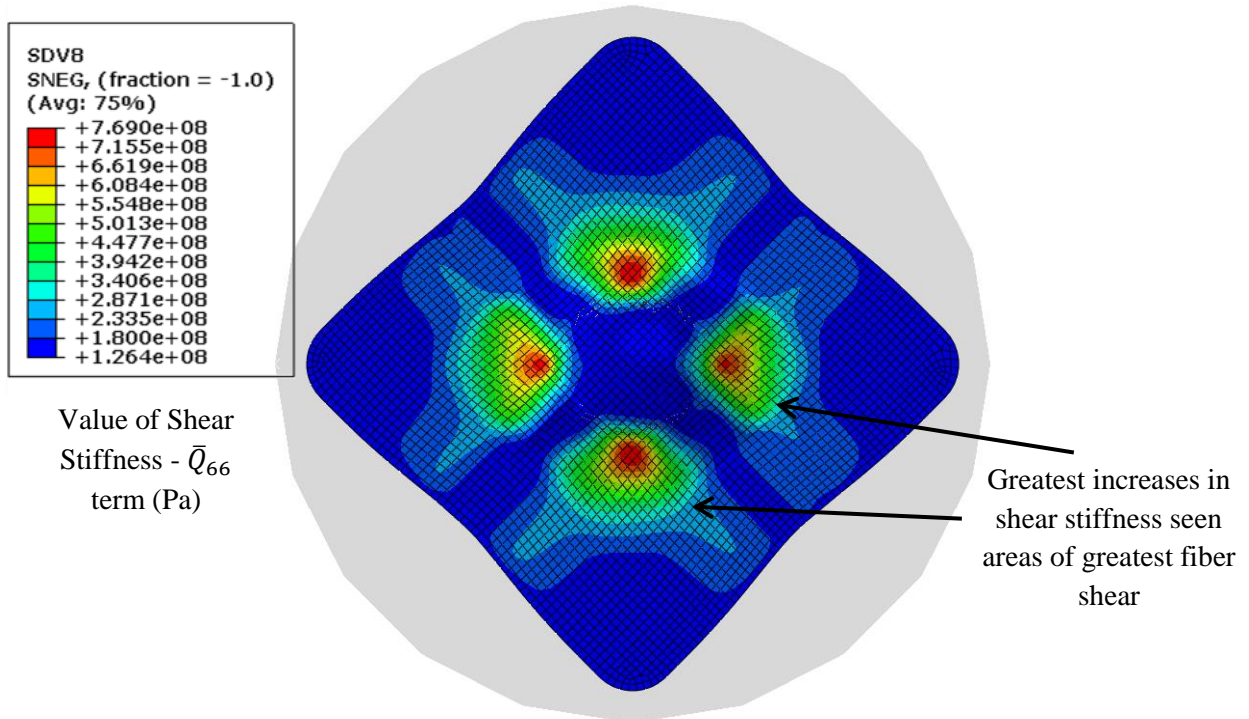


Figure 58 - \bar{Q}_{66} Contour Plot

If the shear stiffness becomes too high, the blank may warp out of plane instead of shearing in plane. This is one of the main reasons that abnormal wrinkling patterns were developing in the simulations depicted in Figure 56. Lower shear stiffness will allow more in plane shearing as opposed to out of plane warping as is seen in the most recent simulations (Figure 55).

Over-prediction of Shear Stiffness

As mentioned above the over prediction of the shear stiffness led to poor results in the initial numerical simulations. This over prediction in the stiffness was not attributed to the empirical relation used to calculate the shear stiffness (equations 21 and 22). In fact, the value for the shear modulus is lower using the empirical formulas than it was found to be in the material characterization (42.1 MPa vs 126.4 MPa). The over prediction of shear stiffness comes from the use of equation 14. This equation is used to predict the increase in volume fraction as a biaxial fiber shears due to matrix squeeze out. When the fibers shear during deformation, the volume fraction predicted by equation 14 increases, which in turn increases the shear stiffness (predicted by equations 21 and 22). This trend can be seen in Figure 59.

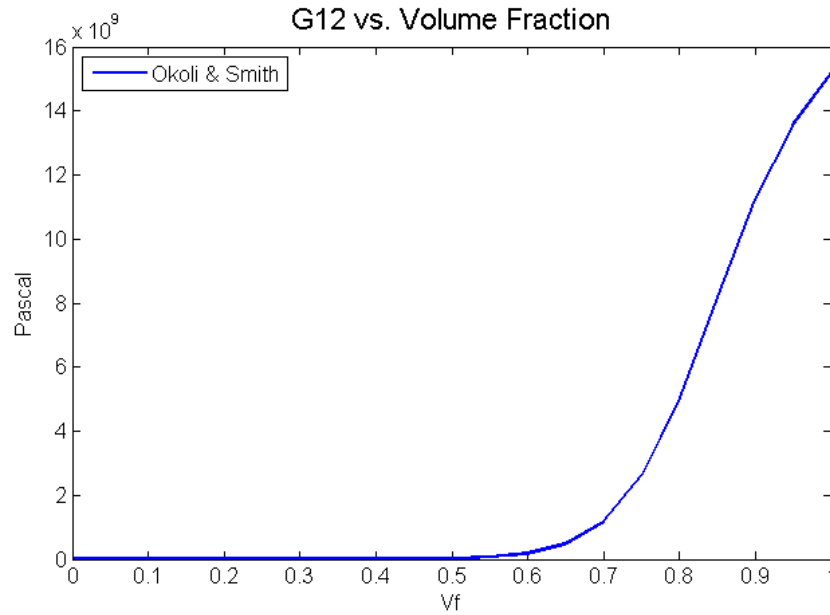


Figure 59 - Shear Stiffness vs Volume Fraction

The shear stiffness is yet again increased as the individual PFO's are rotated to the structural frame using equation 9. The effect of the rotating a single PFO from 0° to 90° on the shear stiffness (\bar{Q}_{66}) can be seen in Figure 60.

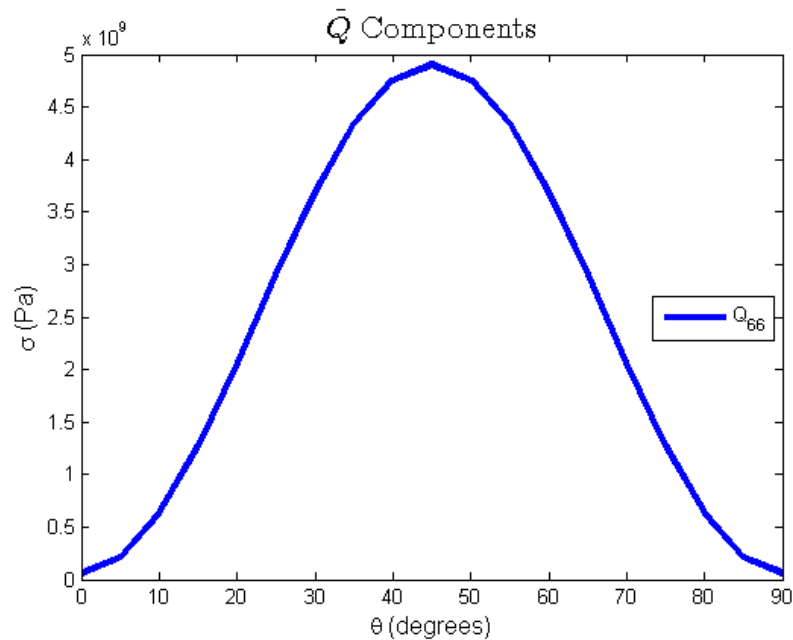


Figure 60 - Frame Rotation Effect on Shear Stiffness

Figure 60 shows that the value of the shear stiffness is increased due to rotation of the material frame to the structural frame. The use of equation 14 increases the shear stiffness twice leading to an over prediction of the parameter. This is evidenced by looking at similar time steps in two simulations; a simulation that utilized equation 14 and a simulation that does not utilize equation 14. In the simulation that utilizes equation 14 the minimum and maximum shear stiffness's are 42.1 MPa and 883.2 MPa. In the simulation that does not use equation 14 the minimum and maximum shear stiffness's are 126.4 MPa and 769.0 MPa. The minimum value indicates the shear modulus in the undeformed configuration of both materials ($\bar{Q}_{66} = G_{12}$ when undeformed). It is clear that the simulation that used equation 14 experiences a much more rapid increase in shear stiffness as well as a much larger gap between the minimum value and the maximum value. The simulation seen in Figure 56 uses equation 14 to update the volume fraction and exhibits wrinkling in unexpected regions. The results in Figure 55 utilize a static value for the volume fraction leading to a more realistic shear stiffness prediction and therefore a more realistic result.

The use of equation 14 (or an equation similar to it) has its uses, however. The artificially high shear modulus prediction can be used to predict the onset of shear locking. Shear locking occurs in woven fabrics that are experiencing high shear. As shear strain increases, eventually the warp and weft fibers will jam over one another leading to increases in the shear stiffness. Equation 14 can be used in this regard to simulate the effects of shear locking. Zampaloni showed good results using this equation when modeling the forming of simple weave fiber glass composites due to this artificial shear locking [3]. The fiber structure in SR-3136 is not woven and therefore will not experience shear locking. Equation 14 has been omitted for this reason.

Comparison to Experimental Results

Making comparisons between numerical simulations and forming experiments is a good way to validate the accuracy of the material model and the boundary conditions. One of the easiest ways in which to do this is to compare the force-displacement curves of the punch for the simulation and experiment. Upon initial comparison the force-displacement plot showed very poor correlation. After realizing that the

forming pressure profile was completely different in the simulation and the experiment, an additional simulation was run with a similar pressure profile similar to the ones observed in the experiments. The comparison showed good results after this change was made. Examples of the pressure profiles used can be seen in Figure 61.

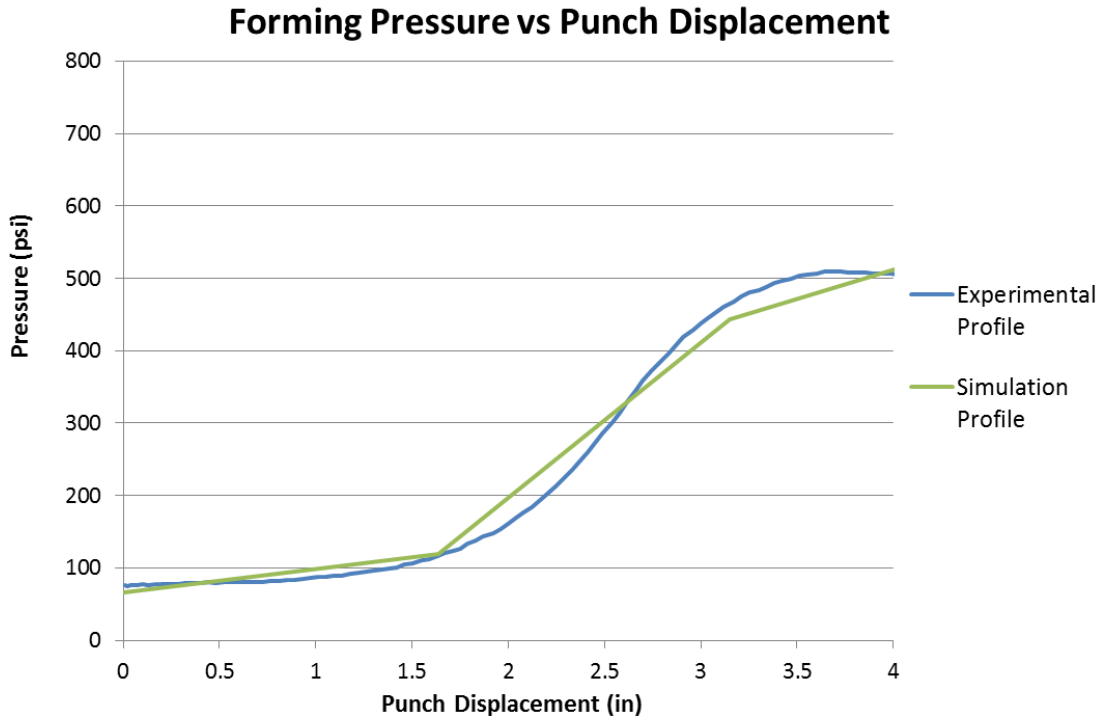


Figure 61 - Pressure Profiles

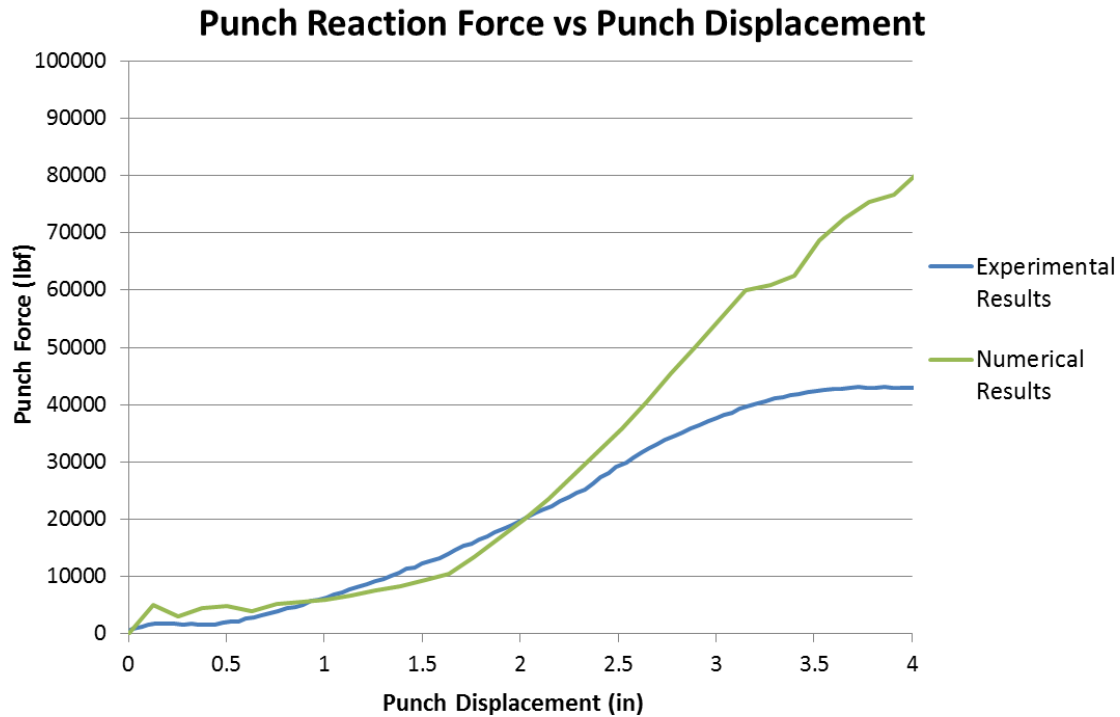


Figure 62 - Force-Displacement Comparison

The pressure profile exhibited in the experiments follow an unusual path due to the limited clamping capability of the clamping rams described in Figure 39. Tailoring a pressure profile to fit the experimental results allows the pressure applied in the simulation to be similar to the pressure applied in the experiment. The displacement of the comparison is restricted to 4 inches to stay within the displacements where pressure is building during the forming experiments.

Figure 62 shows good correlation between the load-displacement curves up to a value of 2.5 inches. After this point the numerical results see a large increase in load while the experimental values taper off. The reason for this is that the numerical simulation begins to exhibit severe wrinkling around this point. The out of plane warping leads to the increased punch load needed to deform the blank. If we restrict the comparison to punch displacements below 2.5 meters then the curves show excellent correlation, showing that the model is able to predict the punch force needed to form the blank accurately.

Another method to compare the simulation results to the experimental results is to compare the shape of the blank clamping areas. This comparison can be seen in Figure 63. The blank shape

comparison shows the same blank shape after forming. This shape is produced primarily by the orientations of the reinforcing fibers. They tend to draw in most along their axial alignment while 45° from these orientations the blank draws in very little, producing the tabs features seen in Figure 63. The biggest difference seen between the two results is the wrinkling on the numerical result is more prevalent than on the experimental results.

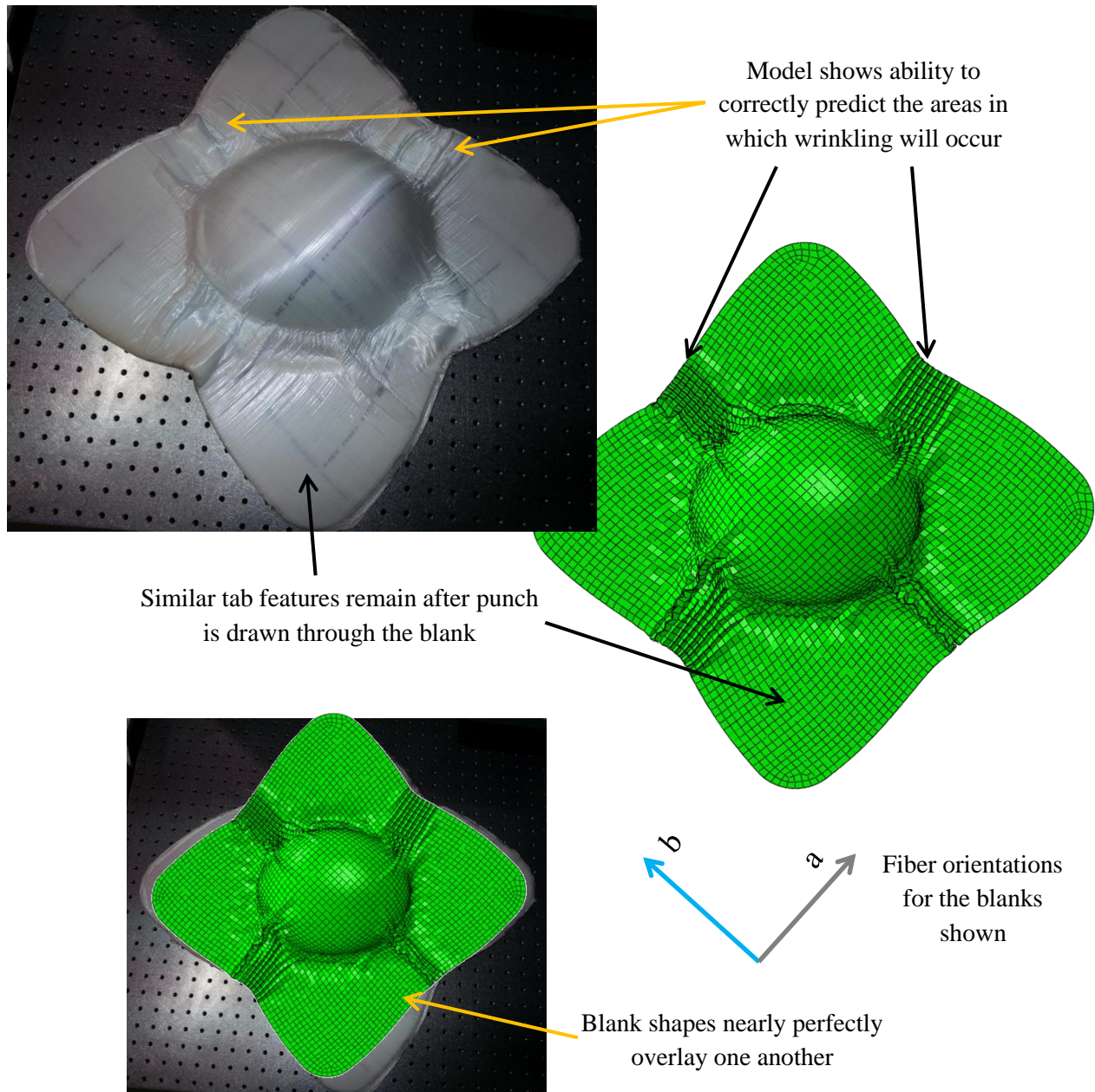


Figure 63 – Blank Shape and Wrinkling Region Comparison

Figure 63 also shows that the model has the ability to predict the location that wrinkling will initiate in effectively. A vast majority of the wrinkling occurs along the blank holding areas in the regions that extend away from the center of the helmet along the fiber orientations. The model shows wrinkling extending a little too far up the dome of the helmet giving room for improvement.

Future Recommendations

The accuracy of the numerical model has been greatly improved with the implementation of the material properties from the material characterizations. Further increases in accuracy could be obtained from obtaining the last few properties need to completely characterize the material and forgo empirical formulas altogether. These last few properties include the transverse shear stiffness and the traction separation properties. The tests required to obtain these properties were not performed due to time constraints and difficulty in machining the specimens required to perform the tests.

The next improvement that should be made is to evaluate the material properties at the temperature at which the composite is formed. All of the properties were evaluated at room temperature. Undoubtedly the properties would deviate significantly if evaluated at the forming temperature. The material is currently treated as an elastic material. This should raise concerns instantly, being that the deformation being simulated is a forming procedure which implies permanent deformation. Therefore, a model which incorporates plasticity is needed order to increase simulation accuracy. More specifically, the model should incorporate a visco-plastic response. Thermoplastic polymers are highly viscous materials when being formed close to their melting temperature so the need for viscous effects in the material response is crucial. Implementing an elasto-viscoplastic material model coupled with the effects of the PFO's was outside the scope of this work and satisfactory results have been obtained without it.

Perhaps a more obtainable improvement could be made by simply increasing the versatility of the transverse shear stiffness. The transverse shear stiffness is implemented as a static value for set of shell elements in the Abaqus input file. The stiffness does not take into account changes in fiber orientation, thickness or any other changes that occur during the simulation. An additional user subroutine should be

written which allows more control over this parameter which has shown to be critical throughout this study.

Conclusions

Throughout the course of this study, composite thermo-hydroforming has been taken from process that only has the ability to form thin composite hemispheres, to a process that has the ability to form thick composite laminates. Better pressure control and temperature control are needed to further increase the quality of the final part. Different clamping mechanisms also need to be investigated to determine which ones give the best final results. Initial results have indicated that composite hydroforming is a viable manufacturing method that has the ability to form deep drawn parts. With additional investigation it is highly likely that this process could be implemented on an industrial scale in the automotive and aerospace industries in order to drastically decrease process time. Processing time for the numerical experiments was on average approximately 5 minutes. This time can be further reduced with better pressure and temperature control in addition to programming the forming steps into the controller software. Additionally, there is a dire need for more clamping force. Future designs should take into account the die shape and desired forming pressure when sizing and selecting the clamping rams.

Numerical results were also obtained that showed good correlation with the experimental results on the basis of wrinkling location, blank draw-in shape and load displacement curves. Out of plane warping prediction is an issue that needs to be investigated further. The general wrinkling area can be predicted but the wrinkling shape is not very accurate. Mesh refine may lead to better results but also leads to decreases in thickness that shell elements can accurately represent. The best way to increase the accuracy of the simulations at this point is to re-measure the material properties at elevated temperatures. This will give the most accurate response of the material as it is being formed.

The ACH is a difficult piece to form, especially since it is the first functional part manufactured with the composite thermo-hydroforming process. It should be noted that ACH's are currently formed using Kevlar that is excessively dented in order to reduce wrinkling and form a part with a high quality surface finish. CTH is nearly able to perform this task using a far simpler blank and using a process that

has the ability to be completely automated. These good results indicate the CTH should be able to form parts with simple curvature as it currently exists. With minimal additional investigation, this process can be implemented on a massive scale.

REFERENCES

REFERENCES

- [1] A. Yousefpour, "Fusion Bonding/Welding of Thermoplastic Composites," *Journal of Thermoplastic Composite Materials*, vol. 17, pp. 303-341, July 2004.
- [2] G. Schinner, "Recycling Carbon-Fiber-Reinforced Thermoplastic Composites," *Journal of Thermoplastic Composite Materials*, vol. 9, no. 3, pp. 239-245, July 1996.
- [3] M. Zampaloni, "A multipreferred fiber orientation constitutive model for fiber mat-reinforced thermoplastics with a random orientation applied to the stamp thermohydroforming process," East Lansing, 2003.
- [4] W. D. Bascom and L. T. Drzal, "The Surface Properties of Carbon Fibers and Their Adhesion to Organic Polymers," 1987.
- [5] T. Semoto, Y. Tsuji, H. Tanaka and K. Yosizawa, "Role of Edge Oxygen Atoms on the Adhesive Interaction between Carbon Fiber and Epoxy Resin," *The Journal of Physical Chemistry*, vol. 117, no. 47, p. 24830–24835, 2013.
- [6] L. Ye, "Manufacture of CF/PEEK composites from powder/sheath fibre preforms," *Composites Manufacturing*, vol. 5, no. 1, pp. 41-50, 1994.
- [7] C. Beyler, "Thermal Decomposition of Polymers," in *SFPE Handbook of Fire Protection Engineering*, 2002, pp. 110-131.
- [8] M. Zampaloni, "Kenaf natural fiber reinforced polypropylene composites: A discussion on," *Composites: Part A*, pp. 1569-1580, 2007.
- [9] Q. Shubhra, "Mechanical properties of polypropylene composites: A review," *Journal of Thermoplastic Composite Materials*, vol. 26, no. 3, pp. 362-391, April 2013.
- [10] N. G. Karsli, "Effects of maleated polypropylene on the morphology, thermal and mechanical properties of short carbon fiber reinforced polypropylene composites," *Materials & Design*, vol. 32, no. 7, pp. 4069-4073, August 2011.
- [11] I. Giraud, "Preperation of aqueous dispersion of thermoplastic sizing agent for carbon fiber by emulsion/solvent evaporation," *Applied Surface Science*, vol. 266, pp. 94-99, 2013.
- [12] Honeywell, *Processing Honeywell Spectra Shield*, 2011.
- [13] T. Xu, "Matrix Free Ultra-High Molecular Weight Polyethylene Fiber-Reinforced Composites: Process, Structure, Properties and Applications," *New Polymertic Materials*, vol. 916, pp. 391-405, September 2005.

- [14] T. Xu and R. J. Farris, "Comparative Studies of Ultra High Molecular Weight Polyethylene Fiber Reinforced Composites," *Polymer Engineering and Science*, vol. 47, no. 10, pp. 1544-1553, 2007.
- [15] E. Greenhalgh, "Fractographic observations on Dyneema composites under ballistic impact," *Composites: Part A*, vol. 44, pp. 51-62, May 2012.
- [16] ASTM International, *Standard Test Method for Tensile Properties of Polymer Matrix Composite Materials*, ASTM International, 2008.
- [17] B. Russell, "The high strain rate response of Ultra High Molecular-weight Polyethylene: From fibre to laminate," *International Journal of Impact Engineering*, vol. 60, pp. 1-9, 2013.
- [18] ASTM International, *Standard Test Method for Shear Properties of Composite Materials by the V-Notched Beam Method*, ASTM International, 2012.
- [19] ASTM International, *Standard Test Method for Shear Properties of Composite Materials by V-Notched Rail Shear Method*, ASTM International, 2012.
- [20] W. Yan-lei, "Evaluation of in plane shear test methods for composite material laminates," *Journal of Chongqing University*, vol. 6, no. 3, pp. 221-226, September 2007.
- [21] G. Liu, "Collapse of a composite beam made from ultra high molecular-weight polyethylene fibres," *Journal of the Mechanics and Physics of Solids*, vol. 63, pp. 320-335, 2014.
- [22] R. Okine, "Analysis of Forming Parts from Advanced Thermoplastic Composite Sheet Materials," *Journal of Thermoplastic Composite Materials*, vol. 2, pp. 50-76, 1989.
- [23] H. Yin, X. Peng and T. Du, "Forming of thermoplastic plain woven carbon composites: An experimental investigation," *Journal of Thermoplastic Composite Materials*, vol. 27, no. 5, pp. 1-13, 2013.
- [24] R. McCool, "Thermofforming carbon fibre-reinforced thermoplastic composites," *Journal of Materials: Design and Applications*, vol. 102, no. L, pp. 91-102, 2011.
- [25] A. C. Karmaker, "Injection Molding of Polypropylene Reinforced with Short Jute Fibers," *Journal of Applied Polymer Science*, vol. 62, pp. 1147-1151, 1996.
- [26] M. Gupta and K. K. Wang, "Fiber Orientation and Mechanical Properties of Short-Fiber-Reinforced Injection-Molded Composites: Simulated and Experimental Results," *Polymer Composites*, vol. 14, no. 5, pp. 367-382, 1993.
- [27] F. Pourboghrat, M. Zampaloni and A. Benard, "Hydroforming of Composite Materials". United States of America Patent 6631630 B1, 14 October 2003.
- [28] M. A. Zampaloni, "Stamp Thermo-Hydroforming: A new Method for Processing Fiber-Reinforced Thermoplastic Composite Sheets," *Journal of Thermoplastic Composite Materials*, vol. 17, no. 1, pp. 31-50, January 2004.

- [29] R. Jones, "Chapter4: Macromechanical Behavior of a Laminate," in *Mechanics of Composite Materials*, Washington D.C., Scripta Book Company, 1975, pp. 147-173.
- [30] W. R. Yu and F. Pourboghrat, "Non-orthogonal constitutive equation for woven fabric reinforced thermoplastic composites," *Composites: Part A*, vol. 33, pp. 1095-1105, 2001.
- [31] W. R. Yu, M. Zampaloni and F. Pourboghrat, "Sheet hydroforming of woven FRT composites: non-orthogonal constitutive equation considering shear stiffness and undulation of woven structure," *Composite Structures*, vol. 61, pp. 353-362, 2003.
- [32] W. R. Yu, M. Zampaloni and F. Pourboghrat, "Analysis of flexible bending behavior of woven preform using non-orthogonal constitutive equation," *Composites: Part A*, vol. 36, pp. 839-850, 2005.
- [33] P. Boisse, "Finite element simulation of textile composite forming including the biaxial fabric behavior," *Composites: Part B*, vol. 28, no. B, pp. 453-464, 1997.
- [34] N. Abedrabbo, M. Zampaloni and F. Pourboghrat, "Wrinkling control in aluminum sheet hydroforming," *International Journal of Mechanical Sciences*, vol. 47, pp. 333-358, 2005.
- [35] P. Harper, "Cohesive zone length in numerical simulations of composite delamination," *Engineering Fracture Mechanics*, vol. 75, pp. 4774-4792, 2008.
- [36] ASTM International, *Standard Test Method for Tensile Properties of Plastics*, ASTM International, 2010.
- [37] D. T. Campbell and D. Cramer, "Hybrid Thermoplastic Composite Ballistic Helmet Fabrication Study," *Advanced Materials and Process Engineering*, 2008.
- [38] U. Mohammed, C. Lekakou and M. Bader, "Experimental studies and analysis of the draping of woven fabrics," *Composites: Part A*, vol. 31, pp. 1409-1420, 2000.
- [39] N. Chang, A. Bellare, R. Cohen and M. Spector, "Wear behavior of bulk oriented and fiber reinforced UHMWPE," *Wear*, vol. 241, no. 1, pp. 109-117, 2000.
- [40] O. Okoli, "Development of a Semi-Empirical Method for Obtaining the Dynamic Young's Modulus in Random Continuous Reinforced Glass/Epoxy Composites," *Journal of Reinforced Plastics and Composites*, vol. 19, no. 4, pp. 292-300, 2000.
- [41] J. Halpin and J. Kardos, "The Halpin-Tsai Equations: A Review," *Polymer Engineering and Science*, vol. 16, no. 5, pp. 344-352, 1976.
- [42] C. G. Davila, "Effective Simulation of Delamination in Aeronautical Structures Using Shells and Cohesive Elements," *Journal of Aircraft*, vol. 45, no. 2, pp. 1-10, 2007.

- [43] V. Kushch, "Explicit Modeling the Progressive Interface Damage in Fibrous Composite: Analytical vs. Numerical Approach," *Composites Science and Technology*, vol. 71, pp. 989-997, 2011.
- [44] J. Davalos, P. Qiao, H. Salim and J. Schlüssel, "Shear Moduli of Structural Composites from Torsion Tests," *Journal of Composite Materials*, vol. 36, no. 10, pp. 1151-1173, 2002.
- [45] A. R. Offringa, "Thermoplastic composites - rapid processing applications," *Composites Part A: Applied Science and Manufacturing*, vol. 27, no. 4, pp. 329-336, July 1996.
- [46] J. Moore, "Manufacture and Mechanical Testing of Kenaf Fiber Reinforced Polypropylene Composites with Aluminum Faces," 2007.
- [47] T. J. Keener, "Maleated coupling agents for natural fibre composites," *Composites Part A*, vol. 35, no. 3, pp. 357-362, March 2004.
- [48] K. Karthikeyan, "The effect of shear strength on the ballistic response of laminated composite plates," *European Journal of Mechanics and Solids*, vol. 42, pp. 35-53, April 2013.
- [49] I. Chang, "Recent Development in Thermoplastic Composites: A Review of Matrix Systems and Processing Methods," *Journal of Thermoplastic Composites*, vol. 1, no. 3, pp. 277-296, July 1988.
- [50] W. J. Cantwell, "The impact resistance of composite materials — a review," *Composites*, vol. 22, no. 5, p. 347-362, September 1991.
- [51] H. Toftegaard, "Determination of In-Plane and Out-of-Plane Elastic Constants for Medium Thickness Sandwich Composite Skins," in *Sandwich Structures 7: Advancing with Sandwich Structures and Materials*, Aalborg, Denmark, 2003.